Western University
Scholarship@Western

Digitized Theses | Digitized Special Collections

2008

DESIGN AND DEVELOPMENT OF IN VITRO TOOLS TO ASSESS FIXATION AND MOTION IN THE SPINE

Stewart D. McLachlin
Western University

Follow this and additional works at: https://ir.lib.uwo.ca/digitizedtheses

Recommended Citation

McLachlin, Stewart D., "DESIGN AND DEVELOPMENT OF IN VITRO TOOLS TO ASSESS FIXATION AND MOTION IN THE SPINE" (2008). *Digitized Theses*. 4118.
https://ir.lib.uwo.ca/digitizedtheses/4118

This Thesis is brought to you for free and open access by the Digitized Special Collections at Scholarship@Western. It has been accepted for inclusion in Digitized Theses by an authorized administrator of Scholarship@Western. For more information, please contact wlswadmin@uwo.ca.

DESIGN AND DEVELOPMENT OF *IN VITRO* TOOLS TO ASSESS FIXATION AND MOTION IN THE SPINE

(Spine Title: Development of Tools to Assess Spinal Fixation & Motion)

(Thesis format: Integrated-Article)

by

Stewart D. McLachlin

Graduate Program in Engineering Science
Department of Mechanical & Materials Engineering

A thesis submitted in partial fulfillment
of the requirements for the degree of
Master of Engineering Science

School of Graduate and Postdoctoral Studies
The University of Western Ontario
London, Ontario, Canada

© Stewart D. McLachlin 2008

THE UNIVERSITY OF WESTERN ONTARIO
SCHOOL OF GRADUATE AND POSTDOCTORAL STUDIES

CERTIFICATE OF EXAMINATION

Supervisor

Cynthia E. Dunning, Ph.D., P.Eng.
Dept. of Mechanical & Materials Engineering
Department of Surgery
Department of Medical Biophysics

Joint-Supervisor

Chris S. Bailey, M.D., FRCSC, M.Sc.
Department of Surgery

Examiners

Thomas R. Jenkyn, Ph.D., P.Eng.
Dept. of Mechanical & Materials Engineering
School of Kinesiology

Michael D. Naish, Ph.D.
Dept. of Mechanical & Materials Engineering
Dept. of Electrical & Computer Engineering

Kevin R. Gurr, M.D., FRCSC
Department of Surgery

The thesis by

Stewart David McLachlin

entitled:

Design and Development of *In Vitro* Tools to Assess Fixation and Motion in the Spine

is accepted in partial fulfilment of the
requirements for the degree of
Master of Engineering Science

Date_____

_____
Chair of the Thesis Examination Board

ABSTRACT

In vitro biomechanical testing of the spine is an important method for evaluating new surgical methods and components, prior to *in vivo* implementation. This relies upon special laboratory tools and techniques to create spinal motion and loading similar to those experienced in the body. In this thesis, two different studies were performed to evaluate the effects of spinal fixation and motion. The first study compared the fixation of a novel hollow screw and a conventional solid screw in an *in vitro* sacral model. Screws were tested in seven cadaveric sacra and subjected to stair-cased cyclic flexion-extension loading to simulate the clinical loading scenario. The hollow screw was less resistant to loosening compared to the solid screw in this model. In the second part of this thesis, a spinal loading simulator was developed as a modification to an existing Instron® materials testing machine to produce motion in a multi-segment spine using applied pure bending moments (*i.e.* flexibility protocol). A custom-designed 2D optical tracking system was used to record the planar motion achieved. An experimental validation study was performed using the developed apparatus, and showed the device was capable of independently producing repeatable and reproducible spine motions (*i.e.* flexion-extension, lateral bending, and axial rotation) in a single cadaveric specimen. Future work will focus on the continued development of the simulator for use in the assessment of spinal orthopaedic interventions.

Keywords: spine, biomechanics, implant fixation, mechanical testing, optical tracking, loading apparatus, flexibility

STATEMENT OF CO-AUTHORSHIP

The research performed in this body of work was a collaborative effort from several individuals. Without the hard work and persistence of those involved, this thesis could not have been completed. Contributions are as follows:

Chapter 1: Stewart McLachlin – wrote manuscript; Cynthia Dunning – reviewed manuscript; Chris Bailey – reviewed manuscript.

Chapter 2: Stewart McLachlin – study design, data collection, data analysis, wrote manuscript; Cynthia Dunning – study design, reviewed data analysis, reviewed manuscript; Chris Bailey – study design, reviewed manuscript; Brendon Beaton – study design, data collection, data analysis; Marlis Sabo – surgical procedures.

Chapter 3: Stewart McLachlin – study design, data collection, data analysis, wrote manuscript; Cynthia Dunning – study design, reviewed data analysis, reviewed manuscript; Chris Bailey – study design, reviewed manuscript; Rebecca Austman – data collection.

Chapter 4: Stewart McLachlin – wrote manuscript; Cynthia Dunning – reviewed manuscript; Chris Bailey – reviewed manuscript.

ACKNOWLEDGEMENTS

First off, I would like to thank my supervisor Dr. Cynthia Dunning for providing me the opportunity to join her research laboratory. She has been an amazing educator, mentor, and friend and I could not imagine a more supportive and helpful advisor, not to mention one who spent a year of my thesis on maternity leave! I have to also thank the most patient person throughout this process, Ms. Chiara Dunning-Zwicker, who spent many long days in the lab with her mom.

I would also like to thank my joint supervisor, Dr. Chris Bailey, for his support and dedication during this work. His research vision provided opportunity to complete this project and I am forever grateful for it. I would like to extend thanks to his surgical colleagues, Dr. Kevin Gurr and Dr. Stewart Bailey, for their contributions to this thesis. I would also like thank Dr. Marlis Sabo for her assistance with the surgical procedures.

An acknowledgement for this project would be remiss without tremendous thanks to my labmates: Brendon, Cheryl, Rebecca, Angela, and Sarah. Having your research experiences to rely on was a huge assistance to this project, especially with LabVIEW™ – thanks Brendon! It was fun to come to the lab each day and the times spent together outside the lab were certainly memorable.

Finally, I would like to thank my family for their love and support throughout my university career and encouraging me to pursue this opportunity. Many others including extended family, roommates and friends have offered support, encouragement and advice along the way so a big thank you goes out to all of you!

TABLE OF CONTENTS

CERTIFICATE OF EXAMINATION ii

ABSTRACT iii

STATEMENT OF CO-AUTHORSHIP iv

ACKNOWLEDGEMENTS v

LIST OF TABLES x

LIST OF FIGURES xi

LIST OF APPENDICES xiv

LIST OF ABBREVIATIONS, SYMBOLS, AND NOMENCLATURE xv

CHAPTER 1: INTRODUCTION 1

1.1 The Human Spine 1

1.1.1. Anatomy and Function 1

1.1.2. Physiologic Motions 7

1.1.2.1. Lumbar & Lumbosacral Spinal Motions 13

1.1.3. Instability and Pathologic Motion 15

1.2 Surgical Treatment of Instability Through Lumbosacral Fusion 18

1.1.4. Pedicle Screw Instrumented Fusion (PSIF) 19

1.2.2 Complications of PSIF 21

1.2.2.1 Instrumentation Failure 21

1.2.2.2 Adjacent Level Effects 22

1.3 Laboratory Investigations of Spinal Fixation and Motion 22

1.3.1 Pedicle Screw Fixation 23

1.3.2 Spinal Loading Simulators 24

1.3.2.1 Stand Alone Devices 25
1.3.2.2 Modified Materials Testing Machines 26
1.3.2.3 Associated Motion Measurement Tools 27
1.4 Study Rationale 29
1.4.1 Pedicle Screw Loosening in the Sacrum 29
1.4.2 Development of a new Spinal Loading Simulator 29
1.5 Objectives and Hypotheses 30
1.6 Thesis Overview 31
1.7 References 31
CHAPTER 2: CYCLIC TESTING OF HOLLOW VERSUS SOLID SCREWS FOR SACRAL PEDICLE FIXATION 35
2.1 Introduction 35
2.2 Materials and Methods 36
2.2.1 Specimen Preparation 36
2.2.2 Screw Insertion 36
2.2.3 Experimental Setup 38
2.2.4 Cyclic Loading Protocol 38
2.2.5 Tracking Screw Loosening 41
2.2.6 Post-hoc Analysis 41
2.3 Results 42
2.4 Discussion 49
2.5 References 53

CHAPTER 3: DEVELOPMENT AND VALIDATION OF A SPINAL LOADING SIMULATOR 55

3.1 Introduction 55

3.2 Materials and Methods 55

3.2.1 Spinal Loading Device 55

3.2.1.1 Instron® Materials Testing Machine 56

3.2.1.2 Modification Components 58

3.2.2 Optical Tracking System for Segmental Motion 62

3.2.3 Experimental Validation Protocol 64

3.2.3.1 Specimen Preparation and Potting Protocol 64

3.2.3.2 Specimen Setup in Simulator 68

3.2.3.3 Loading Protocol 69

3.2.4 Data Analysis of Segmental Motion 70

3.2.4.1 Segmental Rotations 73

3.2.4.2 Range of Motion and Neutral Zone 76

3.3 Results 78

3.3.1 System Performance 78

3.3.2 Experimental Overview 79

3.3.3 Segmental Rotations 79

3.3.3.1 Rotation vs. Applied Moment Hysteresis Curves 80

3.3.3.2 Range of Motion and Neutral Zone 80

3.4 Discussion 94

3.5 References 105

CHAPTER 4: SUMMARY AND FUTURE DIRECTIONS 107

4.1 Summary 107

4.2 Strengths and Limitations 109

4.2.1 Screw Loosening Study 109

4.2.2 Spinal Loading Simulator 110

4.3 Future Directions 111

4.4 Clinical Relevance 113

4.5 References 114

APPENDICES 115

CURRICULUM VITAE 155

LIST OF TABLES

Table 1.1 Literature Review of Segmental ROM in the Lumbar Spine 16

Table 3.1 Segmental Range of Motion (ROM) at the L1-L2 Level 90

Table 3.2 Segmental Range of Motion (ROM) at the L2-L3 Level 91

Table 3.3 Segmental Range of Motion (ROM) at the L3-L4 Level 92

Table 3.4 Overall Range of Motion (ROM) and Neutral Zone (NZ) for L1-L4..... 93

Table 3.5 Reproducibility of the Segmental Range of Motion (ROM) 95

LIST OF FIGURES

Figure 1.1 The Human Spine 3

Figure 1.2 Lumbar Vertebra 4

Figure 1.3 Intervertebral Disc 6

Figure 1.4 Spinal Ligaments 8

Figure 1.5 Spinal Motion Segment 9

Figure 1.6 Spinal Motions 10

Figure 1.7 Motion Parameters 12

Figure 1.8 Facet Joint Orientations in the Lumbar Spine 14

Figure 1.9 Degenerative Disc Disease at the L4-L5 and L5-S1 levels 17

Figure 1.10 Pedicle Screw Instrumented Fusion at L4-L5 20

Figure 2.1 Hollow and Solid Screws Inserted Into Sacral Specimen 37

Figure 2.2 Experimental Test Apparatus 39

Figure 2.3 Cyclic Loading through Applied Flexion-Extension Bending Moments . 40

Figure 2.4 Comparison of Screw Rotation over the Duration of the Test 44

Figure 2.5 Loading Cycles Completed versus Screw Rotation 45

Figure 2.6 Applied Flexion Moment versus Screw Rotation 46

Figure 2.7 Survivability Curve for Screw Designs to Resist Loosening 47

Figure 2.8 Side by Side Comparison of Loosening Developed 48

Figure 3.1 Instron® 8874 Materials Testing Machine 57

Figure 3.2 Custom-designed Loading Arms and Fixturing 59

Figure 3.3 Spinal Loading Simulator 60

Figure 3.4 Marker Blocks and Tracking Beads 63

Figure 3.5 Simulator Orientation for Flexion-Extension Motion Tracking 65
Figure 3.6 Simulator Orientation for Lateral Bending Motion Tracking 66
Figure 3.7 Simulator Orientation for Axial Rotation Motion Tracking 67
Figure 3.8 Three Cycles of Applied Loading 71
Figure 3.9 Experimental Testing Protocol for Simulator Validation 72
Figure 3.10 Frames of Reference for Rotation Matrices 75
Figure 3.11 Typical Rotation Versus Applied Moment Curve 77
Figure 3.12 Hysteresis Curves of Flexion-Extension versus Applied Moment 81
Figure 3.13 Hysteresis Curves of Lateral Bending versus Applied Moment 82
Figure 3.14 Hysteresis Curves of Axial Rotation versus Applied Moment 83
Figure 3.15 Hysteresis Comparison for the Three Applied Moment Levels 84
Figure 3.16 Mean Values for ±ROM and NZ for L1-L4 Motions / Moments 86
Figure 3.17 Mean Values for ±ROM for L1-L2 Segmental Motions / Moments 87
Figure 3.18 Mean Values for ±ROM for L2-L3 Segmental Motions / Moments 88
Figure 3.19 Mean Values for ±ROM for L3-L4 Segmental Motions / Moments 89
Figure 3.20 Comparison of Rotations Achieved at Start and End of Test Protocol 96
Figure B.1 Camera Image from Screw Loosening Study 123
Figure B.2 Camera Images for Segmental Motion 125
Figure C.1 Front Panel from LabVIEW™ Program to Track Screw Loosening 127
Figure C.2 Back Panel from LabVIEW™ Program to Track Screw Loosening 130
Figure C.3 Front Panel from LabVIEW™ Program to Analyze Screw Rotation 131
Figure C.4 Back Panel from LabVIEW™ Program to Analyze Screw Rotation 134
Figure C.5 Front Panel from LabVIEW™ Program to Track Segmental Motion 135

Figure C.6 Back Panel from LabVIEW™ Program to Track Segmental Motion 139

Figure C.7 Front Panel from LabVIEW™ Program to Analyze Spine Motion..... 140

Figure C.8 Front Panel from LabVIEW™ Program to Analyze Spine Motion..... 144

LIST OF APPENDICES

APPENDIX A: Anatomical Glossary 115

APPENDIX B: Tracking Methods for 2D Motion Analysis 120

APPENDIX C: LabVIEW™ Programs for Motion Tracking and Post-hoc Analysis .. 126

APPENDIX D: Detailed Testing Protocol for Screw Loosening Study 145

APPENDIX E: Detailed Testing Protocol for Simulator Validation 149

LIST OF ABBREVIATIONS, SYMBOLS, AND NOMENCLATURE

2D – Two-dimensional

3D – Three-dimensional

ALE – Adjacent-level effects

ANOVA – Analysis of variance

A – Anterior

AR – Axial rotation

B&W – Black and white

BMD – Bone mineral density

cm - Centimeter

C1 – C7 – First to seventh cervical vertebrae

C1 – Atlas, first cervical vertebra

C2 – Axis, second cervical vertebra

DOF – Degree of freedom

EZ – Elastic zone

$\mathbf{F_x}$ – Force along the x-axis (similarly for y and z axes)

FE – Flexion-extension

g - gram

HAM – Helical Axis of Motion

Hz – Hertz

I - Inferior

IEEE – Institute of Electrical and Electronics Engineers

IVD – Intervertebral Disc

K wire – Kirschner wire

L1 – L5 – First to fifth lumbar vertebrae

L5 – S1 – Lumbosacral joint

L - Lateral

LB – Lateral bending

LOS – Line-of-sight

LVDT – Linear variable displacement transducer

LZ – Laxity zone

$\mathbf{M_x}$ – Moment about the x-axis (similarly for y and z axes)

M – Medial

MRI – Magnetic Resonance Imaging

M1 – M4 – Marker blocks 1 to 4

min - Minute

mm - Millimeter

n - Number

N - Newton

Nm – Newton meter

NP – Neutral position

NZ – Neutral zone

P - Posterior

PID – Proportional, integral, and derivative

PSIF – Pedicle screw instrumented fusion

PVC – Polyvinyl chloride

qCT – Quantitative computed tomography

${}^{y}_{x}R$ - Rotation matrix, x with respect to y

ROM – Range of motion

RVDT – Rotational variable displacement transducer

s - Second

SD – Standard deviation

S – Superior

SXGA – Super extended graphics array

S1 – S5 – First to fifth sacral bodies, fused to form sacrum

T1 – T12 – First to twelfth thoracic vertebrae

TZ – Transition zone

UJ – Universal joint

° - Degrees

α – Significance Level

δ – Rotation about the z-axis in Euler angle analysis

^ - Unit vector notation

% - Percentage

% Diff – Percent difference

CHAPTER 1: INTRODUCTION

OVERVIEW: This chapter reviews the background material relevant to this body of work. As such, it provides the basic details of the spinal anatomy and the associated functions, describes the surgical treatment of spinal instability through spine fusion, and highlights the use of laboratory techniques to investigate some of the existing complications for spinal fixation. Due to the clinical aspects of this work, the use of anatomical terms could not be avoided; therefore, a descriptive glossary has been provided in Appendix A.

1.1 THE HUMAN SPINE

1.1.1. Anatomy and Function

The spine is a unique and highly intricate musculoskeletal structure within the human body. Its biomechanical purpose is three-fold: 1) to support the weight of the upper body, 2) to allow physiologic motion of the upper body, and 3) to protect the vitally important spinal cord lying within the centre of the spine from damage (White, III and Panjabi, 1990). These functions are accomplished based on the unique combination of parts working together within the spine: the vertebral bodies, intervertebral discs, synovial joints, and the surrounding muscles and ligaments.

The bony structure of the spine is made up of small, irregular shaped bodies called vertebrae. Similar to other bones within the body, all vertebrae are composed of the same general structure; a hard, compact outer shell of cortical bone surrounding a lighter, spongy cancellous (or trabecular) bone. Starting at the cranial end, there are

seven cervical (*i.e.* C1-C7) vertebrae, twelve thoracic (*i.e.* T1-T12) vertebrae, five lumbar (*i.e.* L1-L5) vertebrae, five fused sacral (*i.e.* S1-S5) vertebrae, and three to four fused coccygeal vertebrae (see White, III and Panjabi, 1990). Together, the vertebrae form the spinal column, which is divided into four main regions based on curvature of the column (Figure 1.1). The lordotic curvature in the cervical and lumbar regions is convex anteriorly, compared to the kyphotic curvature, which is convex posterior, in the thoracic and sacral regions. The size and shape of the vertebrae in each region are reflective of function. For example, as a result of the weight of the torso, a lumbar vertebra at the caudal end of the spine is under significantly more load than a cervical vertebrae, thus it is much larger and more robust.

Excluding the unique anatomy of the Atlas (C1) and Axis (C2), vertebrae in the cervical, thoracic, and lumbar regions similarly consist of two sections: the vertebral body and the vertebral arch (Figure 1.2A) (see White, III and Panjabi, 1990). The body is the large, cylindrical mass of the anterior half of each vertebra. The arch, which contains the spinal canal and functions to protect the spinal cord, forms the posterior portion of each vertebra. It supports seven processes (*i.e.* superior articular (2), inferior articular (2), transverse (2), and spinous (1)) for attachment of muscles and ligaments that induce motion and provide stability to the spine. This motion is guided by the orientation of the facet joints, a set of intervertebral synovial joints formed by the articulation of the inferior and superior articular processes of the cranial and caudal adjacent vertebrae respectively (Figure 1.2B). Connecting the arch to the body are two short, thick sections of bone referred to as pedicles that project posteriorly from the body, one on each side,

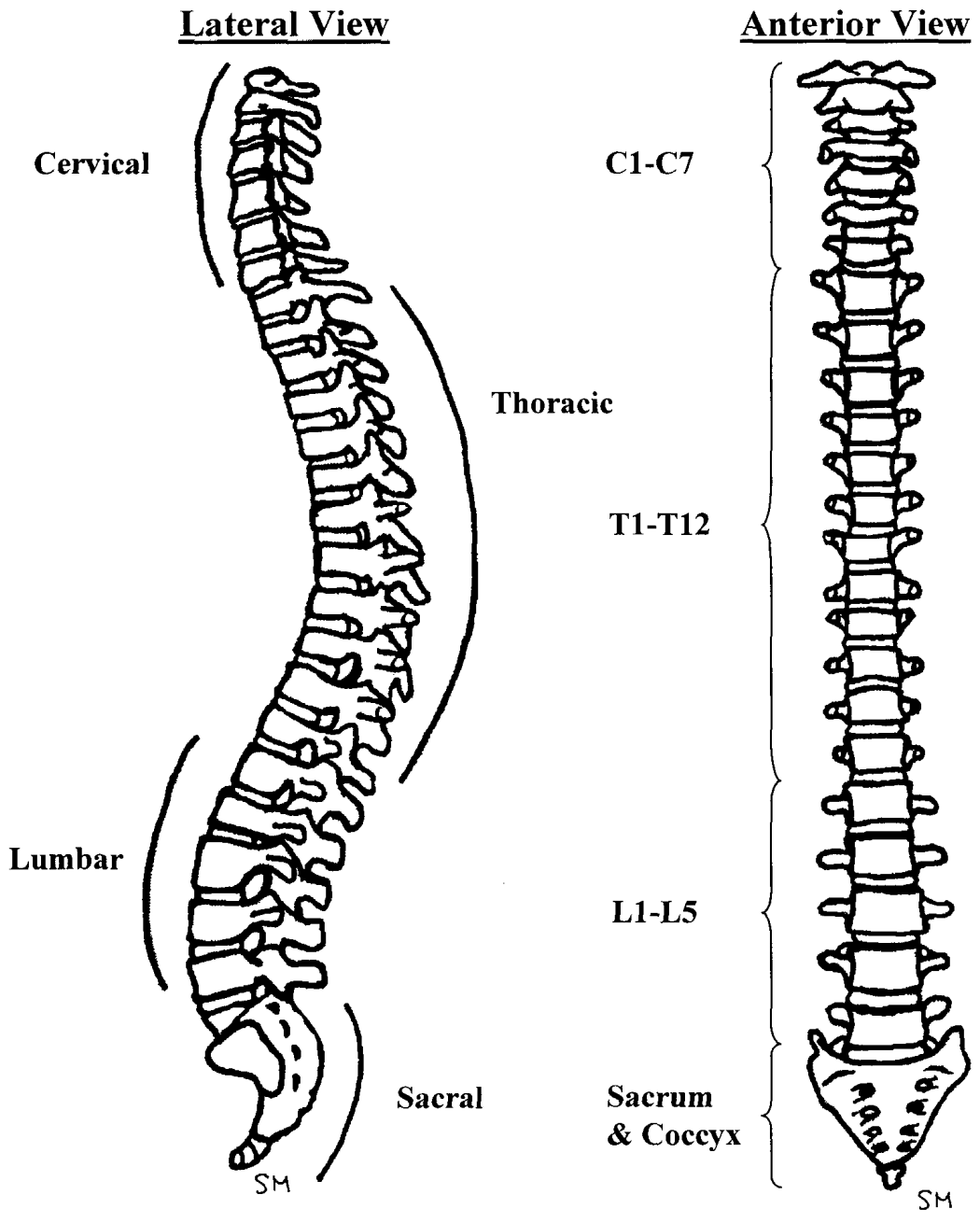

Figure 1.1 **The Human Spine**
In the sagittal plane, as viewed laterally, the anterior-posterior curvature of the human spine is split into 4 unique regions: 1) cervical (C1-C7), 2) thoracic (T1-T12), 3) lumbar (L1-L5), and 4) sacral (sacrum and coccyx). Curvature in the cervical and lumbar spine is lordotic, while the thoracic and sacral regions have kyphotic curvature. From an anterior view, the spine appears straight.

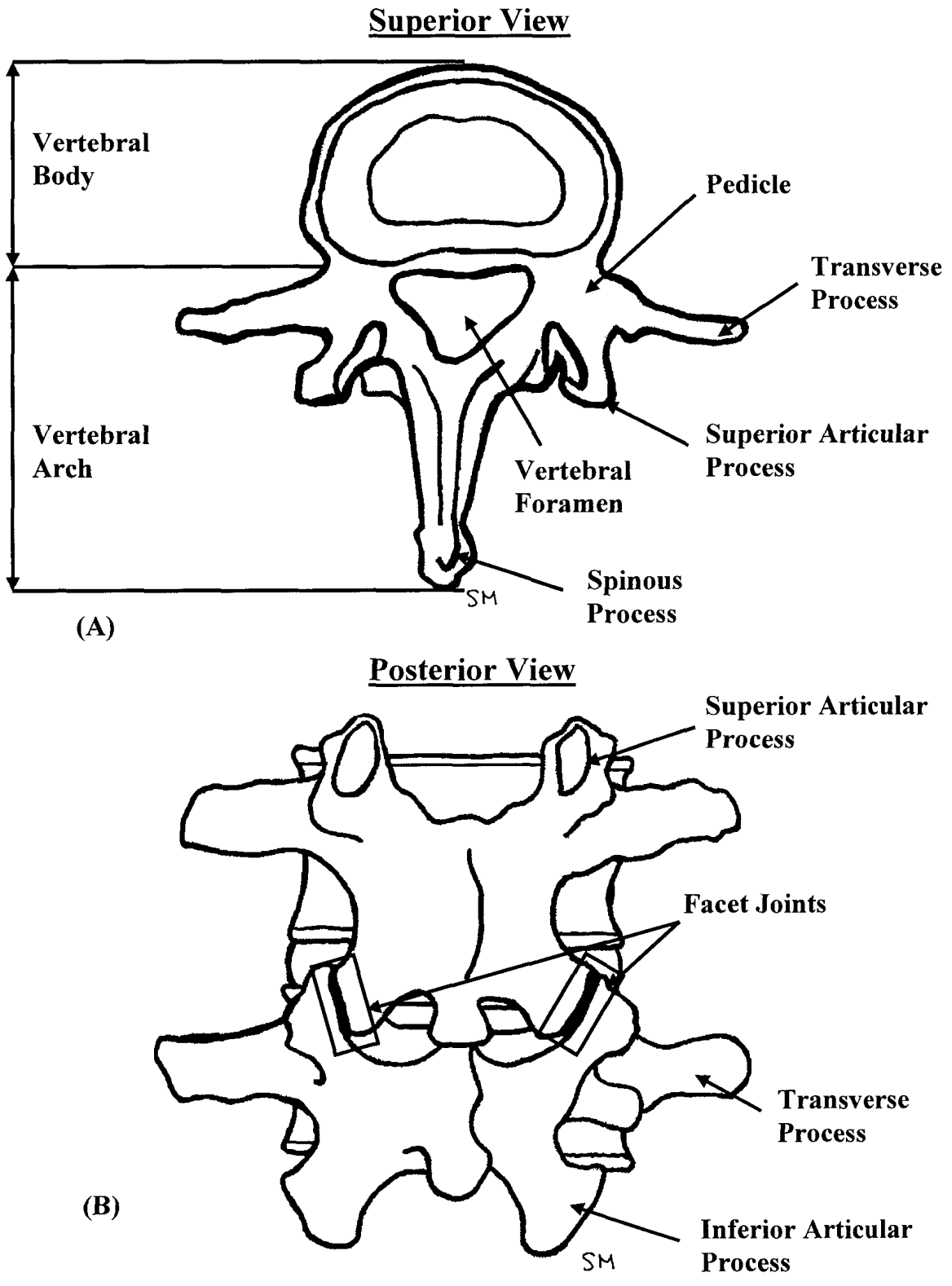

Figure 1.2 **Lumbar Vertebra**
(A) Superior View - The vertebra is split into the body and the arch. The body is the large anterior mass. The arch, positioned posteriorly, is made up by the pedicles and processes, forming the foramen (spinal canal). (B) Posterior View – Facet joints guide the motion of a vertebra against the adjacent vertebrae.

forming the lateral sides of the arch. The posterior arch, including the pedicles, predominately consists of cortical bone.

Different from the similarly-shaped vertebrae in the cervical, thoracic, and lumbar regions, the sacrum is a unique, triangular-shaped vertebra consisting of multiple bodies fused together to form one large bone with its own curvature (see White, III and Panjabi, 1990). The unique geometry of the sacrum contains some of the identifiable features found in other vertebrae, such as pedicles; however, unlike the pedicles in other vertebral segments, those of the sacrum are much larger and consist primarily of cancellous bone. Its unique shape may be a result of function. Residing in the most caudal region of the spine, the sacrum is under the most load of any vertebra and thus is the largest vertebrae in the spine (see White, III and Panjabi, 1990). It interacts with both the lumbar spine (forming the lumbosacral spine) and with the pelvic bone (forming the sacroiliac joints).

Between adjacent vertebral bodies exists a soft tissue known as the intervertebral disc (IVD) (Figure 1.3). This disc characterizes the unique properties of the spine by maintaining alignment, allowing flexibility, and distributing load (see White, III and Panjabi, 1990). The structure of each disc is split into two key components: the annulus fibrosus (a firm, fibrous ring surrounding the periphery of each disc); and the nucleus pulposus (a soft, gelatinous mass contained within the annulus). In their primary roles, the fibrous ring structure of the annulus fibrosus allows for the disc to resist high bending and torsional loads, and the gelantinous mass of the nucleus pulposes acts hydrostatically to store energy to distribute compressive loads (see White, III and Panjabi, 1990). The contrasting properties of each of these components give the disc and the spine its unique abilities of stability and flexibility.

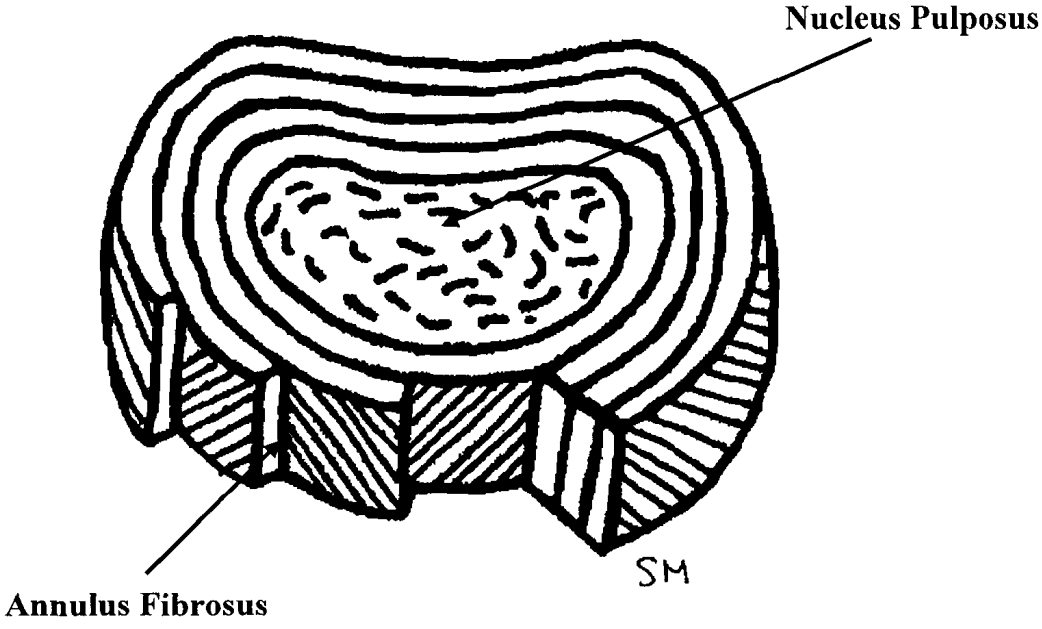

Figure 1.3 **Intervertebral Disc**
The intervertebral disc lies between adjacent vertebrae. The structure of the disc is composed of the Annulus Fibrosus, an outer ring of tough laminates, surrounding a central core of soft, gelantinous material called the Nucleus Pulposus.

Stabilization of the spinal column is accomplished with both passive and active systems working in combination. In addition to the passive stability provided by the vertebral bodies (*i.e.* osseous structures) and IVDs, the ligamentous structures attached to the vertebrae also contribute to the passive stability of a healthy spine (Figure 1.4). The ligaments act to limit the relative motion of the vertebral bodies when placed in tension. The posterior ligaments include the supraspinous and interspinous ligaments as well as the ligamentum flavum. Joining the vertebral bodies are the anterior and posterior longitudinal ligaments. Unlike ligaments, muscles attached to the spinal column provide active stabilization. When "on," they can produce motion in the spine, and add to the overall stability of the spine by compressing adjacent vertebrae together.

1.1.2. Physiologic Motions

One of the critical functions of the spine is to allow physiologic motion of the torso. Movement of the spinal column is best described using the concept of a motion segment. As the smallest unit representing the general mechanical behaviour in a given region of the spine, the motion segment is made up of two adjacent vertebral bodies and their connecting soft tissues (*i.e.* the IVD and ligaments) (Figure 1.5) (see White, III and Panjabi, 1990).

The motion of each segment, while unique, can be defined as a standard six degree-of-freedom system, consisting of three rotations about and three translations along the three-dimensional (3D) coordinate system defined for the human body (*i.e.* sagittal, frontal, and transverse planes) (Figure 1.6) (see Wilke *et al.*, 1998). In a normal spine, the translations of the motion segment are typically small, thus investigations predominately look at rotations. Three standard rotational motions have been defined:

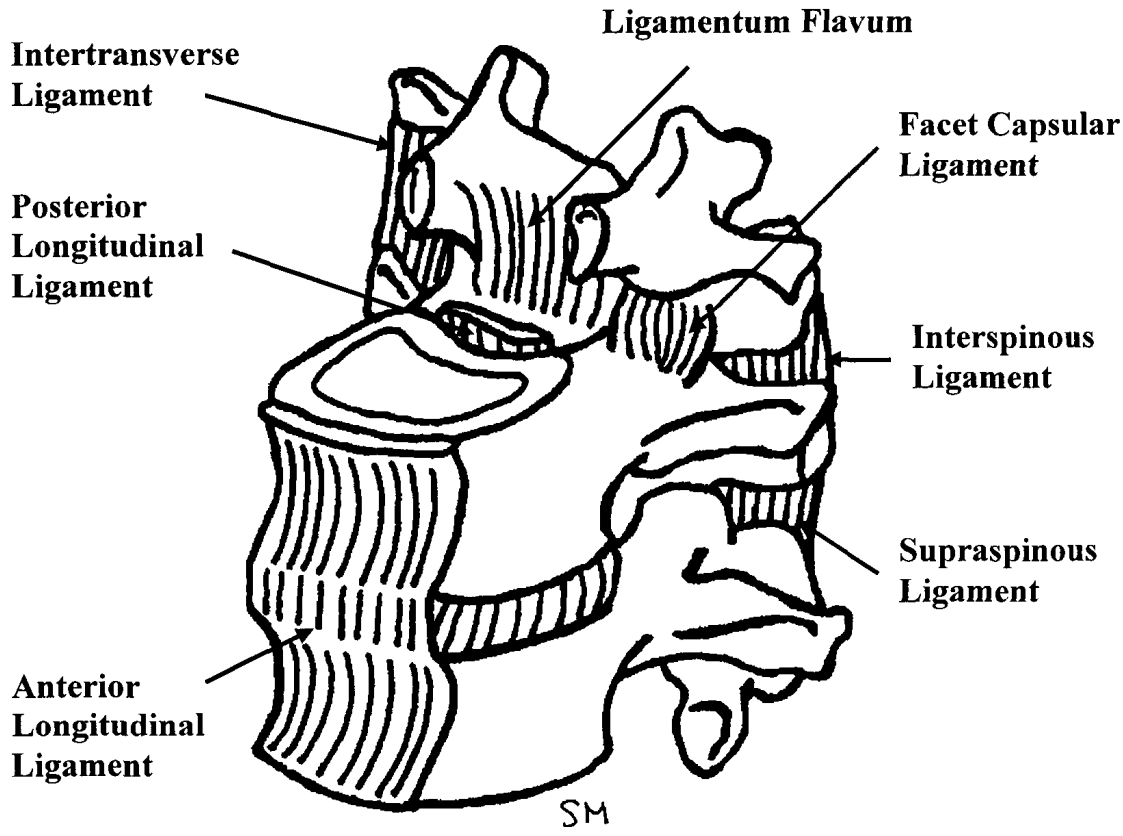

Figure 1.4 **Spinal Ligaments**
The stability of the spine is maintained by its surrounding ligaments, which provide passive support (in addition to the passive support of the osseous structures and active stabilizing influence of muscles).

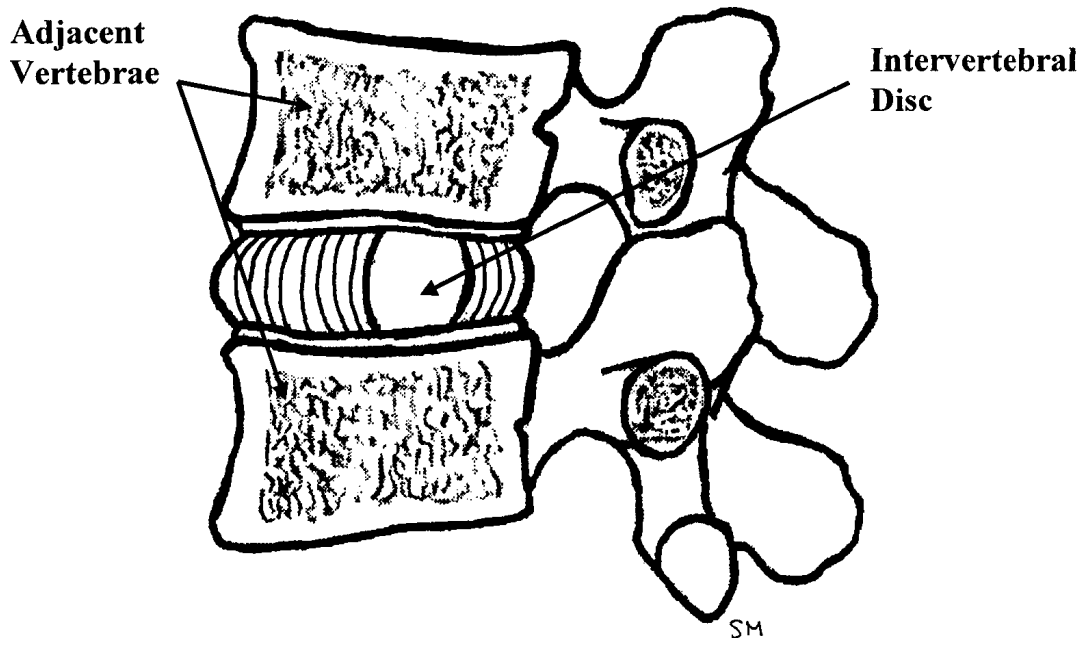

Figure 1.5 Spinal Motion Segment
The motion segment is the smallest unit used to describe motion of the spine. It is consists of two adjacent vertebral bodies, the intervertebral disc, and the connecting ligaments (not shown in the figure).

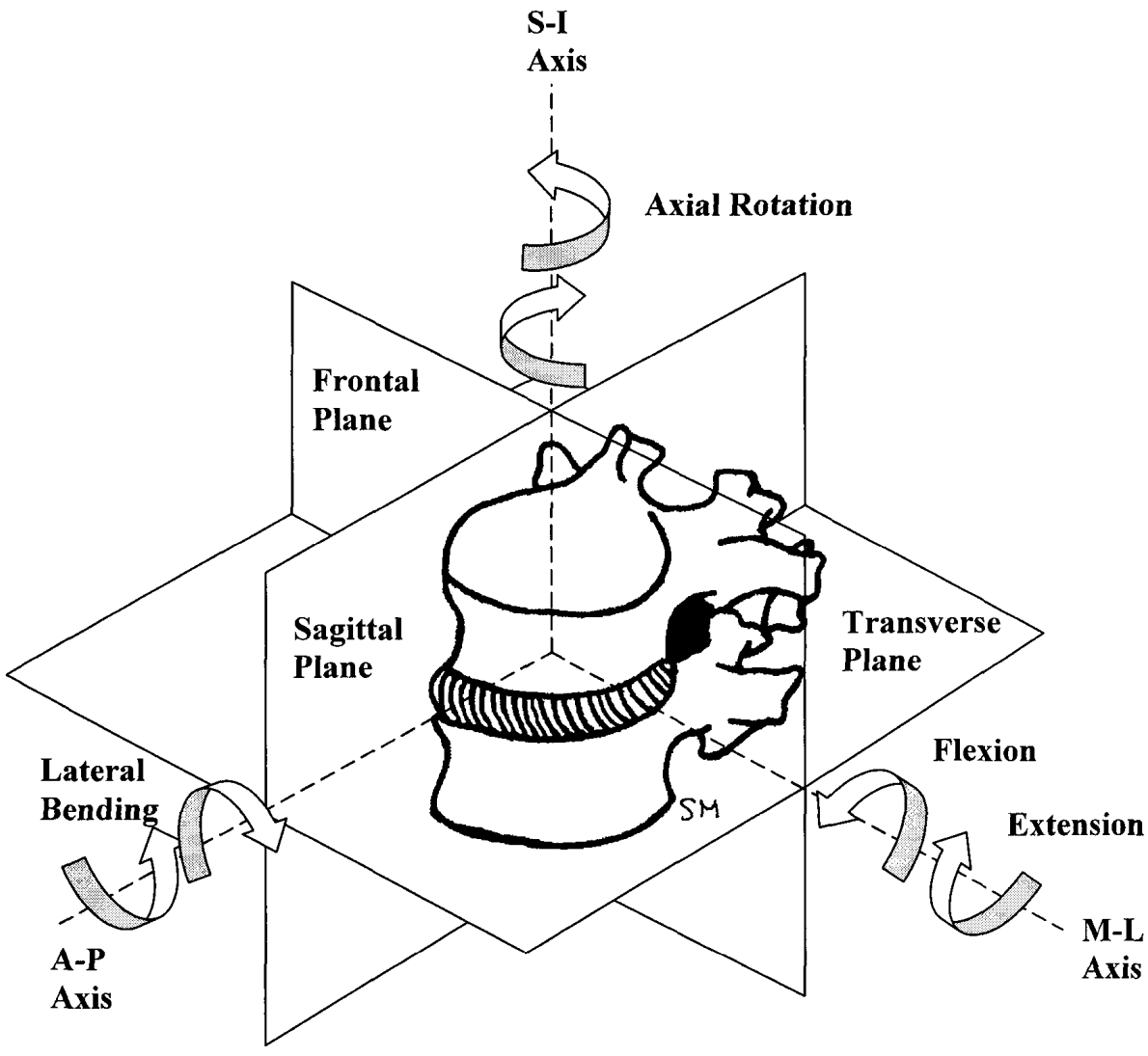

Figure 1.6 **Spinal Motions**
The three physiologic rotations of the spine are Flexion-Extension, Lateral Bending, and Axial Rotation. Flexion-Extension rotates the spine in the sagittal plane about the medial-lateral (M-L) axis; Lateral Bending rotates the motion segment in the frontal plane to left and right sides about the anterior-posterior (A-P) axis; and Axial Rotation, to the left and right, rotates in the transverse plane about the superior-inferior (S-I) axis. Since the motion segment is a six degree-of-freedom system, three translations are also found in the spine in addition to the rotations shown. For clarity purposes, translations have not been included.

flexion-extension, lateral bending, and axial rotation (see White, III and Panjabi, 1990). These motions can occur independently, or in combination to allow for variety of movements. By definition, flexion-extension rotates the spine in the sagittal plane in anterior (flexion) and posterior (extension) directions about the medial-lateral axis; lateral bending rotates the motion segment in the frontal plane to left and right sides about the anterior-posterior axis; and axial rotation, to the left and right, rotates in the transverse plane about the superior-inferior axis.

The overall magnitudes of spinal movement can be defined by several different motion parameters, including range of motion (ROM) and the helical axis of motion (HAM). ROM is defined as the maximum physiologic movement (*i.e.* no plastic deformation) the spine travels through in one loading direction (Panjabi *et al.*, 1975). Thus, there are both a +ROM and a -ROM for each physiologic motion (*i.e.* flexion is +ROM, extension is -ROM) (Figure 1.7A). These values can be considerably different between flexion-extension, lateral bending, and axial rotation depending on the motion segment of interest. While ROM describes the individual measurements of each physiologic motion, the 3D HAM is available to describe the overall motion of the motion segment based on a unique axis about which the segment rotates and parallel to its translation (Panjabi *et al.*, 1981).

In addition to describing overall motion, quantifying the laxity around the spine's neutral position is important for defining the physiologic stability. Two different regions of spinal stiffness are thought to divide the ROM, but accurately describing and defining the boundaries of these regions has proven to be difficult. Thus, numerous parameters have been developed to quantify each region. Early quasi-static studies described the

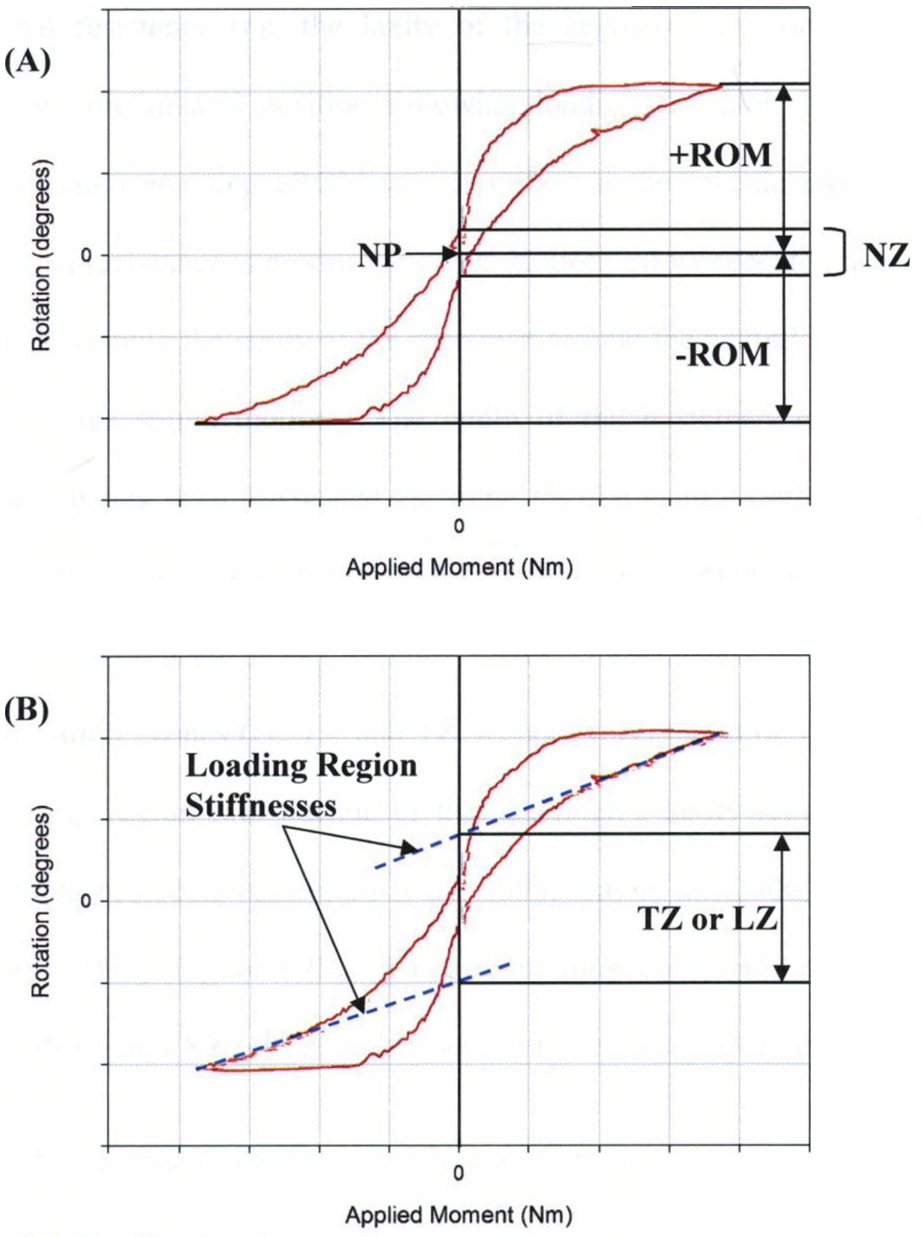

Figure 1.7 **Motion Parameters**

(A) Range of motion (ROM) is the largest physiologic rotation (*i.e.* no plastic deformation) the spine moves through in a specified loading direction (+ROM and -ROM). The neutral zone (NZ) exists as a measure of specimen laxity, shown in the figure as the width of the hysteresis loop at 0 Nm, which is centered about the neutral position (NP). (B) Other definitions have been used to describe specimen laxity based on the stiffness of the loading region. The stiffness is extrapolated back to 0 Nm to define a transition zone (TZ) or laxity zone (LZ) of the specimen, where there is minimal ligamentous resistance. These definitions produce a larger region of specimen laxity compared to the NZ.

"neutral zone" (NZ) as the region of the ±ROM where spine motion is produced with minimal internal resistance (*i.e.* the laxity of the segment), measured as a residual deformation from the neutral position following loading (Panjabi, 1992; Oxland and Panjabi, 1992). The remaining ±ROM was described as the "elastic zone," (EZ) where significant internal resistance is produced against motion. More recently, new parameters have emerged, describing the laxity of the specimen around the neutral position in studies involving continuous spinal motion. The width of the hysteresis loop during cyclic continuous loading has been advocated by some (Wilke *et al.*, 1998; Goertzen *et al.*, 2004). This method describes a "dynamic" NZ, similar to the traditional quasi-static NZ, and is often still referenced as NZ (Figure 1.7A). Others have attempted to define "laxity" or "transition" zones (*i.e.* LZ and TZ, respectively) based on the stiffness of the specimen's loading region (*i.e.* outside of the specimen's laxity region), using cyclic, continuous loading protocols (Crawford *et al.*, 1998; Gay *et al.*, 2006; Gay *et al.*, 2008; Thompson *et al.*, 2003) (Figure 1.7B). To date, the most commonly reported kinematic measures are ± ROM and NZ (either quasi-static or hysteresis loop width).

1.1.2.1.Lumbar & Lumbosacral Spinal Motions

Motion in the lumbar and lumbosacral portions of the spine is of particular interest in this thesis. Guided by the orientation of the facet joints, healthy vertebrae in the lumbar and lumbosacral regions move through a larger range of motion in flexion and extension than any other vertebral motion segments in the spine (White, III and Panjabi, 1978). The facet joints allow adjacent segments to easily rotate through flexion-extension motion, but their geometry and positioning against one another restricts the amount of lateral bend and axial rotation available in these segments (Figure 1.8).

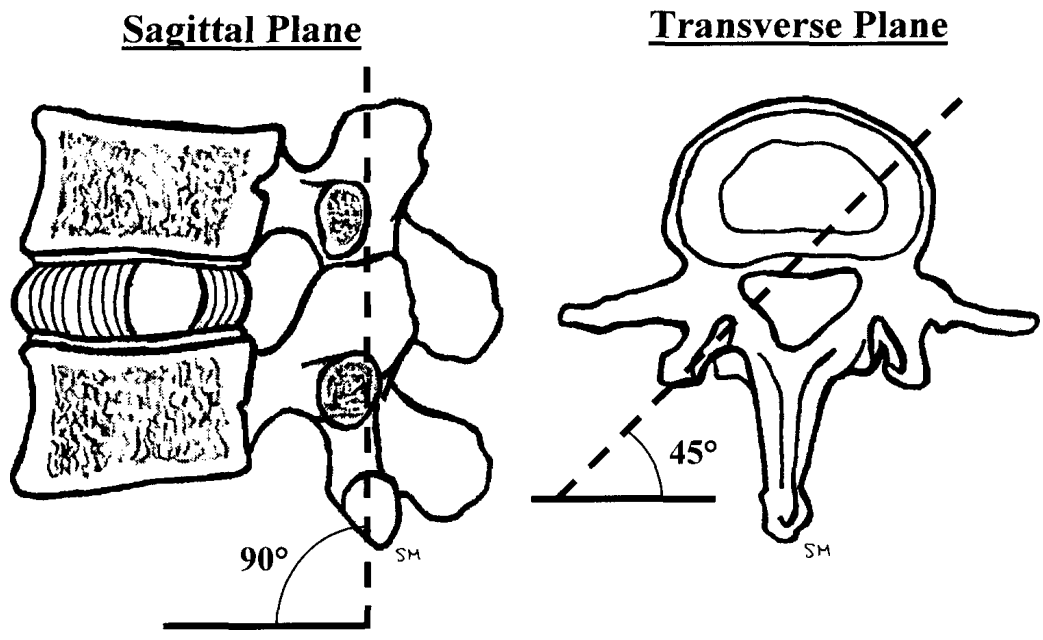

Figure 1.8 **Facet Joint Orientations in the Lumbar Spine**
The orientation of the facet joints in the lumbar spine is at 90° in the sagittal plane to permit a large range of motion in flexion-extension. In the transverse plane, facet joints are oriented at 45°, which reduces the amount of lateral bending range available compared to flexion-extension. In both planes, facet joints permit very little range of motion in axial rotation of the lumbar vertebrae.

Previously reported values for the normal ranges of motion of the lumbar spine are provided in Table 1.1. As the vertebrae in the lumbar and lumbosacral regions are also under more load than any other section, the large range of motion available in flexion and extension may lead to a prevalence of injury in the lower back (White, III and Panjabi, 1990).

1.1.3. Instability and Pathologic Motion

Low back pain affects approximately 8 in 10 people at some point in their life (McKinnon *et al.*, 1997; Andersson, 1999). Severity of the pain can range from a minor annoyance to a serious debilitating injury. Low back pain can result from repeated cyclic motions (*i.e.* a job task involving picking up objects off the ground), or from degenerative, traumatic, or deformity pathologies that may become chronic and severe (Figure 1.9).

Instability of the spinal motion segments is a common source of pain for the low back. White, III and Panjabi (1990) define the spine as being clinically unstable if, under physiological loads, there are changes in the patterns of motion (*i.e.* altered ROM and/or NZ) which may result in neurologic deficit, excessive deformity and/or pain, acutely or with time. Due to this pain and instability, physiologic motions may become limited or altogether impossible. The altered motion is referred to as pathologic motion, and causes a detrimental effect on a person's ability to perform normal daily activities.

			Flexion-Extension					Lateral Bending (Left-Right)					Axial Rotation (Left-Right)				
Author (Date)	Applied Moment	Loading Protocol	L1-L2	L2-L3	L3-L4	L4-L5	L5-S1	L1-L2	L2-L3	L3-L4	L4-L5	L5-S1	L1-L2	L2-L3	L3-L4	L4-L5	L5-S1
Panjabi (1994)	7.5 Nm	QS	5-4	7-3	7-2	8-3	9-5	4-4	5-5	5-5	5-5	4-4	1-1.5	1.5-1.5	1.5-2	0.5-1	0.5-0.5
Yamamoto (1989)	10 Nm	QS	10.7	10.8	11.2	14.5	17.8	4.9	7	5.7	5.7	5.5	2.1	2.6	2.6	2.2	1.3
White and Panjabi (1978)	No Data	QS	12	14	15	17	20	6	6	8	6	3	2	2	2	2	5
Pearcy (1984a,b)	*In vivo*	N/A	13	14	13	16	14	5.5	5.5	5	2.5	1	1	1	1.5	1.5	0.5

Table 1.1 **Literature Review of Segmental ROM in the Lumbar Spine**
Data were compiled from previous literature for segmental motion in the lumbar spine for L1-S1 specimens. The source is shown with the applied moment (AM) used to achieve the segmental rotations at each level. Data are either provided as the total motion achieved (one #), the motion achieved for each loading direction (#-#), or as the one-sided motion achieved (# *). The loading protocol (LP) to quantify this motion is also shown, C being "continuous" loading and QS being "quasi-static". It should be noted that White and Panjabi (1978) compiled their data from previous literature and general knowledge of the lumbar spine, with no applied moment given.

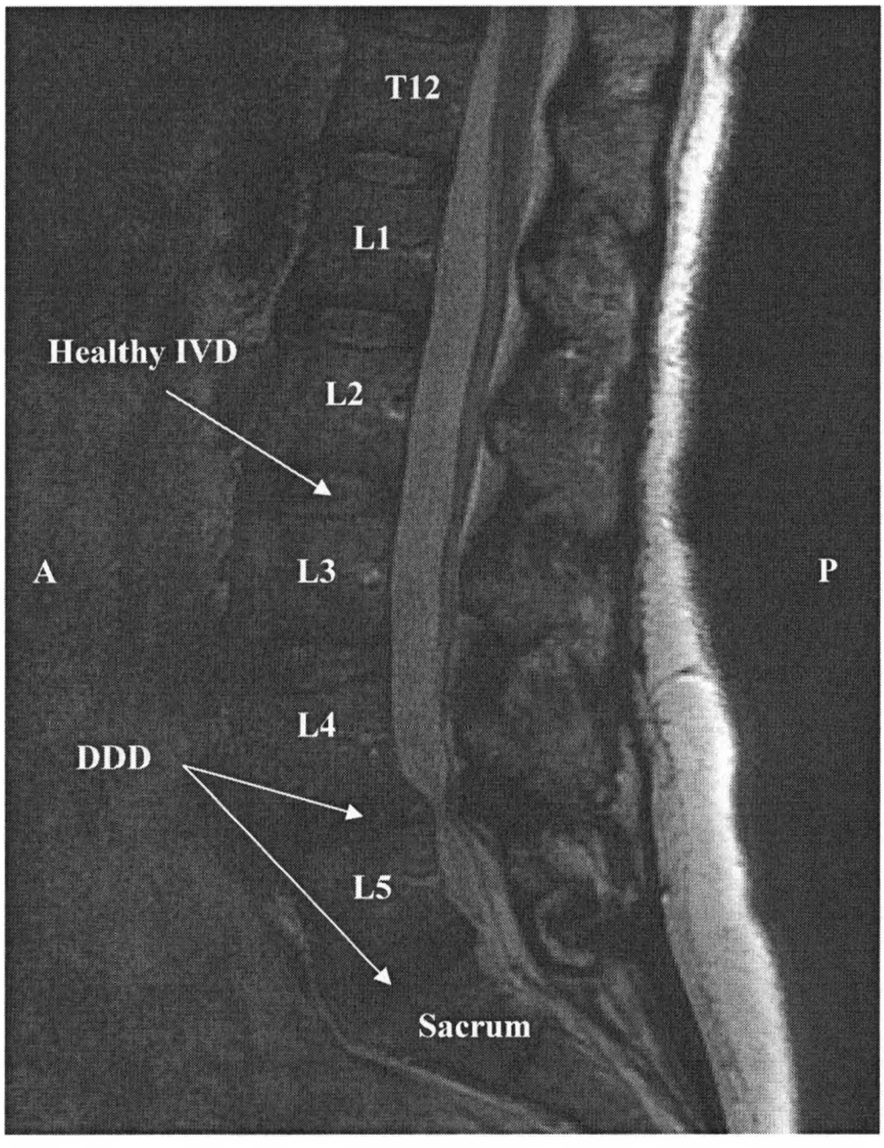

Figure 1.9 **Degenerative Disc Disease at the L4-L5 and L5-S1 levels**
Chronic lumbar spine pathologies such as degenerative disc disease (DDD) can have a drastic effect on a person's ability to achieve a normal lifestyle. Surgical treatment of these conditions is often required to reduce low back pain. The figure, an MRI taken from a lateral perspective (anterior (A) to the left, posterior (P) to the right), shows L4-L5 and L5-S1 degenerative disc disease (the dark discs are consistent with this diagnosis). As a result of DDD, L4-L5 Grade 1 degenerative spondylolisthesis (posterior shift of L5) is apparent.

1.2 SURGICAL TREATMENT OF INSTABILITY THROUGH LUMBOSACRAL FUSION

To treat spinal instability, surgical treatment is often required. Spinal fusion, or arthrodesis, is the most important and frequently used surgical procedure in the spine (White, III and Panjabi, 1990). The goal of this procedure is to achieve bone-to-bone fusion between adjacent vertebrae (*i.e.* the motion segment) to eliminate segmental instability, which can help alleviate the associated pain. Previous literature has shown that spinal fusion can be more effective at relieving chronic low back pain than other more conservative methods (Fritzell *et al.*, 2001).

The popularity of the procedure is a result of its wide variety of applications. As follows, White, III and Panjabi (1990) outlined numerous pathologies treatable using spinal fusion. It has been shown to improve clinical instability, when the structural integrity of the spine has been severely weakened through trauma, tumour, or infection. Maintaining correction is made possible using spinal fusion, following mechanical straightening of the spine in scoliosis or kyphosis, or following osteotomy of the spine. Furthermore, fusion can prevent progression of spinal deformities (*e.g.* scoliosis, kyphosis, or spondylisthesis). Finally, it can help alleviate or eliminate pain by stiffening a region of the spine (*e.g.* diminishing movement between adjacent motion segments).

A variety of methods exist to create fusion in the lumbar spine. Prior to the use of instrumentation, orthopaedic spine surgeons first look to perform *in situ* fusions, where bone graft is laid down between the decorticated transverse processes of the target vertebral level. Over time, bone growth, from the adjacent vertebrae, into this new bone

fuses the segments together, eliminating the segmental pathology. This technique is still used in the pediatric population and in some adult situations. However, fusion is more likely to occur if segmental motion is prevented through stabilization of the motion segment with the use of instrumentation (*i.e.* screw and rod, see Section 1.2.1). This instrumentation is meant as an adjunct to the bone grafting.

1.1.4. Pedicle Screw Instrumented Fusion (PSIF)

Many instrumentation techniques are available depending on the type of fusion required, but a common option and one focus of this thesis is the pedicle screw instrumented fusion. First performed by Cotrel and Dubousset in the 1980's, pedicle screw instrumentation systems fix the adjacent segments in position with connecting rods attached to screws inserted posteriorly into the pedicles, the strongest part of the vertebral anatomy. (Figure 1.10) (Cotrel and Dubousset, 1984; Sidhu and Herkowitz, 1997). This technique is often used in the lumbosacral region, fusing together multiple segments of lumbar vertebrae with the sacrum. Since the required bone growth for fusion takes several months to occur, the screw systems must maintain stability of the instrumented vertebrae throughout this period. This can difficult in the lumbosacral section of the spine where there are highly repetitive motions combined with large applied loads.

Regarding the pedicle screw itself, numerous designs are available. Solid screws are the standard screw type used in this surgery, but a variety of other screw designs have been evaluated in the past with varying success. To accommodate the varying sizes of the vertebrae, screws come in a variety of lengths and diameters, to achieve the ideal

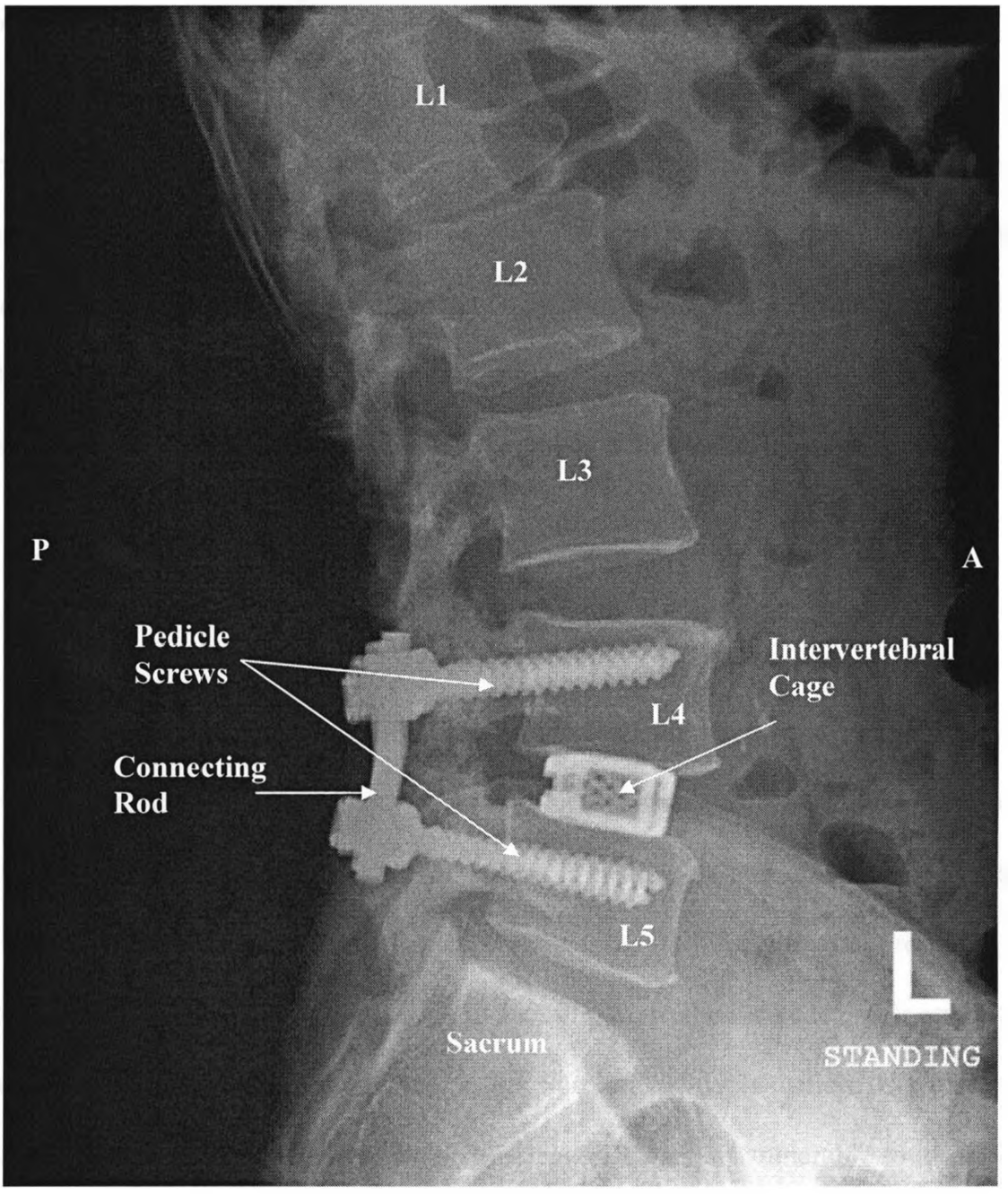

Figure 1.10 Pedicle Screw Instrumented Fusion at L4-L5
Pedicle screw instrumented fusion is a surgical treatment used to assist bone-to-bone fusion at the targeted motion segment. Screws are inserted posteriorly through the left and right pedicles of adjacent vertebrae and connected by metal rods. This effectively eliminates motion at that segment to improve stability. This lateral view of a lumbar spine x-ray shows pedicle screws inserted into the fourth and fifth lumbar (L4, L5) and connected by a metal rod. An intervertebral cage is used to replace the intervertebral disc to correct for the loss of height.

fixation. The diameter of the screw is more important than length, as the majority of screw purchase occurs within the pedicle itself and not the trabecula of the vertebral body (Zindrick *et al.*, 1986). However, screws can also be chosen for cortical purchase, monocortical or bicortical, where bicortical screws would gain cortical fixation from the pedicle but also from the cortical shell in the anterior aspect of the vertebral body (Luk *et al.*, 2005). With numerous hardware options available, the choice is often dependent on the surgical procedure required, as well as the opinion and experience of the surgeon.

1.2.2 Complications of PSIF

1.2.2.1 Instrumentation Failure

While PSIF aims to reduce instability and associated back pain, instrumentation "failure" cannot always be avoided, often leading to pseudoarthodesis (failure of the fusion to take place). One such mode of failure is pedicle screw loosening within the bone, with associated loss of stability at the bone-screw interface, ultimately resulting in failure to obtain fusion. This complication is due, in part, to the increased stiffness of the pedicle screw instrumentation compared to the vertebral body in which it is inserted. Particularly in the case of cancellous bone, this leaves the screw vulnerable to loosening as the large cyclic loads placed upon the pedicle screws "crush" the surrounding bone structure (Zindrick *et al.*, 1986).

High failure rates have been reported for longer lumbar constructs terminating at the sacrum due to inadequate fixation strength at the pedicle screw-bone interface in the early post-operative period (Lebwohl *et al.*, 2002). This may be attributed to the anatomical differences between the sacral pedicles and those of the lumbar spine, where

the majority of screw purchase occurs in cancellous bone for the sacrum as opposed to cortical bone in other vertebral pedicles. New screw designs and surgical techniques are necessary to improve fixation in the sacrum.

1.2.2.2 Adjacent Level Effects

The rigidity of instrumented fusion can lead to additional problems. As aforementioned, physiologic segmental motions are not independent, thus if the motion of a segment is eliminated through spinal fusion, the motion of the adjacent unfused segments may be affected. These adjacent segments will be subjected to additional stresses (due to stress concentrations) and increased motion (from motion re-distribution), as a result of adaptive changes (Panjabi, 2007). This concept is referred to as "adjacent-level effects" (ALE). The alteration in motion has been clinically shown to accelerate degeneration and other adverse effects in these adjacent segments (Lee, 1988; Schlegel *et al.*, 1996). To reduce or eliminate the effects of ALE, dynamic stabilization devices are entering the market, based on the concept of reducing instability of the motion segment without rigid fusion (Niosi *et al.*, 2006; Schmoelz *et al.*, 2003).

1.3 LABORATORY INVESTIGATIONS OF SPINAL FIXATION AND MOTION

While PSIF remains widely used, clinicians would ultimately like to reduce the incidence of the associated complications. Thus, new spinal fusion-related devices are entering the market to counteract these effects. Evaluating the benefits of these devices prior to their *in vivo* application requires dedicated *in vitro* laboratory studies for biomechanical validation. With numerous laboratories conducting simultaneous

research, a standardized testing procedure (*i.e.* applied loads, loading rate, specimen preparation) has been proposed for all *in vitro* spinal testing (Wilke *et al.*, 1998).

1.3.1 Pedicle Screw Fixation

Numerous *in vitro* investigations have been conducted to evaluate fixation of pedicle screws. Previous literature examining fixation at the screw-bone interface in lumbosacral vertebrae has typically been performed using pullout strength as the failure criterion (Luk *et al.*, 2005; Zhu *et al.*, 2000; Carlson *et al.*, 1992; Panjabi, 1992; Zindrick *et al.*, 1986; Zdeblick *et al.*, 1993). While the pullout strength method provides a comparable reference for fixation capabilities, screw pullout is not a typical clinical failure method. Clinically, the high incidence of screw failure due to loosening has been associated with cyclic loading (Esses *et al.*, 1993).

Some of the experimental loading protocols to test pedicle screw fixation have involved the application of cyclic cranial-caudal load directly to the screw head, and perpendicular to the screw axis (Law *et al.*, 1993; Zindrick *et al.*, 1986). In these models, loosening generally involves "teeter-tottering" of the screw, with the outer cortex acting as a fulcrum along the proximal shaft of the screw and the trabecular bone around the distal part of the screw being "swept away" (Zindrick *et al.*, 1986). A similar mode of failure occurs when loads are applied parallel to the screw, but through a connecting rod attached to the screw head (Zdeblick *et al.*, 1993). Applying these loads at a fixed distance from the screw creates flexion-extension bending moments on the screw to produce loosening.

Few studies have specifically examined the fixation of pedicle screws in the sacrum under cyclic loading (Zhu *et al.*, 2000; Lu *et al.*, 2000; Luk *et al.*, 2005; Zindrick

et al., 1986). These studies have tended to employ non-destructive cyclic testing methods followed by axial pullout to test fixation of pedicle screws for various parameters.

1.3.2 Spinal Loading Simulators

In addition to evaluating fixation in a single pedicle, *in vitro* biomechanical investigations have also proven to be effective in evaluating the stabilizing effects of spinal fixation devices in a multi-segment spine specimen. These studies are accomplished through the use of a spinal loading simulator - a test apparatus in which spinal specimens can be mounted and tested under defined loading conditions (Wilke *et al.*, 1998). Use of a spinal loading simulator allows for evaluation and comparison between different spinal constructs (*i.e.* intact, injured, instrumented, etc.) (Adams, 1995).

The principles behind spinal loading simulators are the flexibility methods developed by Goel *et al.* (1987) and Panjabi (1988). Rather than a displacement-based input, the flexibility method uses a load-input protocol, where a known pure bending moment is applied to the multi-segment specimen and at the same time allowing for unconstrained, natural spinal motion. The pure moment is applied to produce one of the three physiologic motions (*i.e.* flexion-extension, lateral bending, and axial rotation), allowing for unconstrained motion in the other two free motions (*i.e.* if applying a flexion-extension moment, the spine should be able to freely move in lateral bend or axial rotation) (Panjabi, 1988). This procedure is repeated for each of flexion-extension, lateral bending, and axial rotation, using the same magnitude of applied moment in all cases. Post-hoc evaluation of the load-displacement curves reveals the segmental motion

based on parameters of range of motion and neutral zone, both measures of spinal stability (Oxland and Panjabi, 1992).

The earliest simulators used systems of pulleys, in combination with manually added dead weights or pneumatic actuators set up in a force couple, to apply a pure moment input on the spine (Panjabi *et al.*, 1981; Goel *et al.*, 1984). Step-wise loading patterns (quasi-static) were used to achieve repeatable physiologic motions, and to calculate the initial data for segmental ranges of motion and neutral zone (using residual deformation methods, see Section 1.1.2). Simulator development has now evolved to the use of continuous loading machines, versus the traditional step-wise methods (Goertzen *et al.*, 2004). These have become the standard testing apparatus, as they provide a better representation of physiologic motion. Customized to fit the needs of each individual laboratory, continuous loading spinal loading simulators can be built as a stand alone device or as a modification to an existing materials testing machine, as detailed in Sections 1.3.2.1 and 1.3.2.2.

1.3.2.1 Stand Alone Devices

To produce accurate *in vitro* representation of physiologic spinal motions, the majority of biomechanical research laboratories have built their spinal loading simulators as stand alone devices. Various continuous loading design approaches have been employed. In a similar approach to the early step-wise designs, continuous loading simulators have been developed using pulleys and cables in combination with linear actuators and motors (Lysack *et al.*, 2000). This traditional design is still quite effective and the use of a linear motor allows for transmission of continuous motion to the specimen; however, pulley and cable systems are hindered by having to reconfigure

either the machine or specimen between motions (*i.e.* modifications are required when changing from flexion-extension to lateral bending). A different approach that has been successfully applied is to suspend motors (servo or stepper) orthogonally above the specimen, where a specially designed gimbal joint and use of XYZ slides allows the motors to follow the natural motion of the specimen (Wilke *et al.*, 1994; Gedet *et al.*, 2007; Gay *et al.*, 2006). Compared to the pulley and cable systems, this technique is advantageous since different physiologic motions can be applied without reconfiguring the specimen within the apparatus; however, a complex control system is necessary. Motors have also been used in combination with linear bearings and universal joints in a setup by Goertzen *et al.* (2004), where the three physiologic motions were achieved by manually rotating the position of the aluminum frame containing the motor to three defined positions.

1.3.2.2 Modified Materials Testing Machines

Spinal loading simulators can be built as a modification to an existing servohydraulic materials testing machine. This can be an advantage in labs where space is an issue (*i.e.* there is no room for a standalone device), and a materials testing machine is available. Callaghan and McGill (2001) designed a custom jig that attached to their Instron® servo-hydraulic dynamic testing machine (Instron, Norwood, MA, USA) to apply loads to single spinal motion segment. The jig allowed the application of axial loads to the specimen using the Instron® actuator, while creating flexion-extension bending moments through a connecting servo motor attached to the jig with universal joints. This modified materials testing machine setup has been used in a variety of

research projects, including one looking at the effects of combined loading modes (*i.e.* compression with torsion) (Drake *et al.*, 2005).

In addition to single-segment motion, materials testing machines have also been modified to create multi-segment spinal motion. Crawford *et al.* (1995) used the actuator of their MTS® testing machine (MTS Systems Corp., Eden Prairie, MN, USA) in combination with the traditional pulley and cable system setup to apply a pure bending moment to a multi-segment spine. This simulator can only apply one physiologic motion at a time, and requires reconfiguration of the specimen to apply other motions, as is true for most simulators of this type.

Spinal loading simulators capable of applying more than one motion at a time in a multi-segment spine have also been developed. In a similar setup to the stand alone device of Wilke *et al.* (1994), where three orthogonal motors were suspended above the specimen in a gimbal design to apply physiologic pure bending moment, Cunningham *et al.* (2003) designed a six degree-of-freedom spine simulator using stepper motors in a gimbal connected to the actuator of their uni-axial MTS® testing machine. This allowed them to produce unconstrained translation of the specimen under an applied bending moment, using the linear actuator in the *y*-axis, combined with two linear bearing rails for the *x* and *z* axes.

1.3.2.3 Associated Motion Measurement Tools

Regardless of the type of loading apparatus used, the outcome measure of interest with these "spine simulators" is spinal motion; therefore, measurement tools are required to quantify spinal kinematics. As simulator development has evolved, numerous measurement techniques have been used to assess segmental motion. Historically,

electro-mechanical methods and stereovision have been employed (Panjabi *et al.*, 1981). In brief, electro-mechanical devices use transducers attached to the object of interest to determine displacement, either for translations or rotations. Placing the transducer directly on the object of interest may not always be possible, especially in the multi-segmented spine. Thus, non-contact measurement techniques, such as stereovision, may be more advantageous. This involves the use of two or more cameras to collect the position of a marker in space relative to a fixed frame of reference. More recently, many marker tracking techniques are available including electro-magnetic, ultrasound, and optical technologies. These methods are valuable in the spine, where markers are attached to different vertebrae. Combined with the kinematic principles of rigid body motion, analyzing translations and rotations of one vertebra relative to another is possible using these devices.

With respect to spinal loading simulators, optical tracking systems are most commonly used to determine segmental motion as they are generally best suited to this type of testing environment (*i.e.* electro-magnetic tracking methods may be affected by the large metal components in either a standalone or modified apparatus). Commercial devices are available for optical tracking, with the Optotrak Certus™ (NDI, Waterloo, ON, Canada) being the most widely used device. However, these "off-the-shelf" devices tend to be very expensive; thus, custom-built devices can be a more cost-effective option. Using the same principles of stereovision, custom-built devices can be created through use of individual camera systems combined with custom-written video analysis programs to determine the rigid body kinematics of the tracking markers.

1.4 STUDY RATIONALE

1.4.1 Pedicle Screw Loosening in the Sacrum

To reduce the incidence of pedicle screw loosening complications related to instrumented fusion extending to the sacrum, dedicated laboratory investigations are needed. To have clinical relevance, these *in vitro* studies must create loosening of the pedicle screw within the cadaveric sacra in a similar manner to that encountered *in vivo* (*i.e.* through cyclic loading). Thus, a relevant cyclic loading protocol should be developed that can effectively create screw loosening within the sacral pedicle in a clinically reasonable number of cycles. Moreover, a system to track the real-time loosening of the screw should be developed to suggest at what number of cycles and applied load the screw becomes grossly loose, rather than waiting to achieve complete screw pullout.

With an appropriate testing protocol established, new options for pedicle screw designs can be assessed, using relevant cyclic loading protocols and accurate tools to track screw loosening. One new design of interest is a hollow screw, designed to achieve improved fixation in cancellous bone, such as that found in the first sacral pedicle. Therefore, application of this screw to lumbosacral fusion may be advantageous. However, before using this clinically, it is important to conduct an *in vitro* comparison to the current gold-standard solid screw.

1.4.2 Development of a new Spinal Loading Simulator

The development of a new device capable of moving a multi-segment cadaveric spine in a physiological manner will be an important tool, allowing future studies to test

various orthopaedic spinal procedures and instrumentation. This would include the assessment of ALE encountered following intervention through instrumented spinal fusion. Thus, the ability to also quantify motion at the segments above and below the fusion is important. To determine the spinal motions created, an optical tracking system is required to measure kinematic motion parameters, such as ROM and NZ. Once the spinal loading simulator is established, it may eventually be used for future studies such as assessing the effects of ALE on the segmental motion of the spine, potentially leading to an improvement in clinical patient care through use of new dynamic stabilization devices.

1.5 OBJECTIVES AND HYPOTHESES

The specific objectives of this study are as follows:

1. To design an *in vitro* testing method, including appropriate loading protocols and motion measurement tools, for quantifying loosening of a novel hollow screw design versus the current standard solid screw in a cadaveric sacral model; and
2. To design and develop an *in vitro* spinal loading simulator (based on modifications to a materials testing machine) capable of producing unconstrained, physiologic spine motions, and to track the planar motion achieved using customized 2D optical methods to quantify ROM and NZ.

The hypotheses of this investigation were:

1. An *in vitro* cyclic loading protocol producing clinically-relevant screw loosening is possible;

2. The novel hollow screw would provide greater resistance to screw loosening in the cancellous bone of the sacrum compared to the solid pedicle screw;
3. A modified materials testing could be used to independently produce flexion-extension, lateral bending, and axial rotation in a multi-segment (L1-L4) *in vitro* spine at various user-selected applied moment levels;
4. The spinal loading simulator and associated motion measurement tools could produce and quantify these motions in a repeatable and reproducible manner.

1.6 THESIS OVERVIEW

This thesis explores the design and development of tools to assess fixation and motion in the human spine. Chapter 2 details a comparison study performed to examine the fixation of a novel hollow screw design versus the conventional solid pedicle screw design under cyclic loading. Chapter 3 details the development of a spinal loading simulator and motion measurement tools to create and quantify physiologic spine motions in an *in vitro* setting through the use of a modified materials testing machine, as well as a validation study performed to assess the repeatability and reproducibility of the apparatus. Chapter 4 describes the conclusions of the research, some strengths and limitations of the studies performed, possible future directions, and the clinical relevance of this body of work.

1.7 REFERENCES

Adams,M.A. (1995) Mechanical testing of the spine. An appraisal of methodology, results, and conclusions. *Spine* **20,** 2151-2156.

Andersson,G.B. (1999) Epidemiological features of chronic low-back pain. *Lancet* **354,** 581-585.

Carlson,G.D., Abitbol,J.J., Anderson,D.R., Krag,M.H., Kostuik,J.P., Woo,S.L., and Garfin,S.R. (1992) Screw fixation in the human sacrum. An in vitro study of the biomechanics of fixation. *Spine* **17,** S196-S203.

Cotrel,Y. and Dubousset,J. (1984) [A new technic for segmental spinal osteosynthesis using the posterior approach]. *Rev.Chir Orthop.Reparatrice Appar.Mot.* **70,** 489-494.

Crawford,N.R., Peles,J.D., and Dickman,C.A. (1998) The spinal lax zone and neutral zone: measurement techniques and parameter comparisons. *J.Spinal Disord.* **11,** 416-429.

Drake,J.D., Aultman,C.D., McGill,S.M., and Callaghan,J.P. (2005) The influence of static axial torque in combined loading on intervertebral joint failure mechanics using a porcine model. *Clin.Biomech.(Bristol., Avon.)* **20,** 1038-1045.

Esses,S.I., Sachs,B.L., and Dreyzin,V. (1993) Complications associated with the technique of pedicle screw fixation. A selected survey of ABS members. *Spine* **18,** 2231-2238.

Fritzell,P., Hagg,O., Wessberg,P., and Nordwall,A. (2001) 2001 Volvo Award Winner in Clinical Studies: Lumbar fusion versus nonsurgical treatment for chronic low back pain: a multicenter randomized controlled trial from the Swedish Lumbar Spine Study Group. *Spine* **26,** 2521-2532.

Gay,R.E., Ilharreborde,B., Zhao,K., Boumediene,E., and An,K.N. (2008) The effect of loading rate and degeneration on neutral region motion in human cadaveric lumbar motion segments. *Clin.Biomech.(Bristol., Avon.)* **23,** 1-7.

Gay,R.E., Ilharreborde,B., Zhao,K., Zhao,C., and An,K.N. (2006) Sagittal plane motion in the human lumbar spine: comparison of the in vitro quasistatic neutral zone and dynamic motion parameters. *Clin.Biomech.(Bristol., Avon.)* **21,** 914-919.

Gedet,P., Thistlethwaite,P.A., and Ferguson,S.J. (2007) Minimizing errors during in vitro testing of multisegmental spine specimens: considerations for component selection and kinematic measurement. *J.Biomech.* **40,** 1881-1885.

Goel,V.K., Clark,C.R., McGowan,D., and Goyal,S. (1984) An in-vitro study of the kinematics of the normal, injured and stabilized cervical spine. *J.Biomech.* **17,** 363-376.

Goel,V.K., Nye,T.A., Clark,C.R., Nishiyama,K., and Weinstein,J.N. (1987) A technique to evaluate an internal spinal device by use of the Selspot system: an application to Luque closed loop. *Spine* **12,** 150-159.

Goertzen,D.J., Lane,C., and Oxland,T.R. (2004) Neutral zone and range of motion in the spine are greater with stepwise loading than with a continuous loading protocol. An in vitro porcine investigation. *J.Biomech.* **37,** 257-261.

Law,M., Tencer,A.F., and Anderson,P.A. (1993) Caudo-cephalad loading of pedicle screws: mechanisms of loosening and methods of augmentation. *Spine* **18,** 2438-2443.

Lebwohl,N.H., Cunningham,B.W., Dmitriev,A., Shimamoto,N., Gooch,L., Devlin,V., Boachie-Adjei,O., and Wagner,T.A. (2002) Biomechanical comparison of lumbosacral fixation techniques in a calf spine model. *Spine* **27,** 2312-2320.

Lee,C.K. (1988) Accelerated degeneration of the segment adjacent to a lumbar fusion. *Spine* **13,** 375-377.

Lu,W.W., Zhu,Q., Holmes,A.D., Luk,K.D., Zhong,S., and Leong,J.C. (2000) Loosening of sacral screw fixation under in vitro fatigue loading. *J.Orthop.Res.* **18,** 808-814.

Luk,K.D., Chen,L., and Lu,W.W. (2005) A stronger bicortical sacral pedicle screw fixation through the s1 endplate: an in vitro cyclic loading and pull-out force evaluation. *Spine* **30,** 525-529.

Lysack,J.T., Dickey,J.P., Dumas,G.A., and Yen,D. (2000) A continuous pure moment loading apparatus for biomechanical testing of multi-segment spine specimens. *J.Biomech.* **33,** 765-770.

McKinnon,M.E., Vickers,M.R., Ruddock,V.M., Townsend,J., and Meade,T.W. (1997) Community studies of the health service implications of low back pain. *Spine* **22,** 2161-2166.

Niosi,C.A., Zhu,Q.A., Wilson,D.C., Keynan,O., Wilson,D.R., and Oxland,T.R. (2006) Biomechanical characterization of the three-dimensional kinematic behaviour of the Dynesys dynamic stabilization system: an in vitro study. *Eur.Spine J.* **15,** 913-922.

Oxland,T.R. and Panjabi,M.M. (1992) The onset and progression of spinal injury: a demonstration of neutral zone sensitivity. *J.Biomech.* **25,** 1165-1172.

Panjabi,M.M. (1988) Biomechanical evaluation of spinal fixation devices: I. A conceptual framework. *Spine* **13,** 1129-1134.

Panjabi,M.M. (1992) The stabilizing system of the spine. Part II. Neutral zone and instability hypothesis. *J.Spinal Disord.* **5,** 390-396.

Panjabi,M.M., Oxland,T.R., Yamamoto,I., and Crisco,J.J. (1994) Mechanical behavior of the human lumbar and lumbosacral spine as shown by three-dimensional load-displacement curves. *J.Bone Joint Surg.Am.* **76,** 413-424.

Panjabi,M.M. (2007) Hybrid multidirectional test method to evaluate spinal adjacent-level effects. *Clin.Biomech.(Bristol., Avon.)* **22,** 257-265.

Panjabi,M.M., Krag,M.H., and Goel,V.K. (1981) A technique for measurement and description of three-dimensional six degree-of-freedom motion of a body joint with an application to the human spine. *J.Biomech.* **14,** 447-460.

Panjabi,M.M., White,A.A., III, and Johnson,R.M. (1975) Cervical spine mechanics as a function of transection of components. *J.Biomech.* **8,** 327-336.

Pearcy M.J. and Tibrewal S.B. (1984a) Axial rotation and lateral bending in the normal lumbar spine measured by three-dimensional radiography. *Spine* **9**, 582-587.

Pearcy M.J., Portek I., Shepherd J. (1984b) Three-dimensional x-ray analysis of normal movement in the lumbar spine. *Spine* **9**, 294-297.

Schlegel,J.D., Smith,J.A., and Schleusener,R.L. (1996) Lumbar motion segment pathology adjacent to thoracolumbar, lumbar, and lumbosacral fusions. *Spine* **21,** 970-981.

Schmoelz,W., Huber,J.F., Nydegger,T., Dipl,I., Claes,L., and Wilke,H.J. (2003) Dynamic stabilization of the lumbar spine and its effects on adjacent segments: an in vitro experiment. *J.Spinal Disord.Tech.* **16,** 418-423.

Sidhu,K.S. and Herkowitz,H.N. (1997) Spinal instrumentation in the management of degenerative disorders of the lumbar spine. *Clin.Orthop.Relat Res.* 39-53.

Thompson,R.E., Barker,T.M., and Pearcy,M.J. (2003) Defining the Neutral Zone of sheep intervertebral joints during dynamic motions: an in vitro study. *Clin.Biomech.(Bristol., Avon.)* **18,** 89-98.

White,A.A., III and Panjabi,M.M. (1978) The basic kinematics of the human spine. A review of past and current knowledge. *Spine* **3,** 12-20.

White,A.A., III and Panjabi,M.M. (1990) *Clinical Biomechanics of the Spine*. J.B. Lippincott Co., Philadelphia.

Wilke,H.J., Claes,L., Schmitt,H., and Wolf,S. (1994) A universal spine tester for in vitro experiments with muscle force simulation. *Eur.Spine J.* **3,** 91-97.

Wilke,H.J., Wenger,K., and Claes,L. (1998) Testing criteria for spinal implants: recommendations for the standardization of in vitro stability testing of spinal implants. *Eur.Spine J.* **7,** 148-154.

Yamamoto,I., Panjabi,M.M., Crisco,T., and Oxland,T. (1989) Three-dimensional movements of the whole lumbar spine and lumbosacral joint. *Spine* **14,** 1256-1260.

Zdeblick,T.A., Kunz,D.N., Cooke,M.E., and McCabe,R. (1993) Pedicle screw pullout strength. Correlation with insertional torque. *Spine* **18,** 1673-1676.

Zhu,Q., Lu,W.W., Holmes,A.D., Zheng,Y., Zhong,S., and Leong,J.C. (2000) The effects of cyclic loading on pull-out strength of sacral screw fixation: an in vitro biomechanical study. *Spine* **25,** 1065-1069.

Zindrick,M.R., Wiltse,L.L., Widell,E.H., Thomas,J.C., Holland,W.R., Field,B.T., and Spencer,C.W. (1986) A biomechanical study of intrapeduncular screw fixation in the lumbosacral spine. *Clin.Orthop.Relat Res.* 99-112.

CHAPTER 2: CYCLIC TESTING OF HOLLOW VERSUS SOLID SCREWS FOR SACRAL PEDICLE FIXATION[1]

2.1 INTRODUCTION

Currently, solid pedicle screws are the standard instrumentation used in sacral screw fixation; however, these screws are prone to loosening in longer constructs terminating at the sacrum (Carlson *et al.*, 1992). The idea of using a hollow screw for sacral screw fixation has recently been proposed. While designed for vertebral body insertion, the hollow screw increases contact area with the surrounding bone both on the outer and inner surface of the screw, potentially improving fixation within trabecular bone. Thus, it may be beneficial in a sacral application, where the majority of the bone composition is trabecular. Schramm *et al.* (2003) have shown a novel hollow screw to have superior pullout strength compared to existing monocortical screws when inserted into the trabecular bone of thoracic vertebral bodies. Other literature has shown varied results, where the hollow screw was less effective at resisting loosening under cyclic loading (Ferguson *et al.*, 2002).

This chapter outlines the use of a clinically-relevant loading protocol, based on the application of flexion-extension bending moments to the screw, to achieve *in vitro* pedicle screw loosening in the sacrum. Quantifying the screw loosening under cyclic loading using only flexion-extension bending moments applied to the screw in an *in vitro* sacral model has yet to be shown. The goal of this study was to determine if the hollow

[1] A version of this chapter has been accepted for publication (McLachlin SD, Beaton BJB, Sabo MT, Gurr KR, Bailey SI, Bailey CS, Dunning CE. (in press) Comparing the fixation of a novel hollow screw versus a conventional solid screw in human sacra under cyclic loading. *Spine.*)

screw would be more resistant to loosening than a solid pedicle screw when inserted into the S1 pedicles from the standard posterior approach and tested under stair-cased cyclic loading. No previous literature has evaluated the hollow screw for use in sacral screw fixation.

2.2 MATERIALS AND METHODS

2.2.1 Specimen Preparation

Seven fresh-frozen cadaveric sacra were used in this study (mean age: 72 ± 4 years). Each sacrum was removed of all soft tissue and stored at -20°C according to institutional protocols. Prior to any instrumentation, each sacrum was scanned using quantitative computed tomography (qCT) for both an initial anatomic scan and a measurement of BMD (g/cm^3) from a 1 cm^3 region of bone at the centre of each S1 body. No underlying pathology was noted in any specimen.

2.2.2 Screw Insertion

Using a standard posterior technique and fluoroscopic guidance, a solid 7.5 mm diameter x 35 mm length Xia® monoaxial titanium screw (Stryker Spine, Allendale, NJ, USA) was placed in one S1 pedicle and a 12 mm diameter x 34 mm length MACS - TL HMA® (hollow monoaxial) titanium screw (Aesculap, Tuttlingen, Germany) was inserted contralaterally in each specimen (Figure 2.1). The choice of insertion into either the left or right pedicle for each screw was randomly selected in all specimens. The desired screw trajectory was in an anteromedial direction beginning at the base of the facet joint (Carlson *et al.*, 1992). Both screws achieved monocortical purchase.

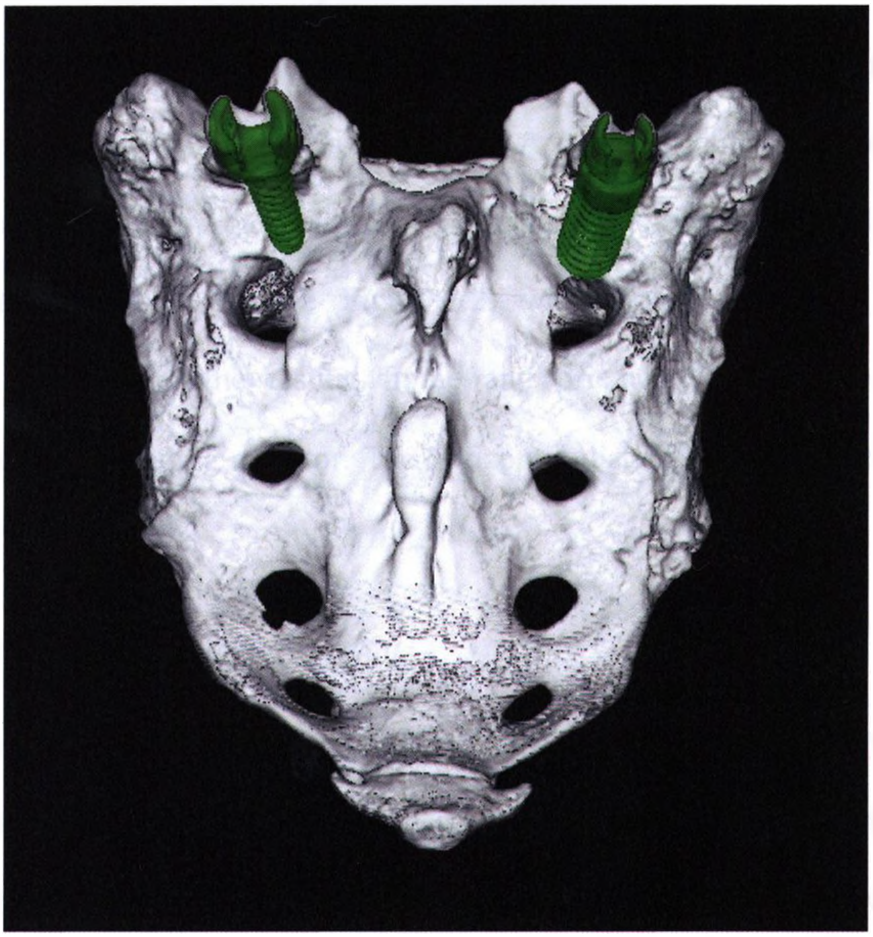

Figure 2.1 **Hollow and Solid Screws Inserted Into Sacral Specimen**
The reconstructed quantitative Computed Tomography scan shows the insertion sites for solid [left] and hollow [right] screws within the S1 pedicles. Screw direction was anteromedially.

2.2.3 Experimental Setup

Each sacrum was potted in 6" diameter PVC pipe, approximately 3" deep, using Denstone™ cement. Due to the irregular shape of the sacrum, additional screws and K-wires were inserted into the lower portion of each sacrum before cementing to increase the available contact area for cement fixation. The PVC pipe was held in place by a custom-designed fixture using several set screws. A standard connecting rod was secured to both the screw and via a ball joint to the actuator of a servohydraulic Instron® 8872 uni-axial materials testing machine (Figure 2.2), with a load cell rated to 250 N. The fixture was mounted to the testing frame and oriented with the connecting rod perpendicular to the loading actuator. The horizontal distance between the actuator and the screw axis was 40 mm.

2.2.4 Cyclic Loading Protocol

A stair-cased cyclic loading protocol was used to simulate the cyclic flexion-extension loading experienced by pedicle screws *in vivo*. With the Instron® in load control, cyclic tension-compression axial loading was applied to the connecting rod in a sinusoidal pattern at a frequency of 1 Hz. As this alternating load was applied to the rod, the pedicle screw was subjected to a corresponding flexion or extension bending moment (*i.e.* compression load created flexion bending moment on the screw) (Figure 2.3). The applied load was selected such that the flexion moments started at 0.5 Nm for the first 1000 cycles and increased by 0.5 Nm after every 1000 cycle steps until the screw was grossly loose based on visual inspection. Extension moments were maintained at 0.5 Nm throughout the entire testing protocol. With limited *in vivo* loading data available, these

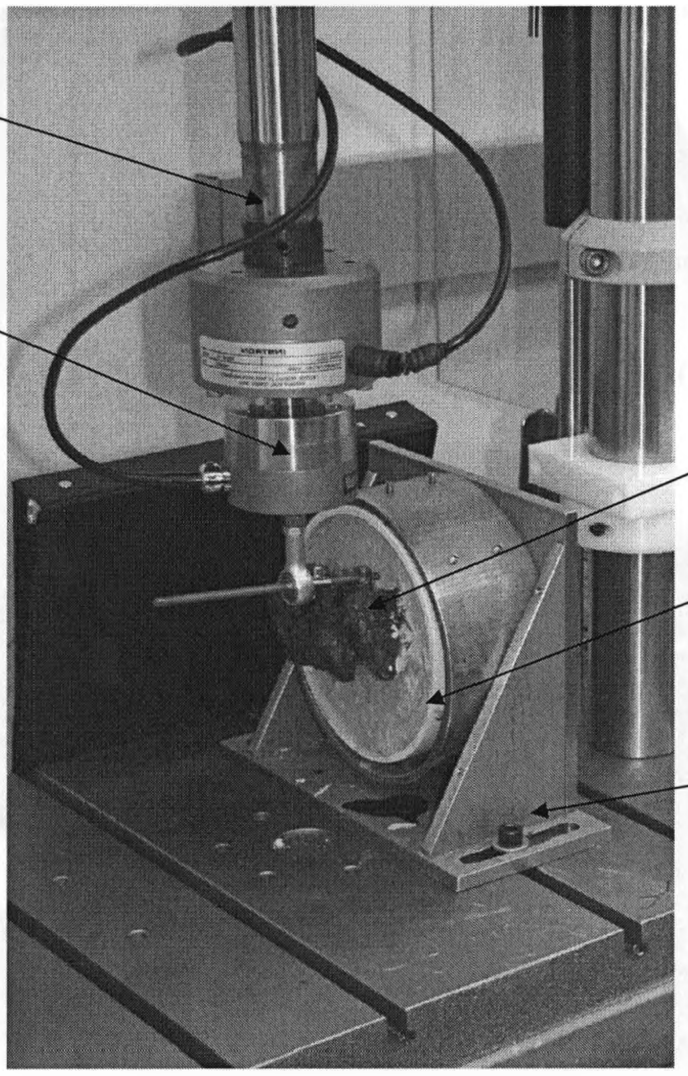

Figure 2.2 **Experimental Test Apparatus**
The actuator of the Instron® materials testing machine applied an axially-directed load, controlled with the attached 250 N load cell, to the rod connected to the pedicle screw in the sacrum. The sacrum, held in a PVC pipe filled with Denstone™ cement, was fixed the the testing platform using a custom-designed mounting fixture.

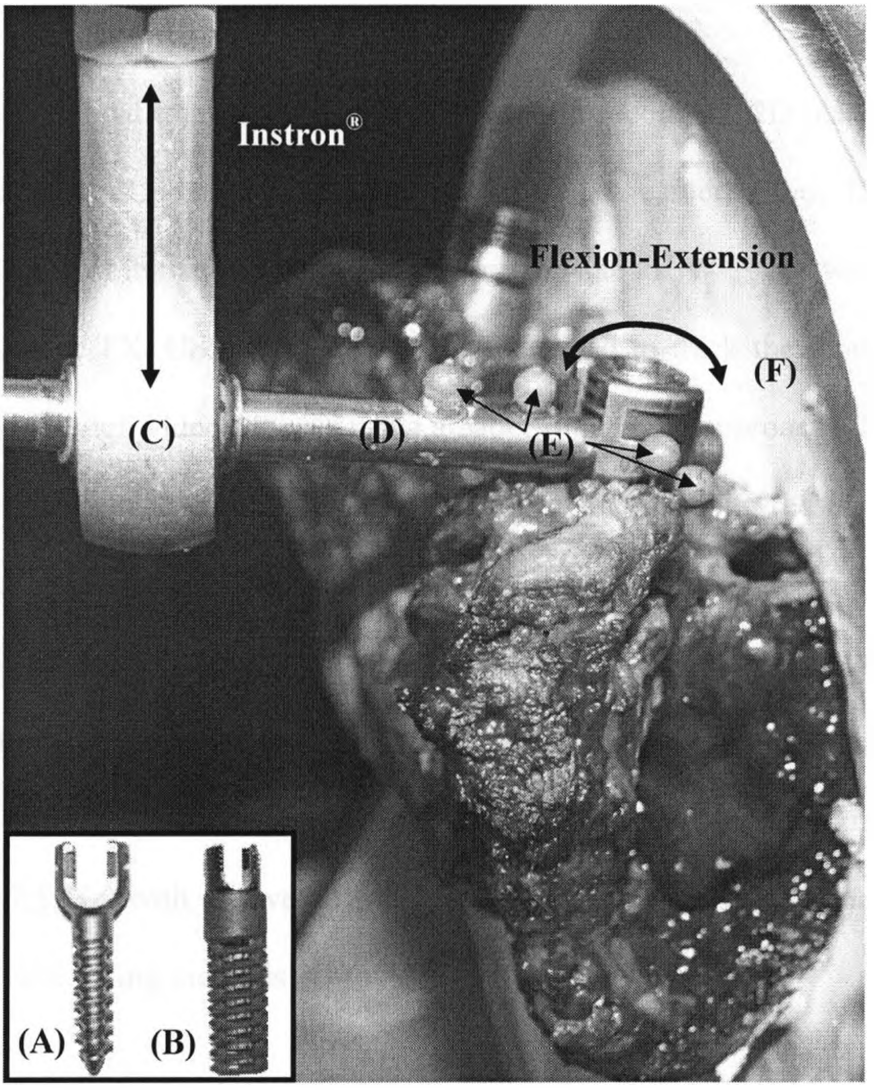

Figure 2.3 **Cyclic Loading through Applied Flexion-Extension Bending Moments** INSET: (A) Solid screw, (B) Hollow screw. APPARATUS: (C) Ball joint connected to the actuator of the Instron® materials testing machine, (D) Connecting rod between ball joint and screw, (E) Optical tracking beads, and (F) Sacrum potted within Denstone™ cement, with caudal endplate exposed.

starting applied moments were determined by pilot studies, and allowed for initial non-destructive loading cycles.

2.2.5 Tracking Screw Loosening

A custom optical tracking system was created to record the 2D-planar motion of both screw and bone. Using an IEEE 1394 colour SXGA camera (Sony DFW-SX910, Tokyo, Japan) in combination with custom-written LabVIEW™ software (National Instruments, Austin, TX, USA), the system was designed to track the loosening of the screw over time through video analysis using a pattern-matching approach. Two tracking beads of the same size and colour were fixed to both the connecting rod (screw motion) and the sacrum (bone motion) to allow tracking of screw motion with respect to the bone. The software program was written to record the real-time x,y locations of all beads within the camera's frame of reference, which was converted to screw rotation relative to bone during a post-hoc analysis (see Section 2.2.6). Data collection was maintained at approximately 7.5 Hz, with an overall precision of approximately 0.1 mm. A detailed description of the tracking methods is provided in Appendix B.

2.2.6 Post-hoc Analysis

Screw loosening was determined based on the magnitude of screw angulation (*i.e.* flexion) relative to the sacrum. Using vector algebra and the nomenclature described by Craig (1989), it was possible to define a coordinate system for both the rod and screw (ROD) and the sacrum (BONE) such that their position and orientation within the camera's frame of reference could be defined using rotation matrices (*i.e.* ${}^{CAM}_{ROD}R$, ${}^{CAM}_{BONE}R$). Since the rotation of the screw relative to bone was of interest, this

relationship was found by multiplying the inverse rotation matrix of the bone in the camera's frame of reference by the rotation matrix of the screw and rod in the camera's frame of reference:

$$ {}^{BONE}_{ROD}[R] = {}^{CAM}_{BONE}[R]^{-1}\ {}^{CAM}_{ROD}[R] = {}^{BONE}_{CAM}[R]\ {}^{CAM}_{ROD}[R] $$

Rotations were calculated using Euler ZYX angle analysis, since the largest rotation in the 2D plane was about the *z*-axis. These rotations could then be evaluated to determine at what point (*i.e.* cycle and loading rate) the screw had failed (*i.e.* became grossly loose within the sacrum). To examine the mode of screw failure, all specimens were re-scanned using qCT following the loading protocol.

Both the magnitude of the applied flexion moment and the required number of loading cycles to cause screw loosening were analyzed using two-way repeated measures analyses of variance (ANOVAs), with factors of screw type and magnitude of screw rotation. These were followed by post-hoc Student-Newman-Keuls tests ($\alpha = 0.05$).

2.3 RESULTS

The initial qCT scans of each specimen following screw insertion were taken to assess bone quality through a BMD measurement, as well as the distance of the screw tip to the far cortex. The average ± standard deviation BMD for all the specimens was 104.6 ± 47.8 g/cm^3. For the solid screw, the average screw tip to cortex distance was 6.4 ± 4.4 mm, and correspondingly for the hollow screw, 8.0 ± 3.2 mm. No screw penetrated the far cortex.

None of the solid or hollow screws bent or fractured during testing. Loading of each screw was allowed to continue until gross screw loosening within the specimen had visibly occurred, confirmed with manual palpation. The screw's failure point was

determined post-hoc, by examining a graph of screw rotation versus time for each specimen (Figure 2.4). From this, it was determined that visible failure of the screw corresponded to an average of 6° of screw rotation. It was after this point that screw rotation tended to increase exponentially. Thus, the relative screw performances were compared at both 3° and 6° of rotation.

Overall, the hollow screw required fewer loading cycles (p=0.004) (Figure 2.5) and less applied moment (p=0.003) (Figure 2.6) to achieve the same magnitude of screw rotation as the solid screw. A survivability curve was created to show the effectiveness of each screw type to achieve a given number of cycles before 6° of screw rotation (Figure 2.7). From this curve, it is evident that no screw failed at less than 2000 cycles, while no screw lasted beyond 18000 cycles.

Scans taken after testing showed that the mode of failure for the solid screws was clearly based on a "teeter-totter" method, where the screw was anchored about the posterior cortex, while trabecular bone was pushed away as the screw rotated (Figure 2.8A). While less defined in some specimens, the hollow screw also experienced this mode of loosening. However, while the solid screw appeared to push cancellous bone out of its path as it teetered, the hollow screw appeared more to cut through the bone as it loosened. This has been surmised based on the smaller void in cancellous bone evident in the post-hoc scans of the hollow screws (Figure 2.8B). These scans also showed that the centre core of the trabecular bone remained within the hollow screw; however, it was no longer fixed to any bone outside the core after screw rotation had occurred. This was verified at the time of retrieval.

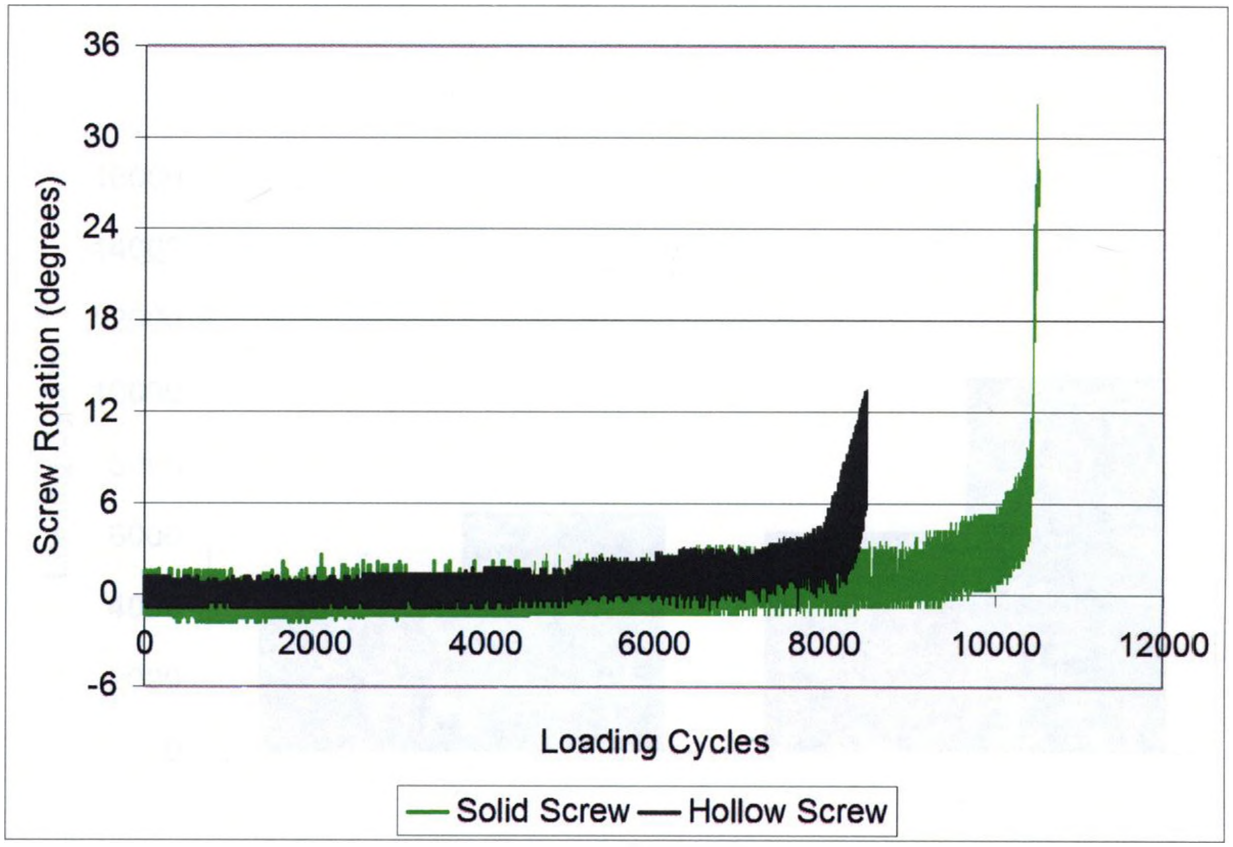

Figure 2.4 **Comparison of Screw Rotation over the Duration of the Test**
Screw rotation for both screw designs increases gradually to six degrees, after which the rotation increases exponentially to drastic failure. Therefore, six degrees was used as the failure point for screw loosening.

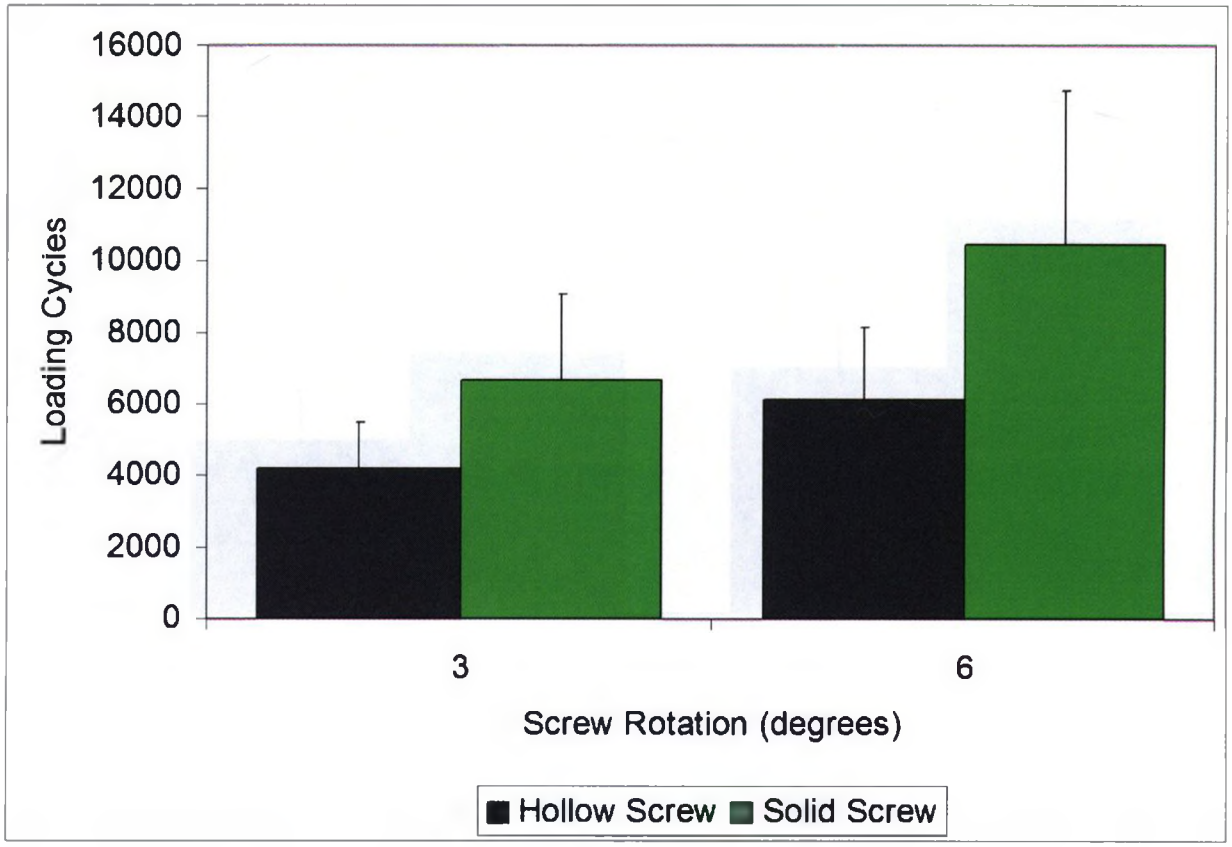

Figure 2.5 **Loading Cycles Completed versus Screw Rotation**
The mean data from the seven specimens for the required number of cycles to achieve three and six degrees of screw rotation are shown for the hollow and solid screws. The solid screw required more cycles to reach both three and six degrees ($p<0.05$). Error bars indicate the standard deviation.

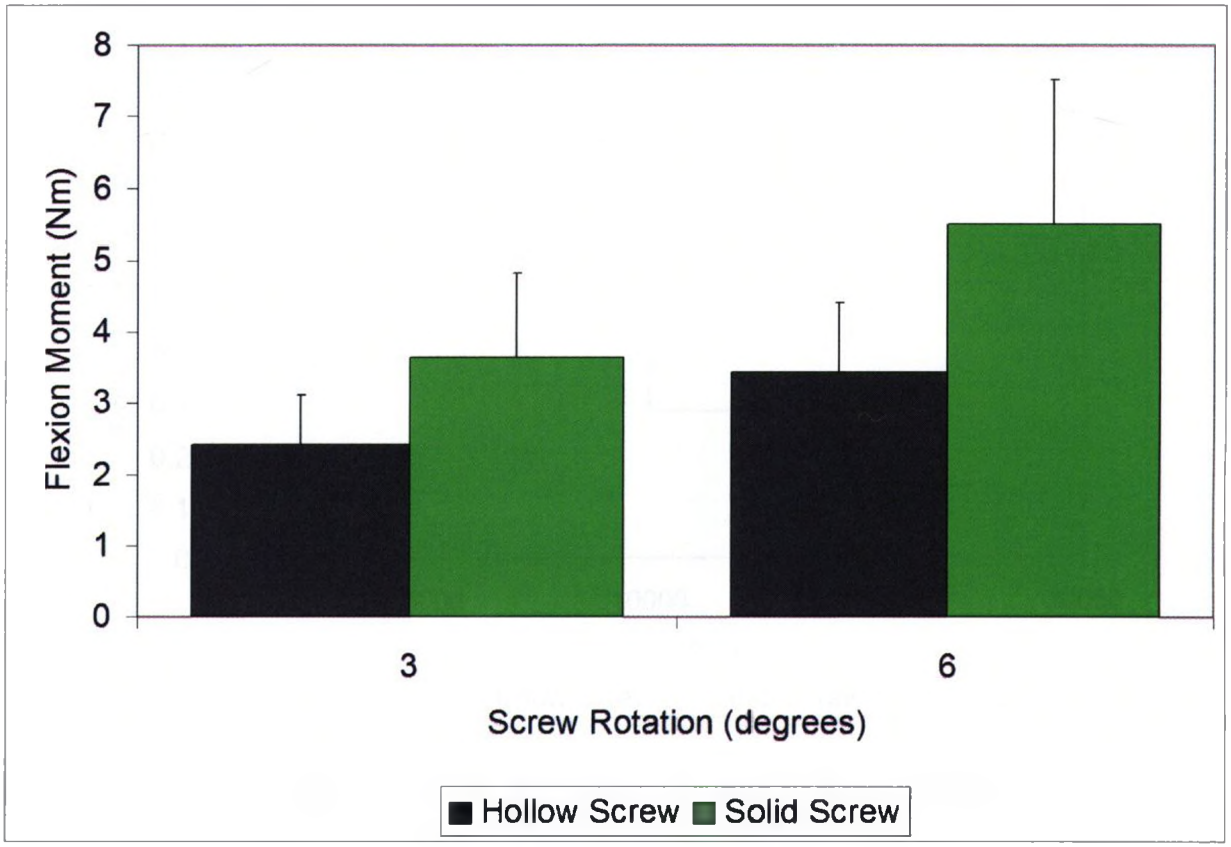

Figure 2.6 **Applied Flexion Moment versus Screw Rotation**
The mean data from the seven specimens for the applied flexion moment (Nm) to achieve three and six degrees of screw rotation are shown for the hollow and solid screws. The solid screw required larger applied moments to reach both three and six degrees ($p<0.05$). Error bars indicate the standard deviation.

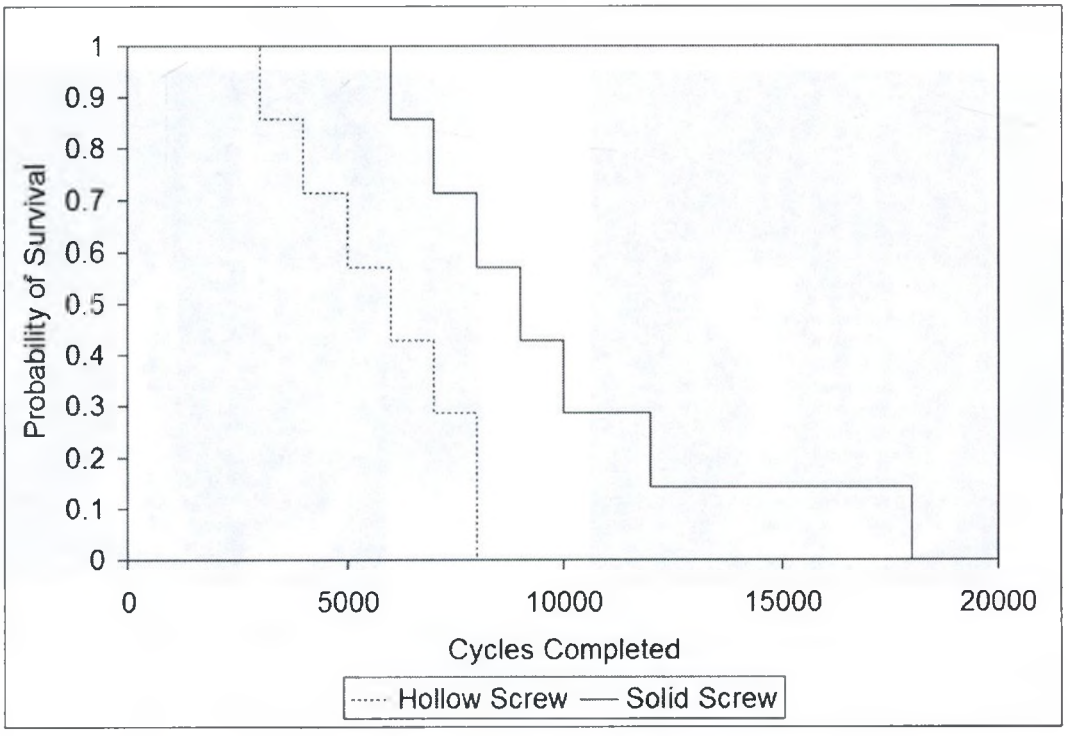

Figure 2.7 **Survivability Curve for Screw Designs to Resist Loosening**
The curve for screw failure at six degrees of screw rotation (n=7). No screw lasted longer than 18000 cycles. The solid screw shows a distinct survival advantage.

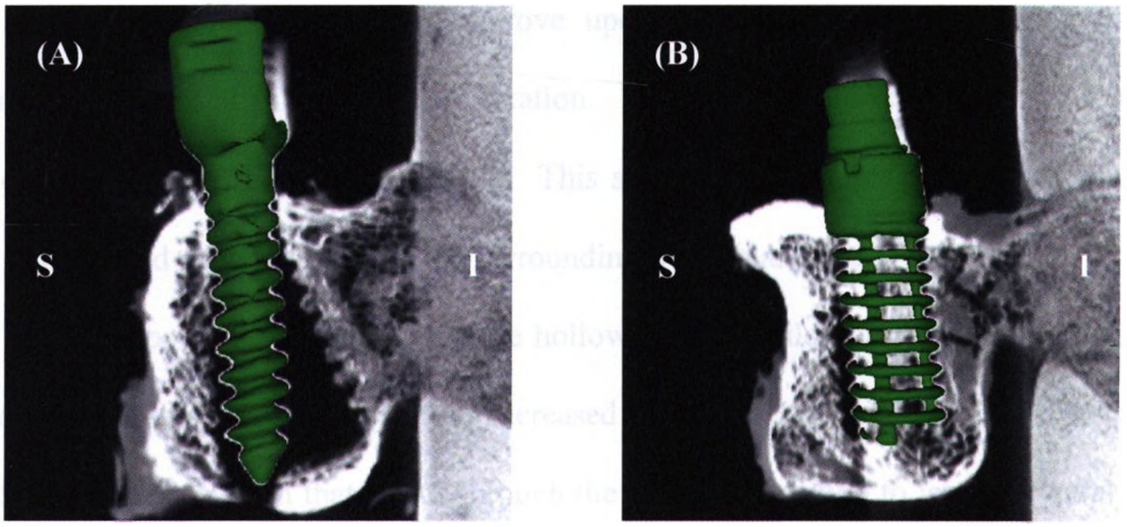

Figure 2.8 **Side by Side Comparison of Loosening Developed**
qCT scans, taken from a lateral view along the superior (S) – inferior (I) axis, obtained following testing for the (A) solid and (B) hollow screws within the same specimen. The hollow screw appears to cut through trabecular bone, with a central core of bone remaining within screw. The solid screw clearly teeters about the cortical shell while sweeping away interior trabecular bone.

2.4 DISCUSSION

Sacral screw loosening continues to be a clinical problem due to the large bending moments applied at the screw-bone interface in the sacrum. To improve the failure rate of lumbosacral instrumented fusion, bicortical fixation has been advocated by some (Lebwohl *et al.*, 2002; Luk *et al.*, 2005; Emami *et al.*, 2002); however, a risk of neurovascular injury is associated with this procedure (Ergur *et al.*, 2007; Mirkovic *et al.*, 1991). Thus, it is important to improve upon existing monocortical methods and instrumentation used in sacral screw fixation. This study evaluates the use of a novel hollow screw in the first sacral pedicle. This screw design offers potential advantages due to increased contact area with the surrounding trabecular bone.

It had been hypothesized that the hollow screw would perform superiorly to the solid screw in this model, based on its increased surface area within bone. The design of the hollow screw is such that it cuts through the bone on insertion to leave a central core of bone intact within the screw. This is different than conventional solid screws, where bone is pushed away from the screw upon insertion. Schramm *et al.* (2003) showed that the HMA hollow screw provided results comparable to a bicortical pedicle screw fixation in an axial pullout test when used from an anterior approach. The opportunity to achieve the same fixation strength as bicortical fixation would be of benefit in the sacrum.

Subjected to the cyclic flexion-extension loading in the present model, the hollow screw proved to be less effective at resisting screw loosening. The current findings are supported by those of Ferguson *et al.* (2002), who also found the hollow screw to be ineffective under cyclic conditions. While their study was designed for anterior fixation in osteoporotic thoracolumbar vertebrae, they found the hollow screw experienced

excessive displacement, through cancellous bone cut-out, in the vertebral body when tested using a cyclic applied moment. The present findings support their recommendation to use caution when applying the hollow screw clinically.

In the current study, the decision was made to standardize the screw length, selecting a solid screw length (35 mm) to closely match the length of the available hollow screw (34 mm). Screw length has been shown in previous literature to increase fixation if the screw can come in contact with the opposing cortex (Zindrick *et al.*, 1986). As the specimens used had a large range in size, the tip of the screw to the far cortex of the sacrum varied significantly as measured by the qCT scan; however, no screw penetrated the far cortex prior to loading. A difference between screw diameters between the solid (7.5 mm outer diameter) and hollow (12 mm outer diameter) screws existed in this study. The use of the solid 7.5 mm screw is a consistent with current clinical practice as the largest diameter available. The 12 mm hollow screw was the smallest diameter made available for this study. Previous research with solid screws has shown that increasing the screw diameter increases fixation strength (Zindrick *et al.*, 1986). The larger diameter hollow screw did not outperform the smaller diameter solid screw in the current study, suggesting that the cause of failure was screw design.

There were a wide range of BMD values in the seven specimens tested, with some indicating osteoporosis. Although BMD has been shown previously to correlate with pullout strength (Zindrick *et al.*, 1986; Halvorson *et al.*, 1994), this would not play a role in the current study due to its repeated-measures design, where each pair of screws are compared within a specimen.

The majority of previous research to examine pedicle screw failure in the sacrum has employed pullout for inducing failure (Luk *et al.*, 2005; Lu *et al.*, 2000; Zhu *et al.*, 2000; Zindrick *et al.*, 1986; Zdeblick *et al.*, 1993; Law *et al.*, 1993; Carlson *et al.*, 1992; Schramm *et al.*, 2003). While this method provides valuable comparison data, it is not indicative of the common mode of failure seen clinically, which involves loosening from cyclic loading (Law *et al.*, 1993; Zindrick *et al.*, 1986; Ashman *et al.*, 1988). Zdeblick *et al.* (1993) showed that cyclic flexion-extension loading applied to pedicle screws creates loosening similar to the clinical situation in lumbar vertebrae. The loads applied *in vivo* to sacral pedicle constructs remain a relative unknown. Thus, the method of Zdeblick *et al.* (1993), who used a ramping cyclic pattern at 0.5 Hz starting at a moment of ±1.5 Nm and increasing the baseline moment at +0.5 Nm/min, has been adapted to this sacral model based on initial pilot testing. As opposed to an increasing ramp, the load was step-wise increased every 1000 cycles in the current study to allow fatigue to be assessed. Initial load magnitudes were also reduced to 0.5 Nm of flexion and extension to ensure the test was initially non-destructive. With the reduced magnitudes, the loading frequency was increased to 1 Hz. As the lumbosacral spine typically has a larger range of motion in flexion compared to extension, the current loading protocol was designed to emphasize larger flexion moments that would be associated with this range of motion, and the propensity for screw failures in this direction. Thus, step-wise loading increments of 0.5 Nm were only added in flexion, with the extension moment maintained at a non-destructive baseline of 0.5 Nm throughout testing. Loading was continued until all screws, both solid and hollow, reached at least 6° of screw rotation in flexion.

While other sacral studies have used non-destructive cyclic methods followed by axial pullout methods to determine fixation strength (Lu *et al.*, 2000; Luk *et al.*, 2005; Zhu *et al.*, 2000; Zindrick *et al.*, 1986), the current study continued to cycle the screws to failure to be more indicative of the clinical scenario. Moreover, this enabled post-hoc qCT scans to be taken with the screws still *in situ*, so as to evaluate the mode of screw failure. Based on these scans, it was determined that the mode of loosening was consistent with previous literature describing a "teeter-totter" method of failure (Zindrick *et al.*, 1986). In all cases, the solid pedicle screw used the posterior cortex as a fulcrum of rotation and the weaker trabecular bone was swept away (Figure 2.7A). Similarly, the hollow screw rotated with the cortical shell as the fulcrum; however, rather than sweeping away bone, the hollow screw also appeared cut through the bone (Figure 2.7B). This is consistent with previous use of the hollow screw under cyclic loading conditions (Ferguson *et al.*, 2002). Evaluation of the post failure qCT scans also showed that the central core of bone remained within the hollow screw, thus fixation benefits from the core were lost once the screw began to rotate.

This *in vitro* experimental work is indicative of the fixation available in the S1 pedicle in the immediate post-operative period. If the pedicle screw designs cannot provide adequate stability under cyclic conditions in this early phase, long-term stability through fusion of the vertebrae, which may take many months, will likely not occur. Thus, the initial stability of the screw is perhaps more important than any additional delayed fixation stability possibly achieved through bone ingrowth into the hollow screw (*i.e.* a factor which cannot be assessed in this *in vitro* investigation). By then, it would be hoped that fusion between the vertebrae would have begun, limiting the necessity of the

screw. If fusion between the vertebrae has not occurred, the construct will, in all likelihood, eventually fail despite bone ingrowth into the screw.

2.5 REFERENCES

Ashman,R.B., Birch,J.G., Bone,L.B., Corin,J.D., Herring,J.A., Johnston,C.E., Ritterbush,J.F., and Roach,J.W. (1988) Mechanical testing of spinal instrumentation. *Clin.Orthop.Relat Res.* **227,** 113-125.

Carlson,G.D., Abitbol,J.J., Anderson,D.R., Krag,M.H., Kostuik,J.P., Woo,S.L., and Garfin,S.R. (1992) Screw fixation in the human sacrum. An in vitro study of the biomechanics of fixation. *Spine* **17,** S196-S203.

Craig,J.J. (1989) Introduction to Robotics: Mechanics & Control. Addison-Wesley Publishing Company Inc.

Emami,A., Deviren,V., Berven,S., Smith,J.A., Hu,S.S., and Bradford,D.S. (2002) Outcome and complications of long fusions to the sacrum in adult spine deformity: Luque-Galveston, combined iliac and sacral screws, and sacral fixation. *Spine* **27,** 776-786.

Ergur,I., Akcali,O., Kiray,A., Kosay,C., and Tayefi,H. (2007) Neurovascular risks of sacral screws with bicortical purchase: an anatomical study. *Eur.Spine J.* **16,** 1519-1523.

Ferguson,S.J., Winkler,F., and Nolte,L.P. (2002) Anterior fixation in the osteoporotic spine: cut-out and pullout characteristics of implants. *Eur.Spine J.* **11,** 527-534.

Halvorson,T.L., Kelley,L.A., Thomas,K.A., Whitecloud,T.S., III, and Cook,S.D. (1994) Effects of bone mineral density on pedicle screw fixation. *Spine* **19,** 2415-2420.

Law,M., Tencer,A.F., and Anderson,P.A. (1993) Caudo-cephalad loading of pedicle screws: mechanisms of loosening and methods of augmentation. *Spine* **18,** 2438-2443.

Lebwohl,N.H., Cunningham,B.W., Dmitriev,A., Shimamoto,N., Gooch,L., Devlin,V., Boachie-Adjei,O., and Wagner,T.A. (2002) Biomechanical comparison of lumbosacral fixation techniques in a calf spine model. *Spine* **27,** 2312-2320.

Lu,W.W., Zhu,Q., Holmes,A.D., Luk,K.D., Zhong,S., and Leong,J.C. (2000) Loosening of sacral screw fixation under in vitro fatigue loading. *J.Orthop.Res.* **18,** 808-814.

Luk,K.D., Chen,L., and Lu,W.W. (2005) A stronger bicortical sacral pedicle screw fixation through the S1 endplate: an in vitro cyclic loading and pull-out force evaluation. *Spine* **30,** 525-529.

Mirkovic,S., Abitbol,J.J., Steinman,J., Edwards,C.C., Schaffler,M., Massie,J., and Garfin,S.R. (1991) Anatomic consideration for sacral screw placement. *Spine* **16,** S289-S294.

Schramm,M., Krummbein,S., Kraus,H., Pitto,R.P., and Schmidt,R. (2003) Anterior vertebral body screw pullout testing with the hollow modular anchorage system--a comparative in vitro study. *Biomed.Tech.(Berl)* **48,** 356-361.

Zdeblick,T.A., Kunz,D.N., Cooke,M.E., and McCabe,R. (1993) Pedicle screw pullout strength. Correlation with insertional torque. *Spine* **18,** 1673-1676.

Zhu,Q., Lu,W.W., Holmes,A.D., Zheng,Y., Zhong,S., and Leong,J.C. (2000) The effects of cyclic loading on pull-out strength of sacral screw fixation: an in vitro biomechanical study. *Spine* **25,** 1065-1069.

Zindrick,M.R., Wiltse,L.L., Widell,E.H., Thomas,J.C., Holland,W.R., Field,B.T., and Spencer,C.W. (1986) A biomechanical study of intrapeduncular screw fixation in the lumbosacral spine. *Clin.Orthop.Relat Res.* 99-112.

CHAPTER 3: DEVELOPMENT AND VALIDATION OF A SPINAL LOADING SIMULATOR

3.1 INTRODUCTION

Spinal loading simulators apply known loads to a cadaveric spine specimen such that physiologic motions, similar to the *in vivo* situation, may be approximated. In addition to producing the physiologic motion of interest (*i.e.* flexion-extension), the simulator should allow for unconstrained motion in other directions (*i.e.* natural translations and rotations of the spine without interference from the loading apparatus) (Panjabi, 1988). Thus, precise loading and control methods are required (Crawford *et al.*, 1995). This chapter details the development and validation of an *in vitro* spinal loading simulator, as well as optical methods to quantify the resulting segmental spinal kinematics. Validation is assessed through a preliminary study to evaluate the simulator's ability to create repeatable and reproducible physiologic spine motions.

3.2 MATERIALS AND METHODS

3.2.1 Spinal Loading Device

Due to the limited space available in the laboratory and the availability of an Instron® materials testing machine, the spinal loading simulator was designed and developed as a modification to the Instron®. The goal was to use the machine's loading and control methods to produce repeatable and reproducible segmental spinal motion. Thus, any modifications had to fit within the testing space available, while still allowing

for all of the necessary requirements of a simulator (*i.e.* produce natural, unconstrained motion). In addition, the design had to allow for the segmental motion to be tracked optically (*i.e.* camera's line of sight could not be obstructed by the design of the device).

3.2.1.1 Instron® Materials Testing Machine

The modified materials testing machine was an 8874 Instron® tri-axial servo-hydraulic apparatus (Figure 3.1). Its overhead "axial" actuator was capable of applying axial load and torque. Its "off-axis" actuator, which could be positioned at angles between 0° and 150° to the axial actuator, provided a secondary torque axis. The testing platform was centered below the axial actuator, with approximately 450 mm x 420 mm of working space available. The positions of the actuators could be adjusted to account for a variety of fixture sizes, but had to remain fixed in position during testing.

The maximum travel distances of this Instron's actuators were ±50 mm and 120° for the linear and rotary axes, respectively. The position of each actuator at any point in time is provided by three position sensors in the testing machine, two in the axial actuator to measure translation (*i.e.* LVDT) and rotation (*i.e.* RVDT), and one in the off-axis actuator to measure rotation (*i.e.* RVDT). These sensors were accurate to ±0.5% of full travel.

To monitor applied loading, individual load cells were connected to each actuator. On the axial actuator, an AMTI (AMTI, Watertown, MA, USA) load cell was used to control both the axial load being applied, F_z, and along with the axial torque, M_z. In addition to controlling these two loading axes, it also had additional sensors to monitor the remaining four degrees-of-freedom (*i.e.* two shear forces, F_x and F_y, and two bending moments, M_x and M_y). The loading range specifications of this load cell were 4000 N in

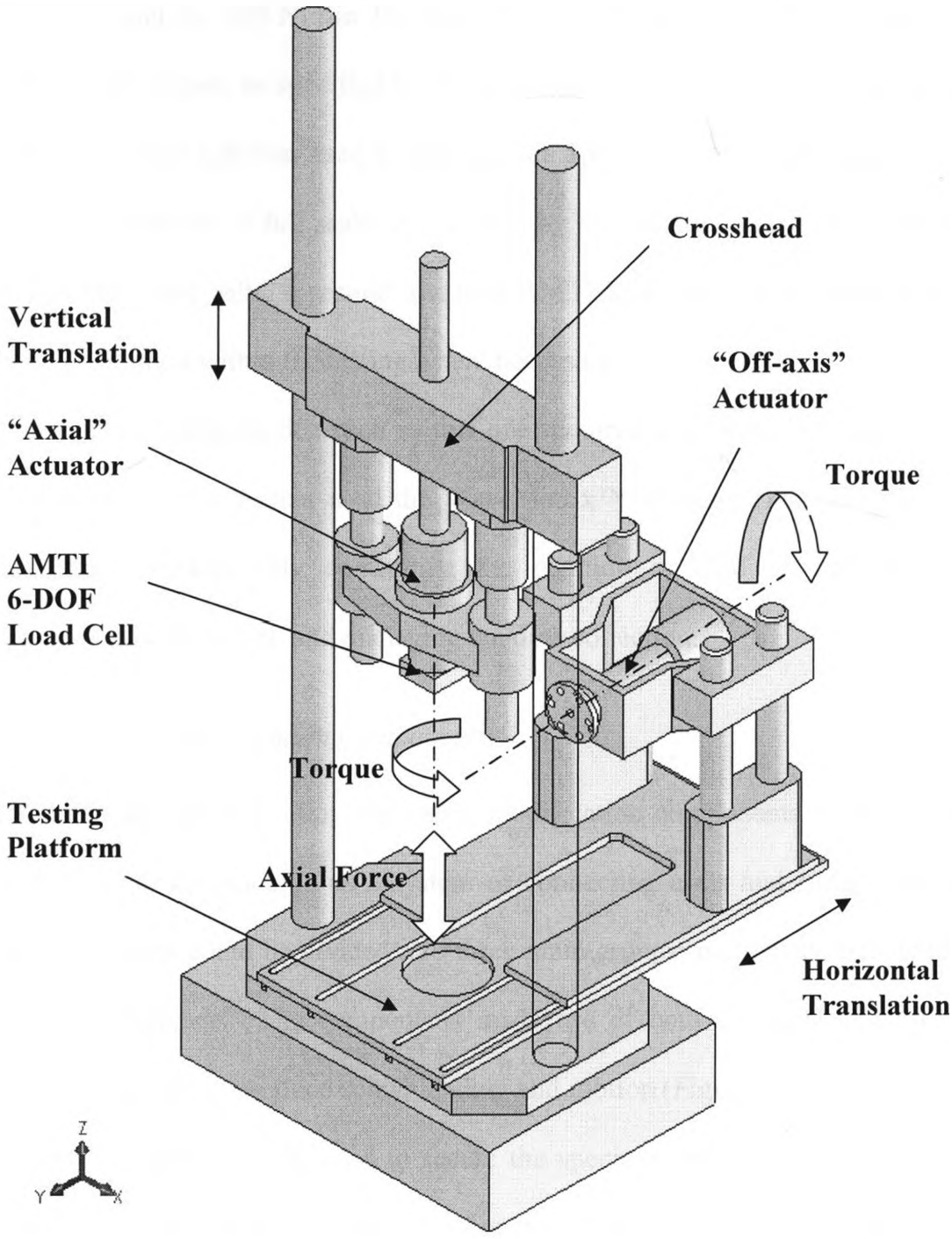

Figure 3.1 **Instron® 8874 Materials Testing Machine**
This servo-hydraulic machine is capable of applying load from two different actuators. The "axial" actuator can apply an axial force, as well as a torque. The "off-axis" actuator can apply a torque about its axis. An AMTI six degree-of-freedom (DOF) load cell is used to control the loading of the axial actuator. Two large columns support and position the axial actuator's crosshead. In addition to the translation available in the axial actuator, the crosshead's position can be vertically adjusted to account for a variety of specimen lengths. Also, the off-axis torque actuator could be moved horizontally if necessary.

F_z, 2000 N in F_x and F_y, 100 Nm in M_z, and 50 Nm in M_x and M_y. The accuracy was ±0.2% of full scale output, as specified by the manufacturer. On the off-axis actuator, a one DOF Instron® load cell was used to measure the applied torque (load range = ±100 Nm, accurate to ±0.005% of full scale as specified by the manufacturer). In addition to these "controlling" load cells, a second identical AMTI load cell was available for use and could be positioned within the testing where necessary.

A complex loading device such as this one required a rigorous software control package. This multi-axis system used the WaveMatrix™ software (Instron, Norwood, MA, USA) for simultaneously controlling the position or load of each actuator, monitoring the load cell output, and managing the data collection.

3.2.1.2 Modification Components

To create the spinal loading simulator, modification components were designed for the materials testing machine as a system of connecting arms and fixtures (Figure 3.2). The components could be divided into three main groups: potting fixtures, loading arms, and counterbalance. The components made use of both the axial and off-axis actuators of the Instron® to produce spinal loading and motion (Figure 3.3).

The potting fixtures were used to secure the specimen to the loading simulator, such that its cranial end would connect to either the off-axis (for flexion-extension and lateral bending motion trials) or axial loading arm (for axial motion trials) of the simulator and its caudal end would be fixed to the testing platform. The fixtures, cranial and caudal, were two stainless steel boxes with removable sides that were designed to fit a cut piece of 4" diameter PVC tubing, rigidly held in place through the use of set screws. Three sets of threaded M6 steel rods were welded to orthogonal sides of the cranial

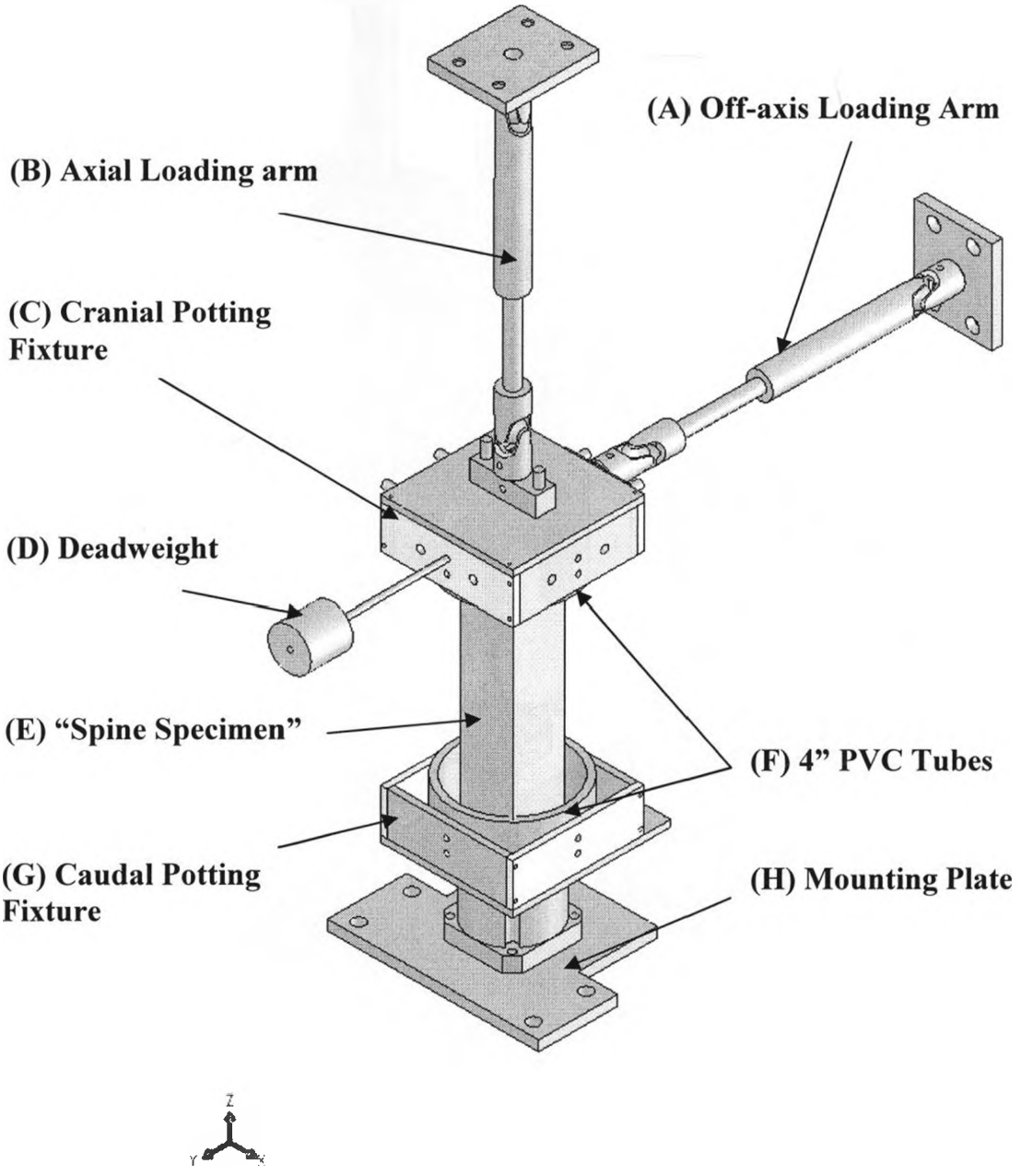

Figure 3.2 **Custom-designed Loading Arms and Fixturing**
(A) The telescoping off-axis loading arm, built with a frictionless linear bearing over a spline shaft connected at each end to a universal joint. (B) The axial loading arm consisted of the same components as the off-axis loading arm, except with the telescoping function removed. (C) The cranial potting fixture with threaded rods attached to connect to both the off-axis and axial loading arms. (D) Deadweight counterbalanced the moment induced on the specimen by weight of the off-axis loading arm. (E) The spine specimen, shown by a placeholder box, was held in (F) 4" PVC tubes in the potting fixtures. (G) The caudal potting fixture attached to the testing platform of the Instron® through the (H) mounting plate.

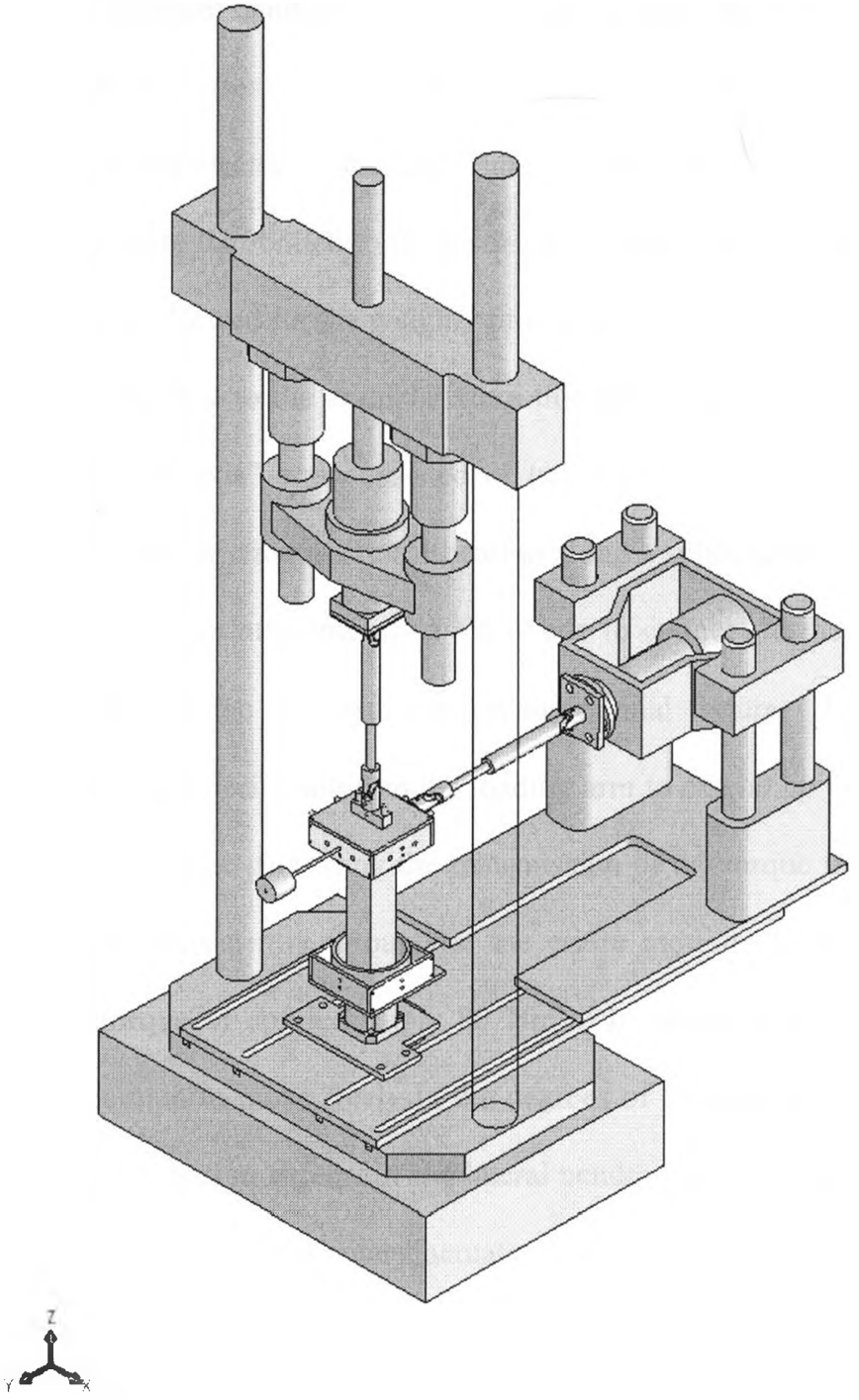

Figure 3.3 Spinal Loading Simulator
The modified Instron® materials testing machine provided the loading actuators to create physiologic spine motion. The simulator made use of both actuators to apply continuous physiologic motions. Custom-fixturing ensured that unconstrained motions were applied through a pure moment design. Flexion-extension and lateral bending were applied through the off-axis loading arm. Axial rotation was applied by the axial loading arm, with the off-axis loading arm removed for these tests.

fixture to allow for different connection sites of a loading arm, set to align with the three physiologic rotations (*i.e.* flexion-extension, lateral bending, and axial rotation). The caudal potting fixture connected to the additional AMTI load cell, which was fixed to moveable mounting plate that bolted to the testing platform of the machine. The use of the additional load cell allowed for the weight of the specimen to be determined.

Torsion was applied to the cranial fixture through the use of specially-designed loading arms. The "off-axis" arm consisted of two universal joints (UJs), connected together by a telescoping, frictionless linear bearing along a spline shaft. The ends of the UJs were welded to custom attachments to allow one to connect to the actuator of the Instron® and the other to the threaded rods on the cranial fixture. The low friction, telescoping element of the design allowed the loading arm to extend up to a maximum of approximately 65 mm, while permitting the transmission of the torque from the actuator to the cranial fixture consistently throughout the entire motion of the spine (up to a maximum applied torque of approximately 80 Nm). In addition, use of the two UJs allowed for the specimen to move freely in the degrees of freedom where there was no applied load. To apply flexion-extension and lateral bending motion, the off-axis loading arm was connected to the off-axis rotary actuator. A second loading arm was created with the same design, minus the telescoping function, to connect to the axial actuator. This "axial" loading arm simulated axial rotation. The telescoping function was not required for this arm since the axial actuator could move "freely" up and down to achieve the same telescoping effect as detailed below.

A counterbalance system was necessary to remove the weight of the fixturing overtop of the specimen. To balance the moment induced on the specimen when the off-

axis loading arm was attached, deadweight was added to the opposing side to the cranial fixture. The weight of these components, in addition to the potting fixtures, on the specimen was removed using the axial actuator of the Instron®, as it was connected to the cranial fixture with the axial loading arm. Furthermore, using the control methods available on the Instron®, the actuator could be set to maintain a pre-defined axial load level; in this case, approximately zero applied load. Thus, as a method of achieving unconstrained motion, the actuator was essentially "free" to move up and down to relieve the machine weight on the spine specimen as it moved through its ROM for each motion. The use of the UJs allowed for the actuator's load point to remain centered over top of the specimen.

3.2.2 Optical Tracking System for Segmental Motion

A custom 2D optical tracking system was used in this study to measure segmental motion of the spine specimen. Capturing 2D planar motion was relevant, as the majority of the individual physiologic motions occur in a single plane.

To assess segmental motion, Delrin® marker blocks (15 mm cubes) were rigidly fixed via threaded rods to mounting brackets attached to each exposed vertebra of the specimen, as well as to the cranial and caudal potting fixtures (Figure 3.4). These markers, rods, and brackets were small and lightweight. Marker placement was such that, in a 2D plane, its *x,y* coordinate axes would lie along the standard anatomical axes defined for the motion segment (Wilke *et al.*, 1998b). The marker attached to the caudal potting fixture was used as the fixed frame of reference since this fixture, and its potted vertebra remained stationary throughout testing. Three beads inserted into the marker block were used to define the coordinate axes on each marker. Depending on the motion

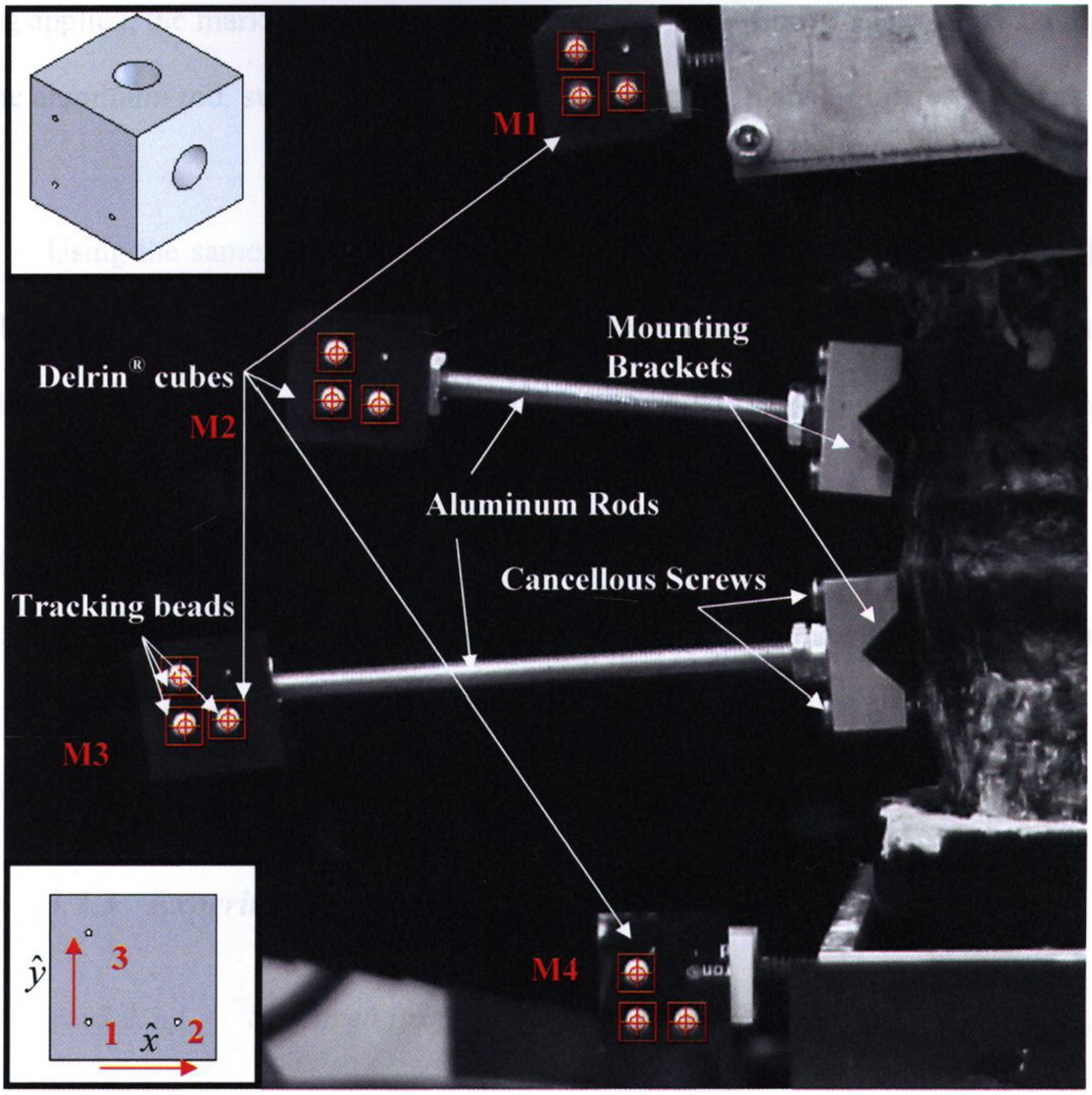

Figure 3.4 **Marker Blocks and Tracking Beads**
Small Delrin® cubes were used as marker blocks for the video motion analysis program. There were four blocks (M1, M2, M3, and M4) used in the study to capture the motion of the four vertebral bodies (L1-L4). M1 and M4 were connected to cranial and caudal potting fixtures. M2 and M3 were attached to the exposed vertebrae along an aluminum threaded rod to a mounting bracket. This bracket was vertically aligned along the vertebra's most anterior point and held in place using cancellous bone screws. The marker blocks could be positioned on the end of the rod in three orthogonal positions depending on the motion being applied (TOP INSET). The positions of the three individual beads set in each marker block were tracked in real-time throughout the spine's motion based on a pattern matching approach. These beads (labeled 1, 2, and 3 in BOTTOM INSET) were located in machine drilled holes to form two orthogonal vectors (1-2 = $\hat{x}$ and 1-3 = $\hat{y}$).

being applied, the marker block could be rotated between orthogonal positions on the end of the aluminum rod, such that the three beads were in the plane of interest (Figures 3.5 – 3.7).

Using the same tracking components as the loosening study (*i.e.* Chapter 2), the IEEE 1394 camera (Sony DFW-SX910, Tokyo, Japan) and custom LabVIEW™ software tracked the *x,y* location of beads again through a pattern-matching technique. In this case, black and white video analysis was used rather than colour analysis (see Appendix B) to allow for more beads to be tracked. Data collection was targeted at approximately 7.5 Hz. The precision of the analysis program was approximately 0.25 mm. The *x,y* position data of each bead was collected in real-time during the motion trials, then segmental rotations were calculated in the post-hoc analysis (Section 3.2.4).

3.2.3 Experimental Validation Protocol

3.2.3.1 Specimen Preparation and Potting Protocol

One fresh-frozen cadaveric multi-segment lumbar spine (L1-L4) was harvested for use in this validation study. The specimen had all musculature removed, but the ligaments and intervertebral discs were left intact. It was stored at -20°C, and allowed to thaw overnight prior to the start of testing.

To fix the specimen within the simulator, the ends of the spine were potted using Denstone™ cement in 4" diameter PVC pipe (1.5" deep). Due to the shape and size of the lumbar vertebrae, limited cement contact area was available. Thus, additional screws and K-wires were inserted into the upper and lower vertebrae to increase cement fixation. The cranial end of the specimen was potted first, with the specimen set cranial end down

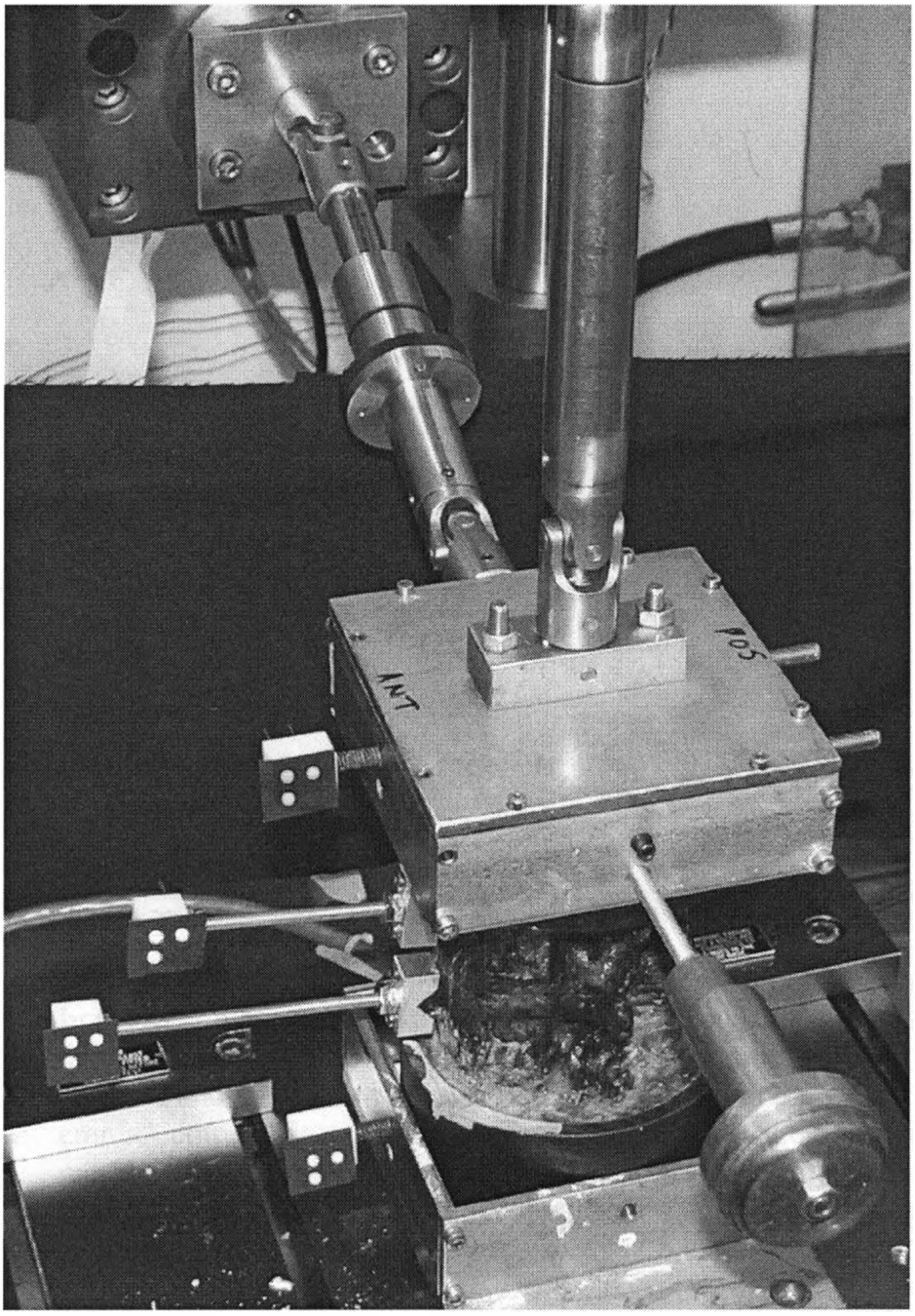

Figure 3.5 **Simulator Orientation for Flexion-Extension Motion Tracking**
In the flexion-extension simulator orientation, the specimen was aligned such that its anterior-posterior axis was positioned perpendicular to both the loading actuator and the camera's field of view. To track the spine motion produced, the marker blocks were attached along the sagittal plane of the specimen to be seen from a lateral perspective, as shown on the left.

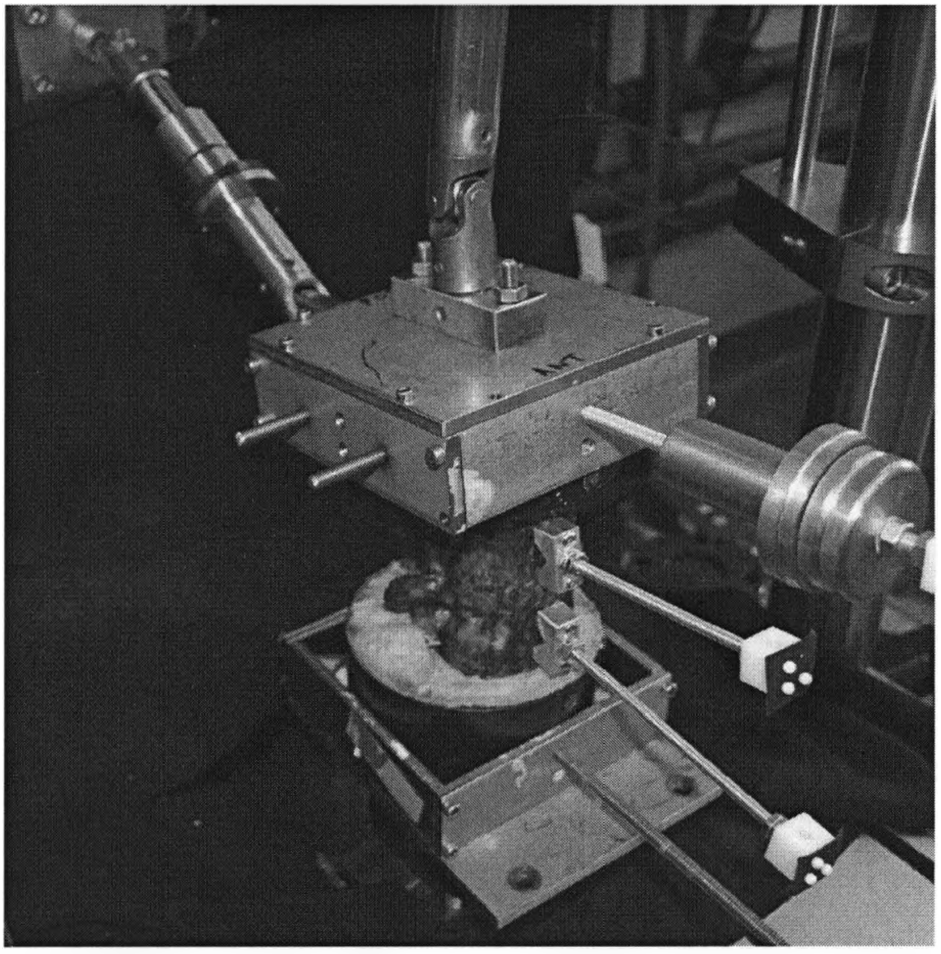

Figure 3.6 **Simulator Orientation for Lateral Bending Motion Tracking**
In the lateral bending simulator orientation, the specimen was aligned such that its anterior-posterior axis was positioned parallel to both the loading actuator and the camera's field of view. This required a 90° rotation of the cranial potting fixture and specimen. To track the motion produced, marker blocks were attached along the sagittal plane of the specimen and the blocks rotated to be viewed from a frontal perspective, as shown on the right.

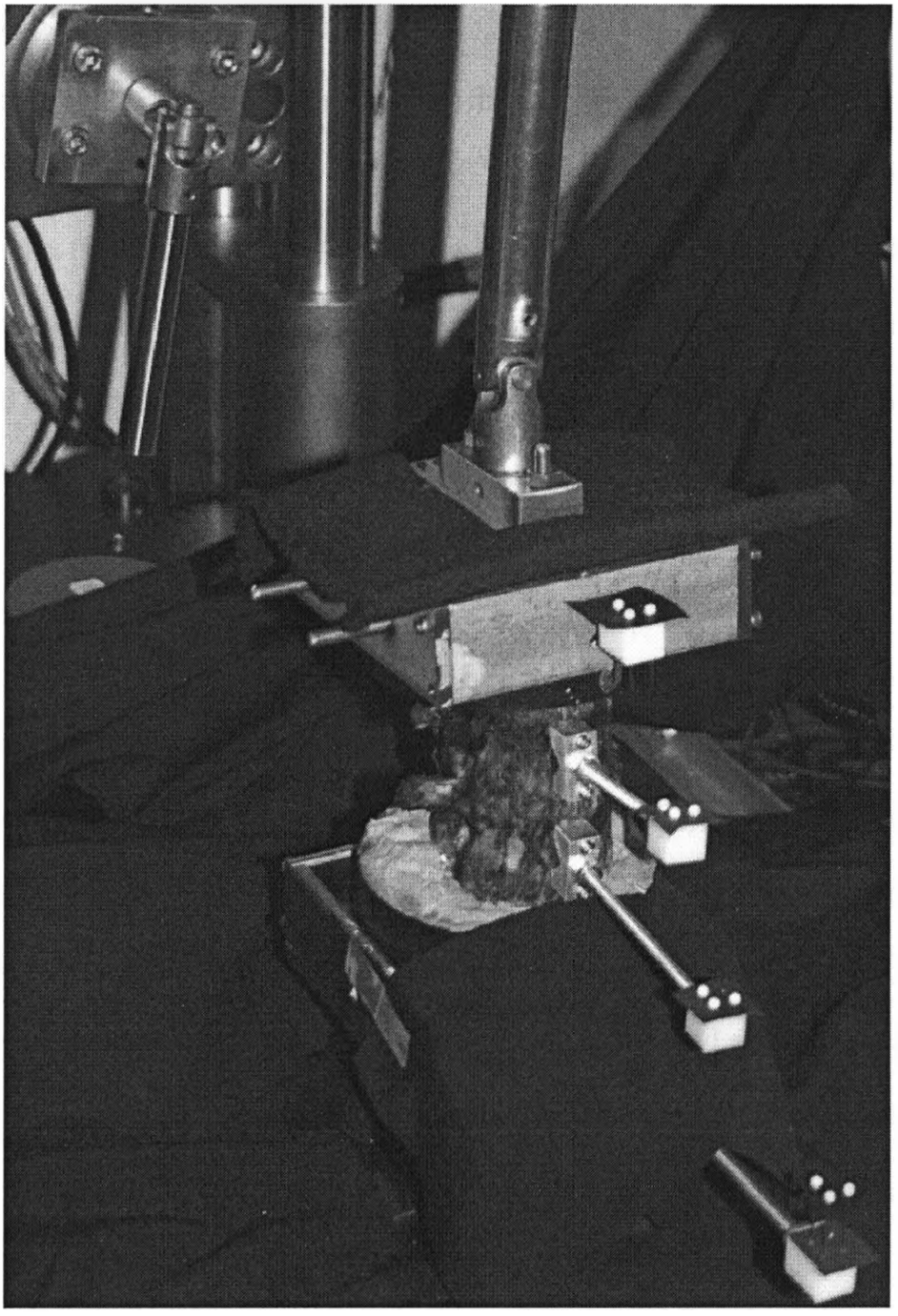

Figure 3.7 **Simulator Orientation for Axial Rotation Motion Tracking**
In the axial rotation simulator orientation, the specimen was aligned such that its anterior-posterior axis was positioned parallel to both the loading actuator and the camera's line-of-sight, similar to the lateral bending setup; however, the off-axis loading arm was removed. To track the motion produced, marker blocks were attached along the sagittal plane of the specimen and the blocks were rotated to be viewed from a superior perspective, as shown on the right.

in the PVC within the potting fixture. After allowing the cement to harden (approximately 20-30 minutes) the cranial fixture, with the specimen attached, was connected to the axial actuator of the Instron®. The specimen could then be correctly positioned into the caudal potting fixture, by lowering the axial actuator, without being shifted by the weight of the cranial fixture. To match *in vivo* orientation, the specimen was aligned such that the mid-plane of the L3-L4 segment was horizontal (Wilke *et al.*, 1998b). Cement was then added around the caudal vertebra (L4) in the PVC to fix it in position.

3.2.3.2 Specimen Setup in Simulator

After potting, the height of the axial actuator was recorded before removing only the specimen (with its PVC pots) from the simulator; all of the fixturing, including the loading arm, upper and lower potting fixtures, and counterbalance arm, remained in the simulator at the specified testing height. The load cells (2 AMTIs and off-axis) were then tared out (*i.e.* balanced to 0 N and 0 Nm for their respective load and torque channels) to remove the machine weight from their readings (the weight of the specimen and cement was approximately 15 N). The specimen was then returned to the simulator and positioned so that its anatomical axes matched up with the motion to be simulated. For example, to apply flexion-extension moments, the specimen was set in the caudal fixture such that its anterior-posterior axis was perpendicular to the off-axis loading actuator and the marker blocks rotated so that the beads could be viewed laterally. The axial actuator was lowered until a small amount of compression was applied to the specimen (approximately -5 N) before attaching the cranial fixture, loading arm, and counterbalance weight. This same procedure was repeated when reconfiguring the

specimen between setups for flexion-extension and lateral bending. (Note: axial rotation used the same setup as lateral bending, minus the off-axis loading arm, and with necessary adjustment to the marker blocks).

Ideally, the axial actuator would move up and down freely along with the produced spinal motion created by the off-axis actuator; however, this was not always possible due to the nature of the servo-hydraulic machine. Thus, steps were taken to adjust the complex control system to the stiffness of the specimen. Using the loop tuning tool, the PID settings for load control of the axial actuator were tuned to a square wave signal using a small cyclic axial load. Tuning the actuator to an aggressive square wave signal allowed for the axial actuator to respond more quickly during testing to load input, thus effectively moving freely with the spine.

3.2.3.3 Loading Protocol

To examine the repeatability and reproducibility of the spine simulator, a relevant loading protocol was devised. Standards previously developed for *in vitro* lumbar spine testing (Wilke *et al.*, 1998b) with pure moment loading recommend ±7.5 Nm be applied for all physiologic motions using continuous loading. This load value falls within the elastic range of the specimen, allowing for multiple tests without destruction of the spine. For other regions of the spine, recommended loading values are significantly lower (*i.e.* ±5 Nm for the thoracic and ±2.5 Nm for the cervical). Regardless of the applied magnitude, it was important that the pure moment loading applied produced normal range of motion (ROM) for each of the three physiologic motions of the spine specimen. Thus, in the current setup, three separate loads were applied, ±2.5 Nm, ±5 Nm, and ±7.5 Nm, to the lumbar specimen to achieve a variety of ROMs.

Using the WaveMatrix™ multi-axis control program, a loading protocol was setup to run three trials consisting of three full loading cycles (Figure 3.8). The goal of loading three full cycles was to precondition the specimen to reduce the viscoelastic effects of the motion segment, where the last cycle was used for data analysis (Wilke *et al.*, 1998b). Loading of the specimen was achieved with the Instron® in rotation control at 2°/s (considered to be a typical physiologic loading rate; Wilke *et al.* (1998a)) to a specified load target. This involved using a position ramp to rotate the specimen to a certain location until the desired load (*i.e.* 2.5, 5, 7.5 Nm) was reached; then the rotation was reversed to the next load step. Before starting the cyclic loading protocol, manual rotations were used to find the approximate locations for the desired load to ensure the load target was reached. As mentioned, during the pure moment loading of the specimen, the axial actuator tried to maintain only a small amount of compression of the specimen (approximately -5 N). This meant the axial actuator would move vertically up and down with the motion of the spine. The testing protocol is shown in Figure 3.9. Instron® data were recorded for the applied moment channel (either off-axis or axial) as well as the associated rotation. These data were simultaneously collected along with the marker tracking data to ensure synchronization. Complete details of the testing procedure, including potting, setup, and loading protocols, are provided in Appendix E.

3.2.4 Data Analysis of Segmental Motion

Custom-written LabVIEW™ software was used to convert the recorded marker position data, based on the *x,y* location of the three beads, into a rotation of the vertebral body based on rigid body kinematics (see Appendix C). Comparing the relative rotations of adjacent vertebrae revealed the segmental motion. Overall motion was defined as the

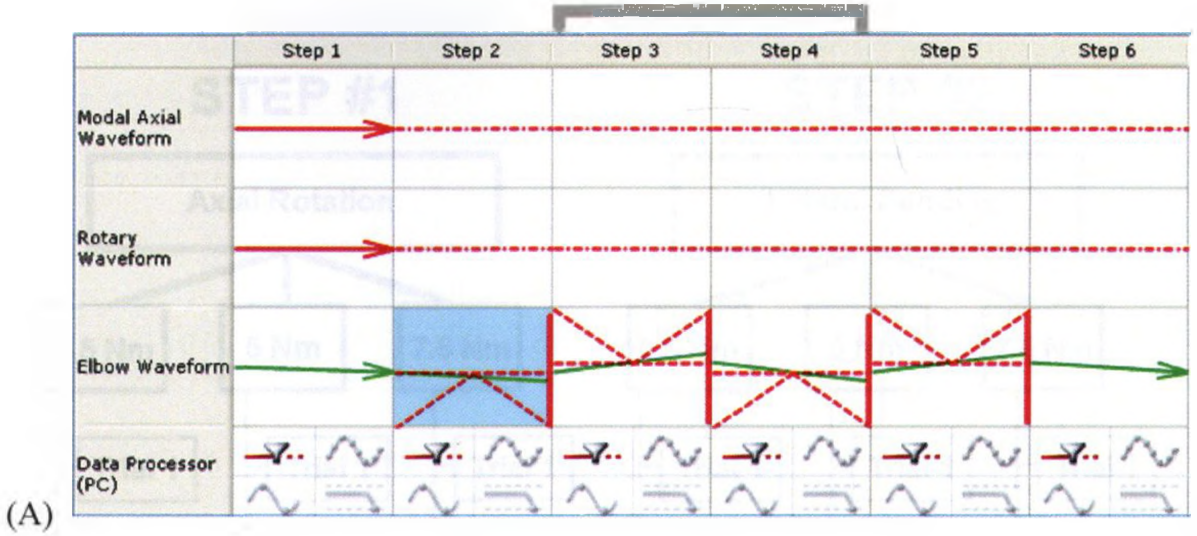

(A)

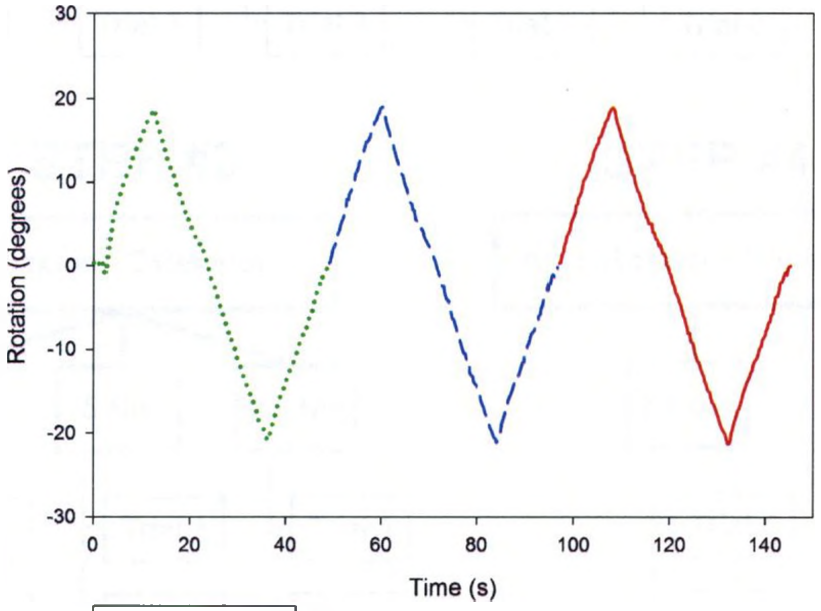

(B)

Figure 3.8 Three Cycles of Applied Loading

(A) The WaveMatrix™ software controlled each loading axis of the Instron® materials testing machine. In flexion-extension and lateral bending, the applied moment was produced from the off-axis actuator, shown above as the "Elbow Waveform," while for axial rotation the "Rotary Waveform" was used to create an applied moment. For all cases, the axial actuator was set to maintain a small, constant, compressive load on the specimen and no applied torque throughout the motion-inducing loading cycles. (B) Three full motion cycles were applied to precondition the specimen, with Cycle 3 data used for kinematic analysis.

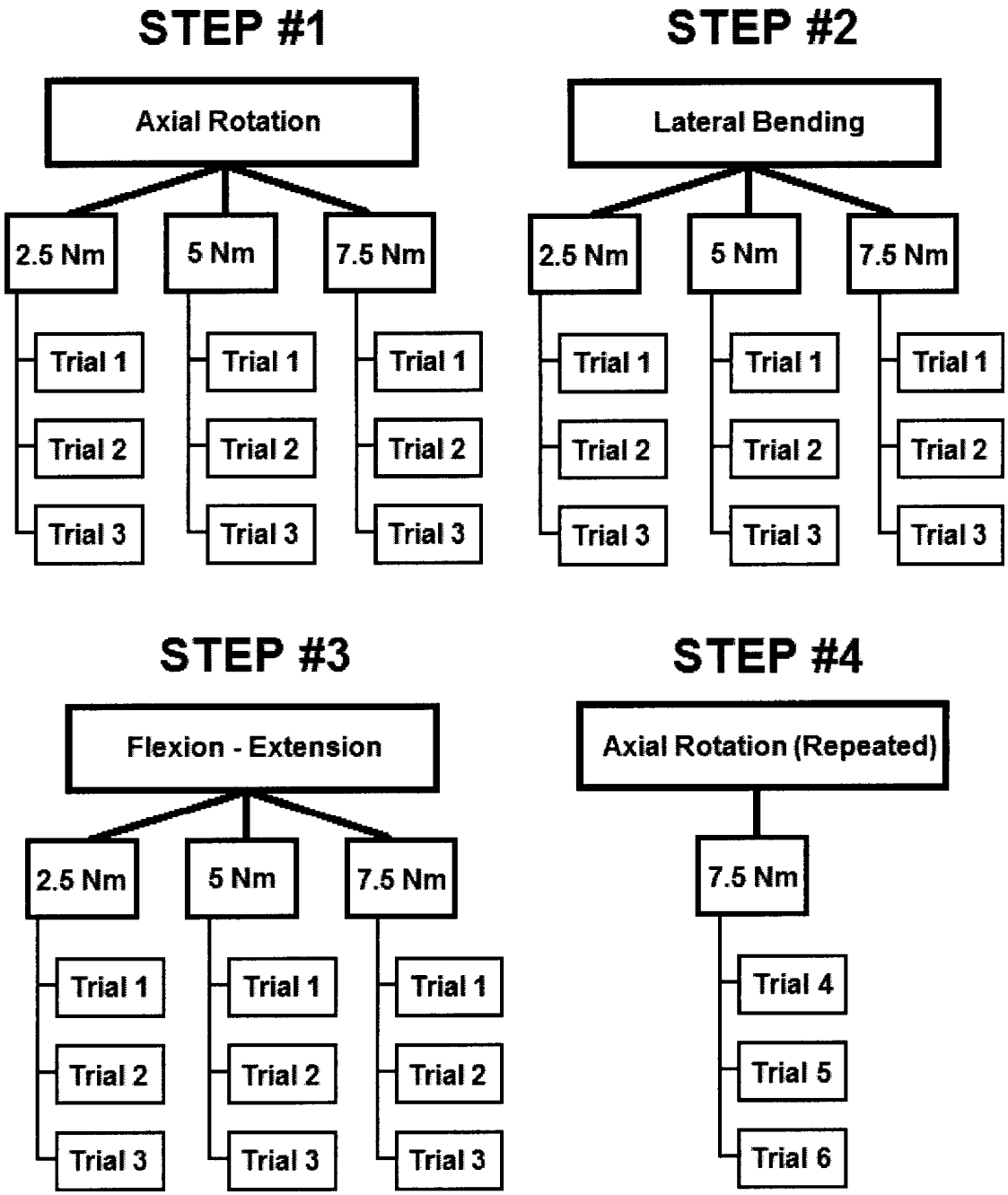

Figure 3.9 **Experimental Testing Protocol for Simulator Validation**
For each of the three physiologic motions (*i.e.* axial rotation, lateral bending, flexion-extension), three individual trials were run for each of the loads of interest (*i.e.* 2.5, 5, 7.5 Nm) to assess repeatability. Each trial consisted of three complete loading cycles, as described in Figure 3.5. Following the three motions, the simulator was reconfigured for three additional trials of ±7.5 Nm for axial rotation to evaluate the reproducibility of the simulator compared to the initial axial rotation setup.

relative rotations between L1-L4. Motion parameters of interest included the +ROM and -ROM (both overall and segmental), as well as the overall continuous neutral zone (NZ) around the neutral position.

3.2.4.1 Segmental Rotations

Before determining segmental rotations, steps were taken to remove any outliers from the raw *x,y* bead position data. The use of a pattern-matching algorithm led to two types of errors in capturing the marker positions: 1) markers were missed (*i.e.* pattern not detected); or 2) markers were "mis-seen" (*i.e.* pattern detected in a non-marker location due to light reflections, etc.). Error #1 manifests itself by including zeroes in the data file for the unfound bead, whereas error #2 was seen as a large "jump" in the bead position between adjacent rows of data. A shift in the recorded bead position of more than ±10 pixels was used as the cut-off, since this would not be physiologically possible due to the applied loading rate. To remove both of these sources of error from the data, a custom-written LabVIEW™ program was devised to search each marker data file for the errors described. If an error case was detected, the entire row of data for all the bead positions at that instance was removed.

To calculate the kinematics of the marker's rotation, it was necessary to define a local coordinate system for each marker attached to a vertebral body (including the marker on the top fixture), as well as for a fixed frame of reference (*i.e.* marker attached to fixed lower potting fixture). It was then possible to define the orientation of the marker throughout its motion with respect to another marker's frame of reference (*i.e.* the orientation of Marker 1 with respect to Marker 2), through the use of a 3x3 rotation matrix (*i.e.* ${}^{M2}_{M1}[R]$).

To establish the local coordinate system on a marker, unit vectors were defined from beads 1-2 and 1-3, based on the beads' *x,y*, and *z* positions (where $z = 0$ for all beads) (Figure 3.4). These unit vectors were defined as the $\hat{x}$-axis for beads 1-2 and $\hat{y}$-axis for beads 1-3 regardless of the motion trial performed (Note: This method ensured that the rotation of interest always took place about the $\hat{z}$-axis). Taking the cross-product of the $\hat{x}$-axis and the $\hat{y}$-axis resulted in the orthogonal $\hat{z}$-axis, which was also made into a unit vector. To ensure all the axes were mutually perpendicular, an additional cross product was taken of the $\hat{z}$-axis crossed with the original $\hat{x}$-axis to obtain a new $\hat{y}$-axis. The rotation matrix was formed by grouping the three unit vectors (*i.e.* $\hat{x}, \hat{y}$, and $\hat{z}$) together as the columns in a 3x3 matrix. This provided the rotation matrix of each marker with respect to the camera's frame of reference.

To change the frame of reference, matrix manipulation was required. Since each marker was expressed in the camera's frame of reference, taking the inverse of the desired frame of reference with respect to the camera, and subsequent multiplication with the desired marker would obtain the segmental rotation matrix between adjacent markers:

$$ {}^{M2}_{M1}[R] = {}^{CAM}_{M2}[R]^{-1} \, {}^{CAM}_{M1}[R] = {}^{M2}_{CAM}[R] \, {}^{CAM}_{M1}[R], \text{ for L1-L2 motion} \qquad \text{(Eq. 3.1)} $$

Figure 3.10 depicts the frames of reference graphically. In a similar manner, rotation matrices were defined for quantifying motion from L2-L3 (*i.e.* ${}^{M3}_{M2}[R]$), L3-L4 (*i.e.* ${}^{M4}_{M3}[R]$), and overall spine motion (*i.e.* L1-L4; ${}^{M4}_{M1}[R]$).

Since the rotation of interest always occurred about the $\hat{z}$-axis, a ZYX Euler angle analysis was used to reveal the individual rotation of one marker against another within the 2D plane (only calculating the rotation about the $\hat{z}$-axis was necessary, which is noted as δ). This was calculated as:

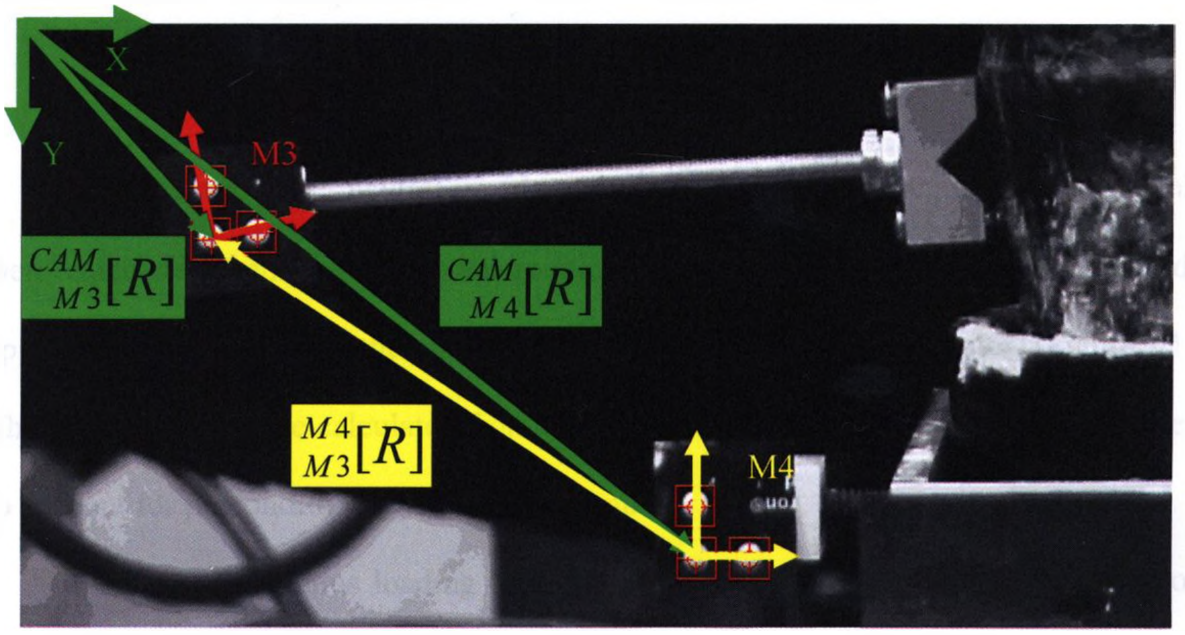

Figure 3.10 Frames of Reference for Rotation Matrices
Initially, the rotation matrices for each marker block were calculated in the camera's frame of reference (as shown by the green lines). Using matrix algebra, the marker block's rotation could be defined in terms of the fixed frame of reference on the caudal potting fixture (M4). This is shown in the figure as M3 in the frame of reference for M4 (yellow line). The same procedure was accomplished for the additional cranial markers, M1 and M2, not shown in this figure.

$$ {}^{M2}_{M1}R = \left[{}^{M2}\bar{X}_{M1} \; {}^{M2}\bar{Y}_{M1} \; {}^{M2}\bar{Z}_{M1} \right] = \begin{bmatrix} r_{11} & r_{12} & r_{13} \\ r_{21} & r_{22} & r_{23} \\ r_{31} & r_{32} & r_{33} \end{bmatrix} \quad \text{(Eq. 3.2)} $$

$$ \delta = A\tan 2\left(\frac{r_{21}}{r_{11}}\right) \quad \text{(Eq. 3.3)}^{2} $$

With the overall and segmental rotations throughout spinal motion calculated, the standard parameters for spinal motion could be defined (*i.e.* ROM and NZ).

3.2.4.2 Range of Motion and Neutral Zone

The neutral zone, neutral position, and range of motion (segmental and overall), were calculated from the segmental rotations, along with the simultaneously recorded applied moment data from the Instron® (torque of the loading arm actuator) (Figure 3.11). These parameters were calculated from the final loading cycle of each trial (*i.e.* Cycle 3) to account for preconditioning of the specimen.

Since a continuous loading protocol was used, the width of the hysteresis loop obtained when plotting the applied moment versus overall segmental motion was chosen as the definition of the NZ, where NZ was the difference between the rotation values at 0 Nm. The neutral position of the specimen was defined as the average of these two rotations (*i.e.* middle of the NZ).

Before calculating the ROM, the recorded segmental rotations (*i.e.* based on the marker beads) were shifted, such that the calculated neutral position was taken as zero rotation. This allowed for the ROM to be split into +ROM and -ROM similar to other studies (*i.e.* flexion could be differentiated from extension). The total ROM (sum of +ROM and -ROM) was also described for each rotation.

---

[2] The Atan2 (r_{21}/r_{11}) function computes $\tan^{-1}(y/x)$, but uses the signs of both x and y to determine the quadrant in which the resultant angle lies (see Craig, 1989)

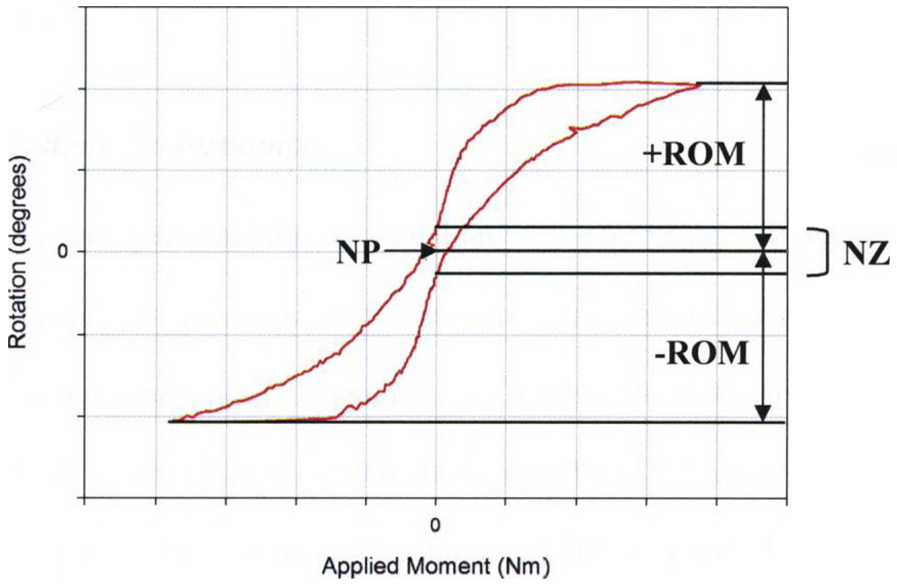

Figure 3.11 Typical Rotation Versus Applied Moment Curve
The visual definitions are shown in the figure for range of motion (+ROM and -ROM), neutral zone (NZ) and the neutral position of the specimen (NP). Width of the hysteresis loop was used to define the NZ of the specimen, a measure of specimen laxity. The NP was set in the centre of the defined NZ. +ROM and -ROM were the largest rotation achieved in each loading direction.

The means and standard deviations for the ROM and NZ over the three trials performed at each load level for each motion were calculated to assess the repeatability of the simulator. Reproducibility of the ROM and NZ was also compared for one load between the initial 7.5 Nm axial rotation setup (*i.e.* Step 1, Figure 3.9) and the final 7.5 Nm axial rotation setup done at the end of the testing day (*i.e.* Step 4, Figure 3.9).

3.3 RESULTS

3.3.1 System Performance

Overall system performance was qualitatively promising. Based upon visual inspection, the specimen appeared to move through normal motion patterns of the spine. Controllable, accurate, and repeatable loading was achieved with the use of the Instron's actuators. The testing environment, in which the simulator was developed, allowed for all "physiologic" motions to be conducted without any interference. The potting fixtures used in the simulator maintained the correct orientation of the specimen throughout its motion, with no visible shift in position. The counterbalance system functioned appropriately, with the axial actuator moving up and down to relieve the load as it moved through its ROM. The maximum axial load seen on the specimen was approximately ±15 N from the set baseline load (-5 N).

The planar tracking program, written to record and sort the 12 marker beads and simultaneously collect the loading actuator's rotation and load, ran smoothly throughout the testing period. The capture frequency of this program was set at 7.5 Hz; however, this target was not always achieved. Nonetheless, sufficient data were recorded for each cycle to define a clear load versus rotation relationship, including the peak load and

rotation values. An additional concern was the amount of data removed due to the propensity of the camera to miss or mis-see bead locations. Evaluating the raw data versus the error-checked data in the final loading cycle revealed an acceptable amount of data was removed (an average of 6.6% of data points removed).

3.3.2 Experimental Overview

The single specimen that was tested functioned well during all phases of the study. It appeared to maintain itself well through multiple freeze-thaw cycles for numerous testing days (both pilot and validation).

The experimental validation testing duration was approximately 16 hours, spread over two days with the specimen allowed to re-freeze overnight. Potting of the specimen required approximately three hours in total, including 45 minutes to allow for the cement to set on the cranial end before potting the caudal end. Checking of the position targets for each load level and any tuning that was required took up a significant portion of the first testing day. Additionally, the specimen setup time between the different orientations was rather lengthy. Testing of each motion and load level for the specimen was relatively quick once setup, with each trial requiring only a few minutes.

3.3.3 Segmental Rotations

Segmental rotations were calculated for L1-L2, L2-L3, L3-L4, and L1-L4. L1-L4 was defined as the overall motion of the specimen for the specific motion applied. After calculating the overall neutral position of the specimen, the segmental rotations were shifted to reflect the neutral position as zero rotation.

3.3.3.1 Rotation vs. Applied Moment Hysteresis Curves

Rotation versus applied moment hysteresis curves for the three loading cycles were created for each load level of the three physiologic motions. In addition to using these curves to calculate the neutral position and neutral zone, the hysteresis curve gives an overall look at the motion created and general repeatability of the spine simulator. The curves created for each motion at 7.5 Nm are shown in Figures 3.12-3.14. This load was chosen as it has been reported as the standard applied moment used for *in vitro* testing in the lumbar spine (Wilke *et al.*, 1998b). Each motion showed highly repeatable data with very little conditioning effects seen between the cycles. Axial rotation qualitatively appeared to be the smoothest data, when compared to the flexion-extension and lateral bending curves.

Additional hysteresis curves were created in Figure 3.15 for the last cycle (cycle 3) of the three applied moments for axial rotation. This figure shows not only the difference in motion achieved at the three load levels, but also that the curve is similarly shaped at all applied moment levels.

3.3.3.2 Range of Motion and Neutral Zone

ROM and NZ were calculated using the segmental rotation and applied moment data from the final loading cycle. The applied moment data were only known for the entire specimen, not at the segment levels. Thus, NZ could only be shown for the overall motion of the specimen.

With three trials run for each motion and applied moment, the overall (L1-L4) mean and standard deviation were calculated for the overall +ROM (*i.e.* flexion, left lateral bending, and left axial rotation), -ROM (*i.e.* extension, right lateral bending, and

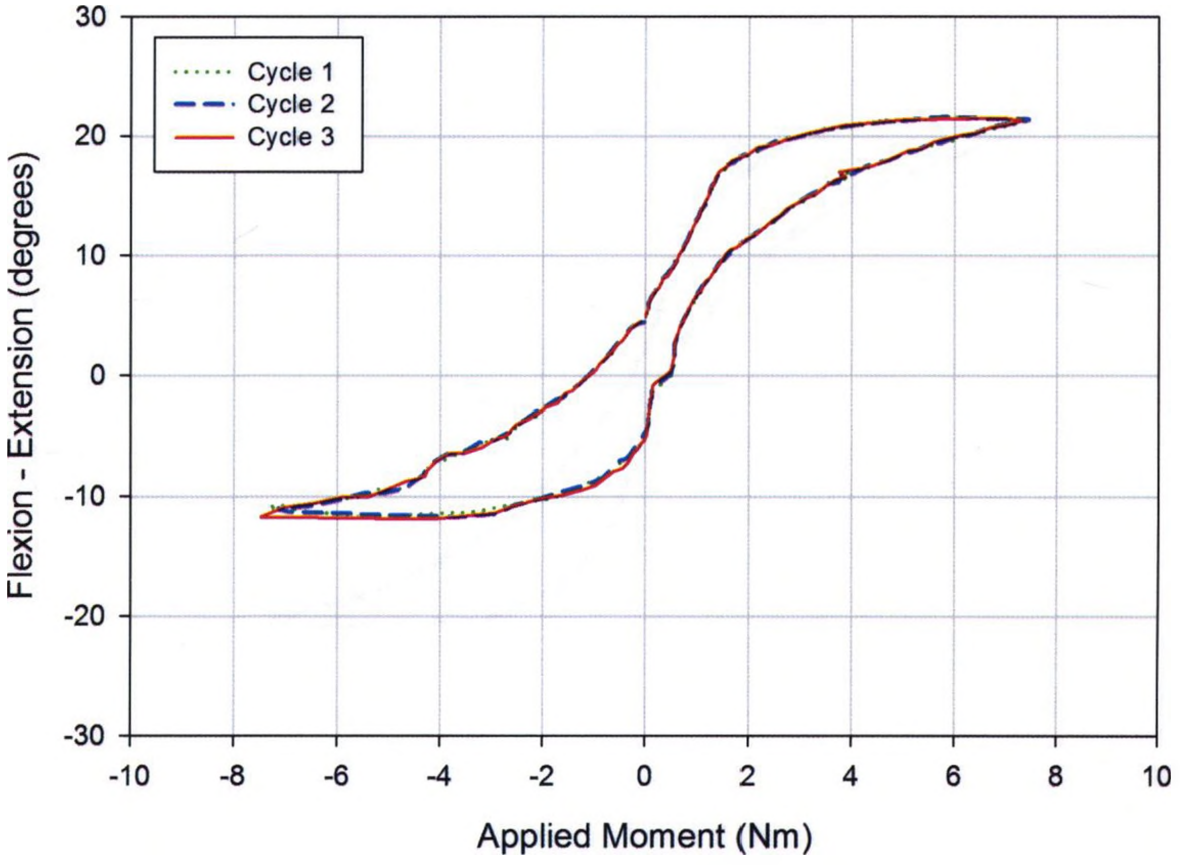

Figure 3.12 Hysteresis Curves of Flexion-Extension versus Applied Moment
The three loading cycles are shown for the flexion-extension rotation achieved with the application of a 7.5 Nm pure bending moment. The final cycle (red solid line) was used for calculation of NP and NZ, based difference in the cycle at 0 Nm.

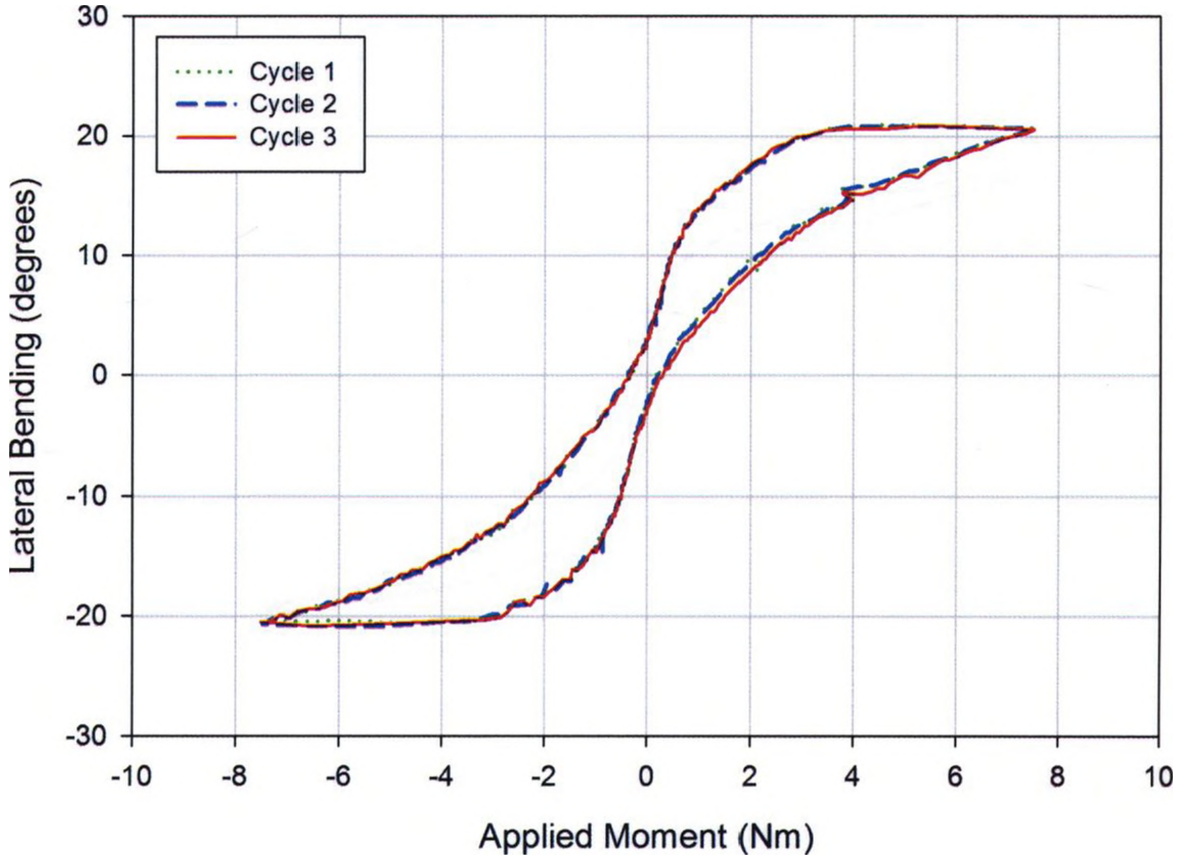

Figure 3.13 Hysteresis Curves of Lateral Bending versus Applied Moment
The three loading cycles are shown for the lateral bending rotation achieved with the application of a 7.5 Nm pure bending moment. The final cycle (red solid line) was used for calculation of NP and NZ, based difference in the cycle at 0 Nm.

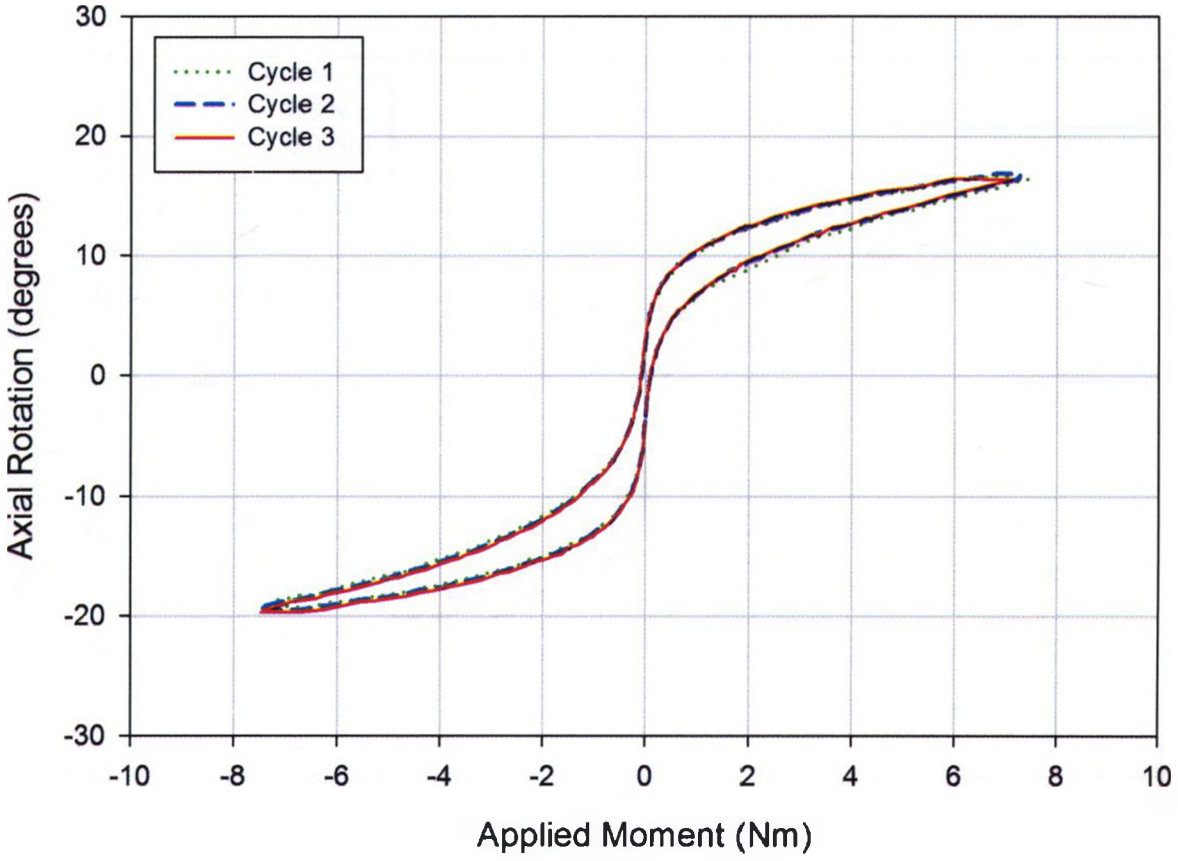

Figure 3.14 **Hysteresis Curves of Axial Rotation versus Applied Moment**
The three loading cycles are shown for the axial rotation achieved with the application of a 7.5 Nm pure bending moment. The final cycle (red solid line) was used for calculation of NP and NZ, based difference in the cycle at 0 Nm.

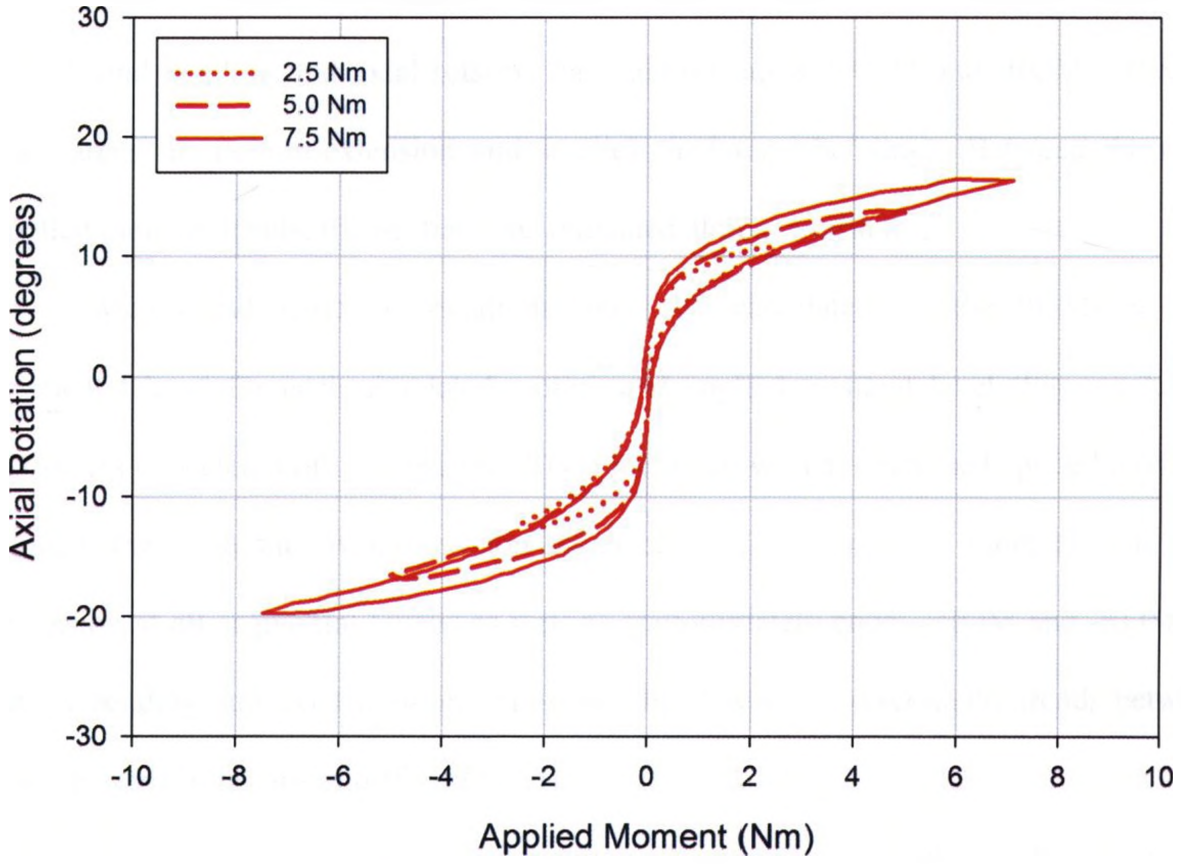

Figure 3.15 Hysteresis Comparison for the Three Applied Moment Levels
The hysteresis curves from the final loading cycle for each of the three applied moments (2.5, 5, and 7.5 Nm) are shown for the axial rotation trials. A similar shape is seen for each of the three curves. The other cycle curves have been omitted for clarity.

right axial rotation), and NZ. Figure 3.16 shows the mean data for these motion parameters for each of the simulated motions and applied moment levels. As expected, both +ROM and -ROM increase with an increase in applied moment. Also, this chart reveals that the largest ROM occurred in flexion (+ROM) for the lumbar specimen used and the smallest ROM was seen in extension. Different from the flexion-extension case, both lateral bending and axial rotation have almost equal +ROM and -ROM. The NZ was largest in flexion-extension and smallest in lateral bending. Between the three applied moment levels, the neutral zone remained almost constant.

Means and standard deviations were also calculated for the ROMs at each segmental level for each simulated motion and applied moment level (Figures 3.17 – 3.19). As expected, both +ROM and -ROM increased with an increased applied moment. Similar trends to the overall motion mean data existed, such as more flexion than extension at all segmental levels, as well as approximately equal +ROM and -ROM for lateral bending and axial rotation. However, there were no discernable trends between the segmental rotations at different levels.

Repeatability of the simulated motions was assessed by comparing the means and standard deviations for all motion parameters calculated. Complete tables of these data including +ROM (segmental and overall), -ROM (segmental and overall), and NZ (overall) are shown in Tables 3.1 – 3.4. Examining each table shows that the motions created at each load level were highly repeatable for both the overall motion, as well as the segmental motion, with nearly all standard deviations being less than one degree.

The reproducibility was also measured by comparing the means and standard deviations of ROM and NZ of axial rotation at 7.5 Nm in the starting setup (*i.e.* Step #1,

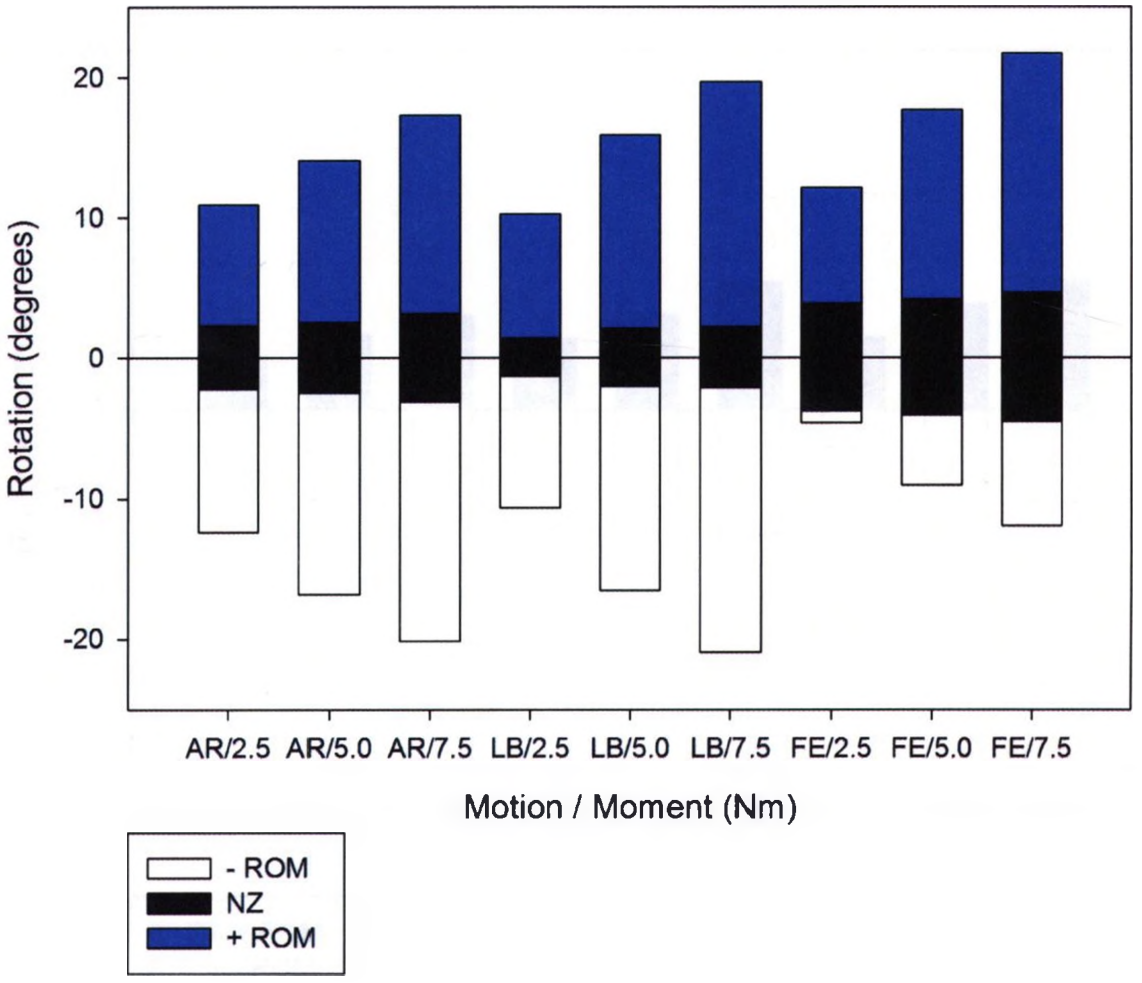

Figure 3.16 Mean Values for ±ROM and NZ for L1-L4 Motions / Moments
The values shown for +ROM, -ROM, and NZ represent the averaged value from the three trials for each motion / moment (AR = axial rotation; LB = lateral bending; FE = flexion-extension). In all cases, the standard deviations were less than 1.3°, and therefore have not been included due to visualization difficulties at this scale.

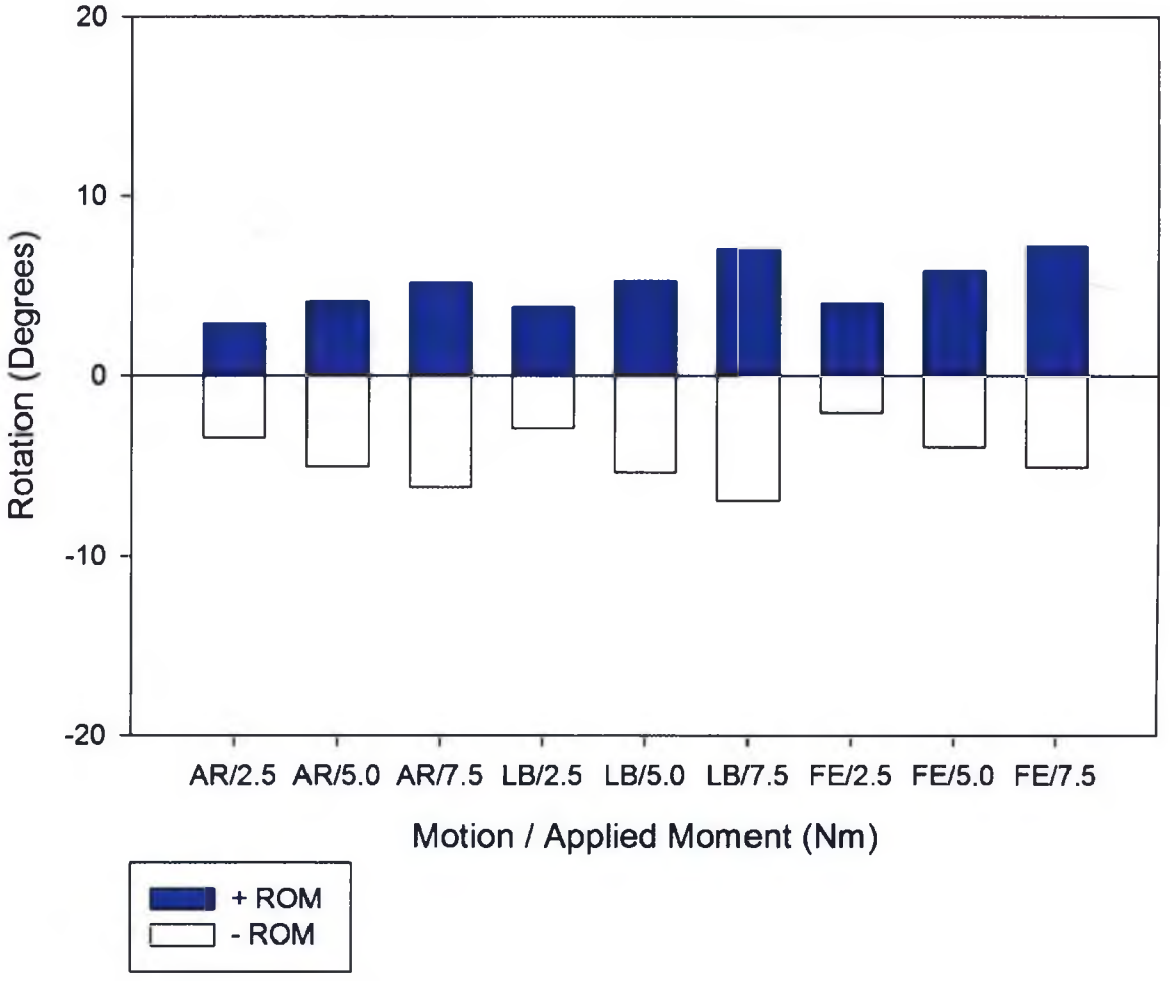

Figure 3.17 Mean Values for ±ROM for L1-L2 Segmental Motions / Moments
The values shown for +ROM and -ROM represent the averaged value from the three trials for each motion / moment (AR = axial rotation; LB = lateral bending; FE = flexion-extension). In all cases, the standard deviations were less than 1°, and therefore have not been included due to visualization difficulties at this scale.

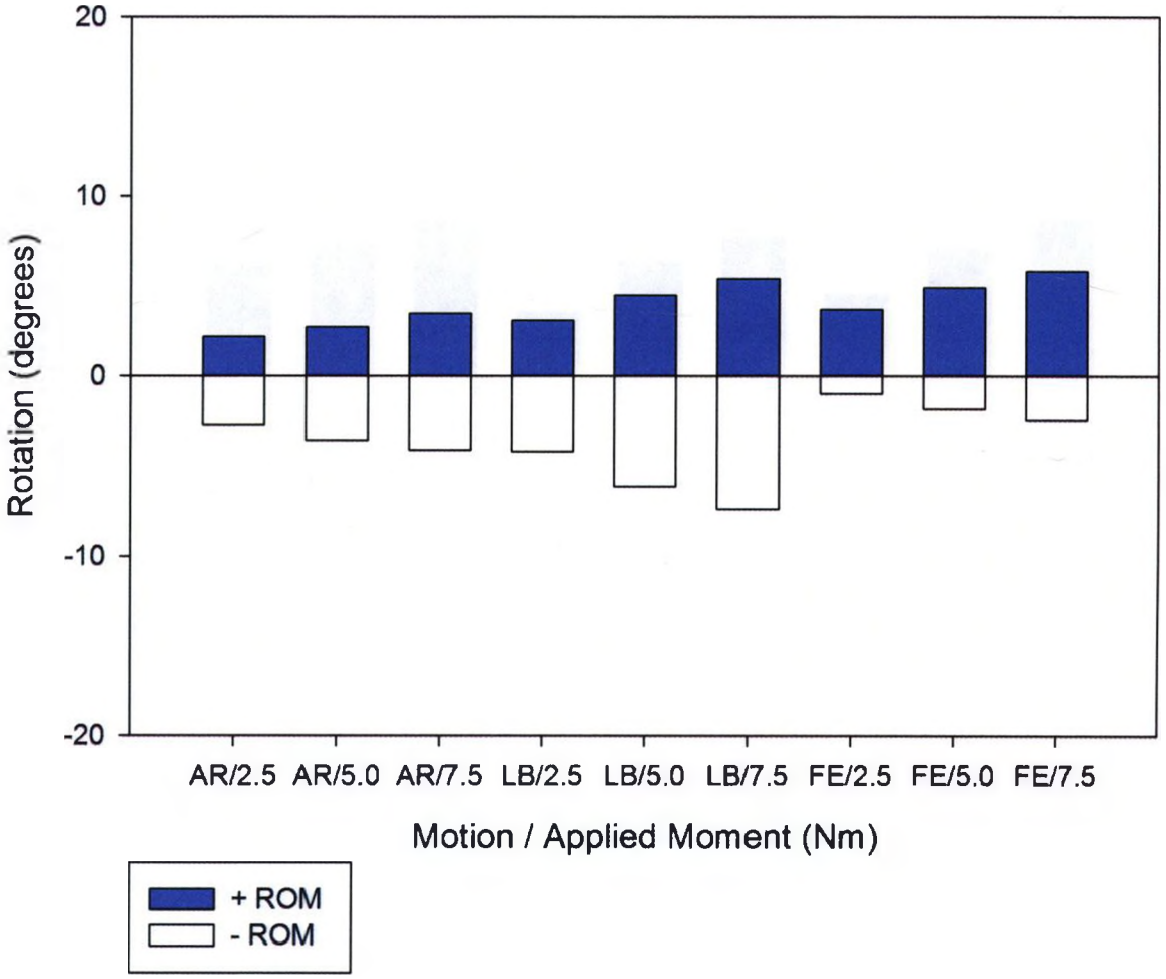

Figure 3.18 **Mean Values for ±ROM for L2-L3 Segmental Motions / Moments**
The values shown for +ROM and -ROM represent the averaged value from the three trials for each motion / moment (AR = axial rotation; LB = lateral bending; FE = flexion-extension). In all cases, the standard deviations were less than 0.44°, and therefore have not been included due to visualization difficulties at this scale.

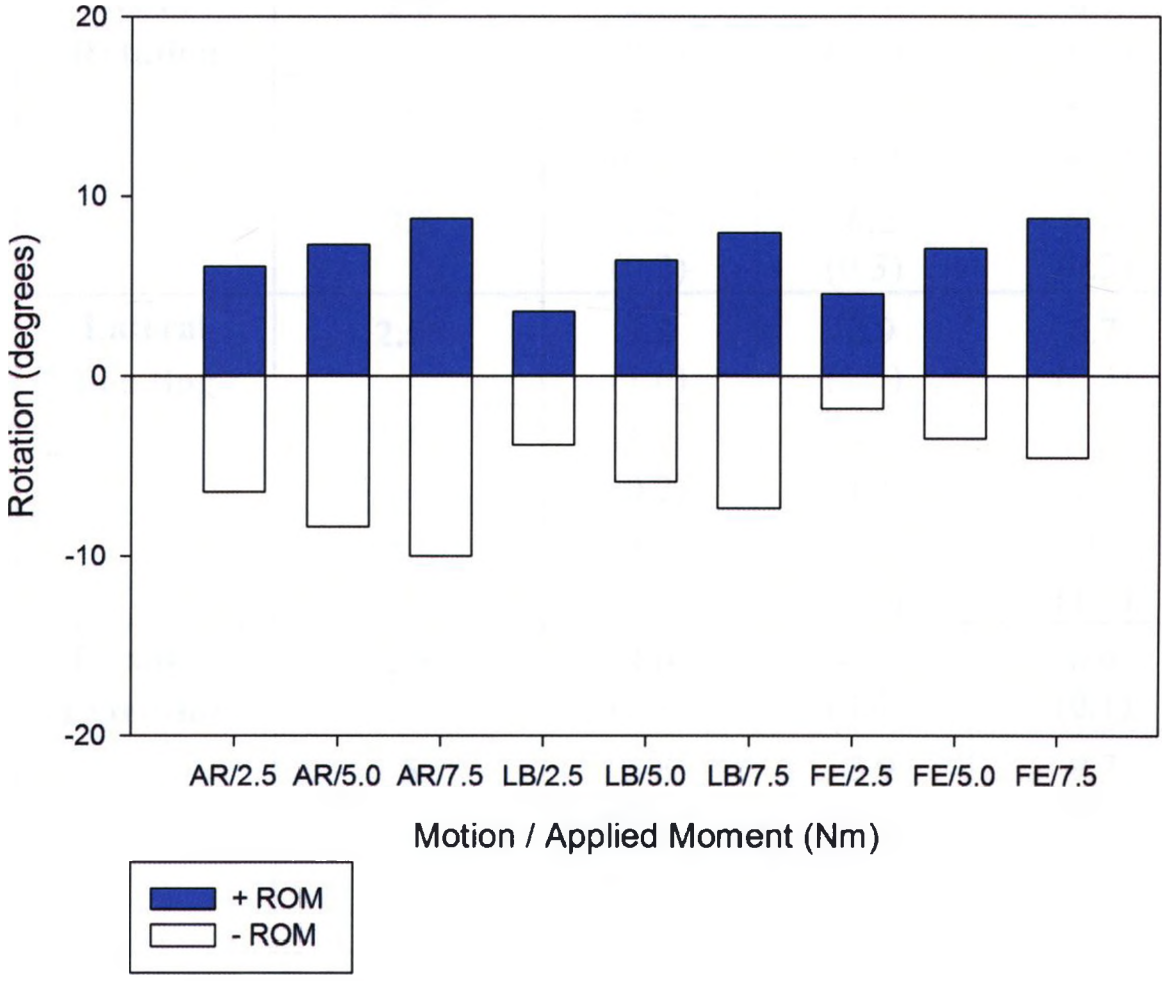

Figure 3.19 Mean Values for ±ROM for L3-L4 Segmental Motions / Moments
The values shown for +ROM and -ROM represent the averaged value from the three trials for each motion / moment (AR = axial rotation; LB = lateral bending; FE = flexion-extension). In all cases, the standard deviations were less than 0.66°, and therefore have not been included due to visualization difficulties at this scale.

L1-L2				
Motion	**Load (Nm)**	**Mean +ROM (°) (SD)**	**Mean -ROM (°) (SD)**	**Mean Total ROM (°) (SD)**
Axial Rotation	**2.5**	2.9 (0.2)	-3.4 (0.2)	6.3 (0.1)
	5	4.1 (0.2)	-5.0 (0.2)	9.1 (0.1)
	7.5	5.2 (0.2)	-6.2 (0.3)	11.3 (0.3)
Lateral Bending	**2.5***	3.8 (1.0)	-2.9 (1.3)	6.7 (0.3)
	5	5.2 (0.2)	-5.3 (0.9)	10.5 (1.1)
	7.5	7.0 (1.3)	-6.9 (0.4)	14.0 (1.7)
Flexion - Extension	**2.5**	4.0 (0.1)	-2.0 (0.0)	6.0 (0.1)
	5	5.8 (0.2)	-3.9 (0.3)	9.7 (0.2)
	7.5	7.2 (0.2)	-5.1 (0.1)	12.3 (0.1)

Table 3.1 **Segmental Range of Motion (ROM) at the L1-L2 Level**
The means and standard deviations (SD) are shown for the +ROM and -ROM, as well as total ROM for three trials of each motion and applied moment. The simulator achieves a high level of repeatability at nearly every load level, with the overall maximum standard deviation being 1.7°. (* Only two trials were used for the 2.5 Nm lateral bending case, due to data loss.)

L2-L3				
Motion	**Load (Nm)**	**Mean +ROM (°) (SD)**	**Mean -ROM (°) (SD)**	**Mean Total ROM (°) (SD)**
Axial Rotation	**2.5**	2.2 (0.2)	-2.7 (0.2)	4.9 (0.1)
	5	2.7 (0.2)	-3.6 (0.2)	6.3 (0.0)
	7.5	3.4 (0.1)	-4.1 (0.2)	7.5 (0.2)
Lateral Bending	**2.5***	3.1 (0.3)	-4.2 (0.4)	7.3 (0.2)
	5	4.5 (0.1)	-6.1 (0.0)	10.6 (0.1)
	7.5	5.4 (0.4)	-7.4 (0.3)	12.8 (0.5)
Flexion - Extension	**2.5**	3.7 (0.1)	-1.0 (0.1)	4.7 (0.1)
	5	4.9 (0.0)	-1.9 (0.1)	6.7 (0.1)
	7.5	5.8 (0.1)	-2.4 (0.1)	8.2 (0.2)

Table 3.2 **Segmental Range of Motion (ROM) at the L2-L3 Level**
The means and standard deviations (SD) are shown for the +ROM and -ROM, as well as total ROM for three trials of each motion and applied moment. The simulator achieves a high level of repeatability at nearly every load level, with the overall maximum standard deviation of 0.5°. (* Only two trials were used for the 2.5 Nm lateral bending case, due to data loss.)

L3-L4				
Motion	**Load (Nm)**	**Mean +ROM (°) (SD)**	**Mean -ROM (°) (SD)**	**Mean Total ROM (°) (SD)**
Axial Rotation	**2.5**	6.1 (0.3)	-6.4 (0.2)	12.5 (0.2)
	5	7.3 (0.1)	-8.4 (0.3)	15.6 (0.2)
	7.5	8.8 (0.5)	-10.0 (0.2)	18.8 (0.7)
Lateral Bending	**2.5***	3.6 (0.2)	-3.8 (0.4)	7.4 (0.2)
	5	6.4 (0.3)	-5.9 (0.2)	12.3 (0.2)
	7.5	7.9 (0.3)	-7.3 (0.1)	15.3 (0.4)
Flexion - Extension	**2.5**	4.6 (0.0)	-1.9 (0.1)	6.4 (0.1)
	5	7.1 (0.1)	-3.4 (0.1)	10.5 (0.2)
	7.5	8.7 (0.3)	-4.5 (0.1)	13.2 (0.4)

Table 3.3 **Segmental Range of Motion (ROM) at the L3-L4 Level**
The means and standard deviations (SD) are shown for the +ROM and -ROM, as well as total ROM for three trials of each motion and applied moment. The simulator achieves a high level of repeatability at nearly every load level, with the overall maximum standard deviation of 0.7°. (* Only two trials were used for the 2.5 Nm lateral bending case, due to data loss.)

L1-L4					
Motion	**Load (Nm)**	**Mean +ROM (°) (SD)**	**Mean -ROM (°) (SD)**	**Mean Total ROM (°) (SD)**	**Mean NZ (°) (SD)**
Axial Rotation	**2.5**	10.9 (0.1)	-12.4 (0.2)	23.3 (0.1)	4.5 (0.2)
	5	14.0 (0.2)	-16.8 (0.2)	30.9 (0.3)	5.0 (0.2)
	7.5	17.3 (0.7)	-20.2 (0.5)	37.4 (1.2)	6.3 (0.4)
Lateral Bending	**2.5***	10.2 (0.5)	-10.7 (0.5)	20.9 (0.0)	2.7 (0.3)
	5	15.8 (0.3)	-16.6 (0.3)	32.4 (0.4)	4.1 (0.6)
	7.5	19.7 (1.1)	-21.0 (0.2)	40.6 (1.0)	4.4 (0.8)
Flexion - Extension	**2.5**	12.1 (0.1)	-4.7 (0.1)	16.8 (0.1)	7.7 (0.2)
	5	17.7 (0.0)	-9.0 (0.3)	26.7 (0.3)	8.2 (0.3)
	7.5	21.7 (0.1)	-11.9 (0.2)	33.6 (0.3)	9.2 (0.4)

Table 3.4 **Overall Range of Motion (ROM) and Neutral Zone (NZ) for L1-L4** The means and standard deviations (SD) are shown for the +ROM and -ROM, as well as total ROM for three trials of each motion and applied moment. In addition, the mean and standard deviation data are shown for the NZ in this overall case. The simulator achieves a high level of repeatability at nearly every load level, with the overall maximum standard deviation of 1.2°. (* Only two trials were used for the 2.5 Nm lateral bending case, due to data loss.)

Figure 3.9) and from a second repeated setup done at the end of the testing day (*i.e.* Step #4, Figure 3.9). Additionally, the percent differences were compared between the two steps. These values are shown in Table 3.5. The reproducibility table showed that, even with a reposition of the specimen in the simulator, overall motion achieved was nearly the same value, with slight changes to the +ROM and -ROM based on the calculation of the neutral position. The percent difference between steps at all segmental levels was relatively small, with an average percent difference of 7.4%. Reproducibility of the simulator was further verified by comparing the results from Step #1, Trial 1 with those achieved in the second setup in Step #4, Trial 6. Figure 3.20 shows the comparison of the overall rotations achieved at 0.5 Nm increments between the two tests, with a strong correlation seen between the trials performed at the beginning and end of the testing protocol ($R^2 = 0.998$)

3.4 DISCUSSION

Dedicated *in vitro* biomechanical studies are needed to pre-clinically evaluate new spinal devices entering the market. To properly evaluate these devices in the laboratory environment, spinal loading simulators are required to move the specimen in a physiologic manner. Such a spinal loading simulator has been developed in this study, built as a modification to an existing Instron® materials testing machine and validated for repeatability and reproducibility of spine motion produced.

The spinal loading simulator developed in this body of work applies pure moment loads to a multi-segment cadaveric spine specimen and measures the resulting displacement (*i.e.* the flexibility protocol) (Panjabi, 1988). This was the first known, non-commercial device to use a multi-axis materials testing machine to simulate spinal

Segment	Start/End	Mean +ROM (°) (SD)	Mean -ROM (°) (SD)	Mean Overall ROM (°) (SD)	Mean NZ (°) (SD)
L1-L2	**Step 1**	5.2 (0.2)	-6.2 (0.3)	11.3 (0.3)	
	Step 4	5.9 (0.2)	-5.2 (0.3)	11.1 (0.2)	
	% Diff.	13.5	-17.1	1.9	
L2-L3	**Step 1**	3.4 (0.1)	-4.1 (0.2)	7.5 (0.2)	
	Step 4	3.7 (0.3)	-4.3 (0.2)	8.0 (0.2)	
	% Diff.	8.6	-4.5	6.4	
L3-L4	**Step 1**	8.8 (0.5)	-10.0 (0.2)	18.8 (0.7)	
	Step 4	9.7 (0.2)	-10.3 (0.5)	19.9 (0.7)	
	% Diff.	9.7	-2.8	6.0	
L1-L4	**Step 1**	17.3 (0.7)	-20.2 (0.5)	37.4 (1.2)	6.3 (0.4)
	Step 4	19.2 (0.3)	-19.6 (0.5)	38.8 (0.8)	6.9 (0.2)
	% Diff.	10.4	-2.8	3.5	8.9

Table 3.5 **Reproducibility of the Segmental Range of Motion (ROM)**
The means and standard deviations are shown for the +ROM and -ROM, as well as total ROM for three trials of axial rotation at 7.5 Nm to compare the initial Step #1 data versus the repeated data collected in Step #4. In addition, the mean and standard deviation data are shown for the neutral zone (NZ) in the overall L1-L4 case for comparison. The simulator demonstrates a strong level of reproducibility at nearly every segmental level as well as the overall case, with an average percent difference (% diff.) of 7.4%.

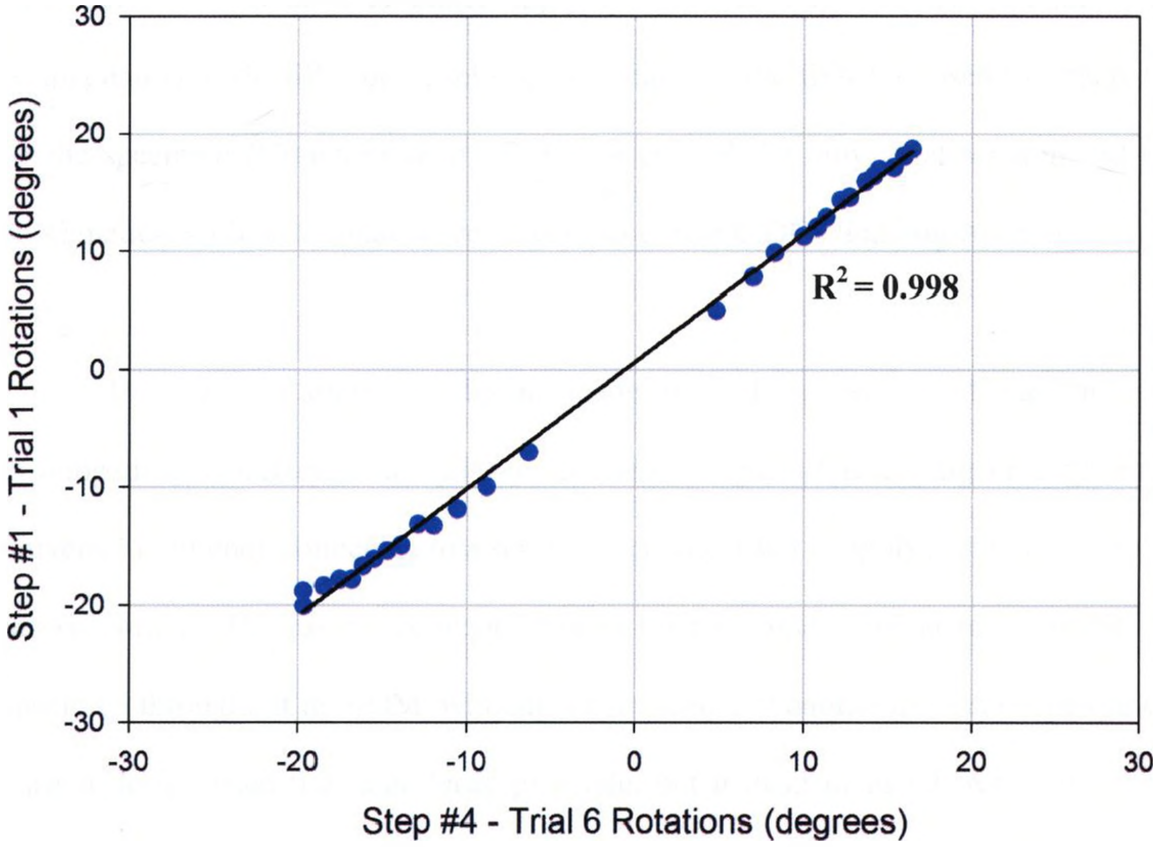

Figure 3.20 Comparison of Rotations Achieved at Start and End of Test Protocol Reproducibility was assessed by comparing the overall (L1-L4) rotations achieved between the axial rotation setup completed at the beginning of the protocol (*i.e.* Step #1 - Trial 1) and the one performed at the end of the protocol (*i.e.* Step #4 - Trial 6). Rotations were recorded at 0.5 Nm increments. A strong correlation was seen between the two setups with an $R^2 = 0.998$.

motion using only servo-hydraulics. The simulator made use of the tri-axial (two torque actuators and one axial actuator) design of the Instron® 8874 to create spine motion. Previously developed simulators, built as modifications to materials testing machines, were limited to bi-axial machines, capable of producing only one torque and axial load. This limited the effectiveness of the materials testing machine as a simulator, since the axial actuator was used to either apply an axial compressive load on the specimen (Callaghan and McGill, 2001), relieve the weight of the fixturing used to impart motion on the specimen (Crawford *et al.*, 1995), or control the only axial rotation and load in combination with additional servo motors to create 6 DOF loading (Cunningham *et al.*, 2003).

The current simulator design made use of unconstrained motion concepts developed by Goertzen *et al.* (2004). In their design, a telescoping loading arm, with universal joint ends connected to a servo motor, was used to apply a pure moment load to the specimen. This useful concept allowed for the same moment to be applied to the specimen throughout its ROM, without constraining the natural motion of the spine. The current design used the same basic principle, but instead included two loading arms to create unconstrained motion of the spine. In flexion-extension and lateral bending, the off-axis loading arm was used to create the desired motion by attaching to the off-axis actuator, while the axial loading arm connected to the axial actuator to act as a counterbalance. In axial rotation, only the axial loading arm was required to create motion, with the off-axis arm removed. The telescoping function of the axial loading arm was not required to produce unconstrained motion, since the axial actuator would move freely up and down with the spine, thus providing the same effect. With the same off-

axis loading arm used to create both flexion-extension and lateral bending, a reconfiguration of the specimen was required. While this was not an ideal design decision, the time to reconfigure the specimen was not significant and could be performed with little difficulty.

The majority of previous literature on spinal loading simulators has described the use of stand alone machines as a way to create pure moment loading (Wilke *et al.*, 1994; Gedet *et al.*, 2007; Goertzen *et al.*, 2004; Panjabi *et al.*, 2007). These independent devices were preferred over materials testing machine designs as they were capable of applying a pure moment to the specimen, where the moment-inducing device followed the motion of the spine such that the same moment was always being applied. This was historically a flaw with a fixed loading apparatus, such as a materials testing machine. With the fixed loading actuator, the moment applied along the specimen changed as the specimen rotates, or the motion of the specimen was constrained to the rotation of the actuator (Panjabi, 2007; Panjabi *et al.*, 2007). With the addition of the telescoping loading arm, the problems associated with a fixed loading actuator were non-evident. Thus, the modified materials testing machine design in the current study had the same capabilities as the popular stand alone designs.

The Instron® 8874 materials testing machine modified was a servo-hydraulic unit, thus there were associated positive and negative benefits. The hydraulic nature of this machine did allow for continuous loading of the specimen, which would be a more physiologic representation of *in vivo* motion compared to the traditional quasi-static deadweight design (Goel *et al.*, 1984; Panjabi *et al.*, 1981). Since the machine operates through the use of a physical system (hydraulics), a finite amount of time would always

exist before the actuator could respond. This was evident in the use of the axial actuator as a counterbalance system design to move up and down with the spine motion. While the actuator could be tuned to respond quicker, it could never respond instantly to the change in direction, thus a small load would always been seen on the specimen when it switched between rotations (*i.e.* from flexion to extension).

The potting fixtures used in the simulator worked well to keep the PVC fixed throughout the spine motion. However, in the pilot studies, there was noticeable specimen rotation in the cement as it appeared to have loosened. This was not completely unexpected as there was only a small amount of bone surface area available for contact with the cement, even with the additional screws added before potting. Any additional tissue remaining on the bone to which the cement fixed to could lead to loosening under an applied load with compression of the tissue. This was corrected with additional screw fixation through the PVC pipe directly into the vertebral body at multiple insertion sites for both the cranial and caudal vertebrae. After this additional fixation, no visible rotation of the vertebra within the cement was seen.

In addition to the loading simulator, a custom-designed 2D optical tracking program was developed using LabVIEW™ software to track the real-time *x,y* pixel locations of tracking beads in the camera's field of view. This allowed for the recording of segmental rotation as a marker blocks, containing three beads each, were connected to each potting fixture and the exposed vertebrae. Marker blocks and their connecting rods and fixtures were designed to be lightweight, so that they did not affect the motion of the spine. A necessary component of the design was that the connecting rods were different lengths, so that from the top-down view for axial rotation, all markers were visible.

Thus, the lower vertebra had a longer connecting rod than the upper adjacent vertebra. As a result, a slightly larger moment would be applied to the lower vertebrae, but the magnitude of the moment would be negligible with the weight of the marker block being less than 50 g at a maximum distance of 125 mm. This minimal effect (less than 0.1 Nm) would be similar to the other simulators using optical tracking methods.

The 2D tracking system developed was used to measure the planar motion created in the specimen. With these methods, it was possible to validate the repeatability and reproducibility of the simulator. While the majority of the rotation for each motion would occur in a single plane, motion of the spine was 3D. Thus, a limitation of this study was that certain motions were missed due to rotations in other planes than the one being recorded. This was evident in the data in that the actuator rotation was always greater than the overall motion seen in L1-L4. While most simulators in the literature use 3D tracking methods, the majority of these are expensive, commercial tracking systems and the design of a custom 3D tracking system was beyond the scope of this project.

The capture frequency of the camera was set at 7.5 Hz; however, this target was not always achieved, with the frequency often slowing to 4 to 5 Hz. While not as much data were collected, at the lower frequencies the pattern-matching tracking program tended to lose fewer markers than at higher frequencies. Thus, there was a trade-off between higher frequencies and more error in the data. This tendency to lose markers was reduced with the covering of all the fixtures with black cloth within the testing space to prevent any mis-seen objects. Even at the lower data collection frequencies, a clear applied moment versus rotation curve could be identified due to the modest applied loading rate of 2°/s.

A significant amount of time for this study was spent developing the data analysis programs in LabVIEW™ to analyze the calculated segmental rotations to define +ROM, -ROM, NZ, and NP. This analysis process was completely automated to calculate the described values for each trial of a specific motion and load, as well as computing the mean and standard deviation of the data for all three trials. Following this long development process, the data analysis itself took only a few minutes to compute the motion parameters for all motions and loads.

The validation of the spinal loading simulator and its motion measurement system involved evaluation of the means and standard deviations of the ROMs (segmental and overall) and NZ achieved for the moments applied for each motion. In this regard, the simulator created highly repeatable results for all motions and moments applied. In general, the standard deviations recorded were less than one degree for nearly all applied moments, with a few exceptions in lateral bending at the L1-L2 level where some standard deviations were between one and two degrees. These higher standard deviations at the most cranial level may have been affected by the mechanical set-up, where a full functional segment does not exist at the L1 level (*i.e.* no cranial T12 vertebrae), but in all likelihood can be attributed to the planar camera set-up used, where the beads on the marker block attached to L1 in the lateral bending case are furthest from the camera and most impacted by any out-of-plane motions occurring in the spine. Although the standard deviations were higher at L1-L2 in lateral bending, the initial level of repeatability was a strong case for the validity of the simulator created.

In addition to repeatability, reproducibility was assessed between the tests at the start and end of the testing day for axial rotation at 7.5 Nm. Percent differences were

calculated between the two testing times, with an average segmental percent difference of 7.4%. While this may seem high, it was possible that the material properties of the disc at this level of the specimen had changed over the course of the testing day (*i.e.* due to drying). Future testing should try to maintain hydration between tests using saline-soaked cloths wrapped around the specimen to prevent drying of the tissue. The reconfiguration of the simulator, as well as the positioning of the marker blocks (*i.e.* rotating the face to orient to the camera's field of view), could have also contributed to the difference seen between the two setups. As such, methods should be implemented (*i.e.* marking the specimen's position in the fixtures) in future tests to ensure the same setup is achieved.

The range of values found for the segmental and overall +ROM, -ROM, and NZ for each specific motion are for the most part within the range of values reported in previous literature. Using the literature data compiled in Table 1.1, the ROM values found in the current study for flexion-extension and lateral bending applied moments of 7.5 Nm are comparable to previously reported data found with similar loads. The overall flexion-extension motion for an L1-L4 specimen, summing the segmental ROMs, was reported as 19° of flexion, with 9° of extension by Panjabi *et al.* (1994). In the current work, ROM values for the same motion and load were recorded as 21.7° of flexion and 11.9° of extension. Yamamoto *et al.* (1989) recorded lumbar segmental motion for a complete lumbar spine using quasi-static loads of ±10 Nm. For similar segments in the current study, the ROM found for flexion-extension and lateral bending were quite similar for the overall motion achieved. The data found in the current study for flexion-

extension also were comparable to *in vivo* data captured by Pearcy *et al.* (1984a,b); however, knowledge of the body's loading scheme to achieve these values was unknown.

The overall and segmental ROM reported in the current study for axial rotation were larger than any previously reported data. Previous literature has typically reported values of ± 1 – 2° of axial rotation in each lumbar motion segment (Panjabi *et al.*, 1994; Yamamoto *et al.*, 1989). The values reported in the current study were approximately ± 3 – 10° for individual segments, and almost 38° of overall axial rotation for the entire segment. Previous literature has reported, however, that a large increase in axial rotation occurs in the lumbar spine with disc degeneration (Mimura *et al.*, 1994). This increase in axial rotation has been reported to be as large as 300% in some male specimens (Fujiwara *et al.*, 2000). Thus, the values seen in the current study are not unreasonable if serious disc degeneration had occurred. The level of disc degeneration was not assessed in the current study as it requires deconstruction of the specimen to expose the disc.

In the current study, NZ was only reported for the entire specimen as a whole, since only the overall applied moment was known. To quantify segmental NZs, the applied moment would have to be known at each segment. This has typically been performed in previous literature by evaluating only a single motion segment. Thus, it was difficult to compare the range of NZ found in the current study for a L1-L4 specimen as no previous literature had evaluated the NZ in such a specimen.

A limitation of this validation study was that only one specimen was used to quantify the ROM and NZ. Thus, the data recorded for ROM and NZ may not be that representative of the population as a whole; however, it did provide a means for validating the repeatability of the simulator. It was possible that the specimen used in

this study was the reason for large increase in axial rotation compared to previous literature, as well as the increased NZ. It was known that the specimen had been previously used to demonstrate a surgical procedure at the L3-L4 level, thus it was highly likely that this contributed to some altered performance compared to an intact specimen. While this possible change in performance may have altered the ROM and NZ seen in the specimen, it would not have an effect on producing repeatable motion in the simulator.

The same specimen was used for multiple pilot studies as well as for the experimental validation study. Therefore, it required multiple freeze-thaw cycles between testing dates. While these multiple freeze-thaw cycles may have had an effect on the motions seen, previously reported literature has shown that spine specimens could be put through three freeze-thaw cycles without a change in motion characteristics (Hongo *et al.*, 2008). The specimen had also experienced some drying of the IVD's after multiple testing dates, but was rehydrated with saline-soaked cloths before testing.

In conclusion, the spinal loading simulator created was able to produce unconstrained motions of the spine using the actuators of a modified Instron® materials testing machine. Through the use of a custom-developed motion measurement system, it was determined that the motions produced were highly repeatable, as well as reproducible following reconfiguration of the device. Therefore, the validation of the apparatus should allow for the spinal loading simulator to be used in a variety of future pre-clinical studies to assess biomechanical complications (*i.e.* ALE) related to orthopaedic spine surgery.

3.5 REFERENCES

Callaghan,J.P. and McGill,S.M. (2001) Intervertebral disc herniation: studies on a porcine model exposed to highly repetitive flexion/extension motion with compressive force. *Clin.Biomech.(Bristol., Avon.)* **16,** 28-37.

Craig,J.J. (1989) Introduction to Robotics: Mechanics & Control. Addison-Wesley Publishing Company Inc.

Crawford,N.R., Brantley,A.G., Dickman,C.A., and Koeneman,E.J. (1995) An apparatus for applying pure nonconstraining moments to spine segments in vitro. *Spine* **20,** 2097-2100.

Cunningham,B.W., Gordon,J.D., Dmitriev,A.E., Hu,N., and McAfee,P.C. (2003) Biomechanical evaluation of total disc replacement arthroplasty: an in vitro human cadaveric model. *Spine* **28,** S110-S117.

Fujiwara,A., Lim,T.H., An,H.S., Tanaka,N., Jeon,C.H., Andersson,G.B., and Haughton,V.M. (2000) The effect of disc degeneration and facet joint osteoarthritis on the segmental flexibility of the lumbar spine. *Spine* **25,** 3036-3044.

Gedet,P., Thistlethwaite,P.A., and Ferguson,S.J. (2007) Minimizing errors during in vitro testing of multisegmental spine specimens: considerations for component selection and kinematic measurement. *J.Biomech.* **40,** 1881-1885.

Goel,V.K., Clark,C.R., McGowan,D., and Goyal,S. (1984) An in-vitro study of the kinematics of the normal, injured and stabilized cervical spine. *J.Biomech.* **17,** 363-376.

Goertzen,D.J., Lane,C., and Oxland,T.R. (2004) Neutral zone and range of motion in the spine are greater with stepwise loading than with a continuous loading protocol. An in vitro porcine investigation. *J.Biomech.* **37,** 257-261.

Hongo,M., Gay,R.E., Hsu,J.T., Zhao,K.D., Ilharreborde,B., Berglund,L.J., and An,K.N. (2008) Effect of multiple freeze-thaw cycles on intervertebral dynamic motion characteristics in the porcine lumbar spine. *J.Biomech.* **41,** 916-920.

Mimura,M., Panjabi,M.M., Oxland,T.R., Crisco,J.J., Yamamoto,I., and Vasavada,A. (1994) Disc degeneration affects the multidirectional flexibility of the lumbar spine. *Spine* **19,** 1371-1380.

Pearcy M.J. and Tibrewal S.B. (1984a) Axial rotation and lateral bending in the normal lumbar spine measured by three-dimensional radiography. *Spine* **9**, 582-587.

Pearcy M.J., Portek I., Shepherd J. (1984b) Three-dimensional x-ray analysis of normal movement in the lumbar spine. *Spine* **9**, 294-297.

Panjabi,M., Malcolmson,G., Teng,E., Tominaga,Y., Henderson,G., and Serhan,H. (2007) Hybrid testing of lumbar CHARITE discs versus fusions. *Spine* **32,** 959-966.

Panjabi,M.M. (1988) Biomechanical evaluation of spinal fixation devices: I. A conceptual framework. *Spine* **13,** 1129-1134.

Panjabi,M.M. (2007) Hybrid multidirectional test method to evaluate spinal adjacent-level effects. *Clin.Biomech.(Bristol., Avon.)* **22,** 257-265.

Panjabi,M.M., Krag,M.H., and Goel,V.K. (1981) A technique for measurement and description of three-dimensional six degree-of-freedom motion of a body joint with an application to the human spine. *J.Biomech.* **14,** 447-460.

Panjabi,M.M., Oxland,T.R., Yamamoto,I., and Crisco,J.J. (1994) Mechanical behavior of the human lumbar and lumbosacral spine as shown by three-dimensional load-displacement curves. *J.Bone Joint Surg.Am.* **76,** 413-424.

Wilke,H.J., Claes,L., Schmitt,H., and Wolf,S. (1994) A universal spine tester for in vitro experiments with muscle force simulation. *Eur.Spine J.* **3,** 91-97.

Wilke,H.J., Jungkunz,B., Wenger,K., and Claes,L.E. (1998a) Spinal segment range of motion as a function of in vitro test conditions: effects of exposure period, accumulated cycles, angular-deformation rate, and moisture condition. *Anat.Rec.* **251,** 15-19.

Wilke,H.J., Wenger,K., and Claes,L. (1998b) Testing criteria for spinal implants: recommendations for the standardization of in vitro stability testing of spinal implants. *Eur.Spine J.* **7,** 148-154.

Yamamoto,I., Panjabi,M.M., Crisco,T., and Oxland,T. (1989) Three-dimensional movements of the whole lumbar spine and lumbosacral joint. *Spine* **14,** 1256-1260.

CHAPTER 4: SUMMARY AND FUTURE DIRECTIONS

4.1 SUMMARY

In vitro biomechanical testing allows researchers to quantify some positive, or negative, effects of new surgical methods and components, prior to *in vivo* implementation. Specific to spine biomechanics, spinal fixation and motion are two of the most frequently evaluated concepts; however, a complete understanding of these concepts does not yet exist. Complications, such as pedicle screw loosening or adjacent-level effects, resulting from the treatment methods (*i.e.* pedicle screw instrumented fusion) are still prevalent. Thus, further biomechanical testing of spinal fixation and motion is required in an effort to ultimately improve patient care.

The main goal of this work was to design and develop relevant *in vitro* testing methods to evaluate spine fixation treatments and motion. This has been accomplished through two approaches: 1) the development of a loading protocol to produce screw loosening (*i.e.* loss of fixation) in a single vertebra (Chapter 2), and 2) the design of a spinal loading simulator and associated motion tracking system, to produce and record physiologic multi-segment motion of a cadaveric spine specimen (Chapter 3).

The initial study (Chapter 2) was conducted to examine pedicle screw loosening in the human sacrum under cyclic loading, a probable cause of this mode of instrumentation failure. Using a repeated-measures study design, two screw types (one solid and one hollow) were compared against each other in terms of the initial fixation achieved within cadaveric sacra. The hollow screw was a novel concept for the sacrum; its design a possible benefit for the pedicle of the sacrum (mostly trabecular bone), based

on previous research (Schramm *et al.*, 2003). Results from the testing protocol showed that screw rotation, for each design, tended to gradually increase to six degrees, after which point both screws were grossly loose. The solid screw required more cycles and load than the hollow screw to achieve six degrees of screw rotation (*i.e.* Objective #1 – to quantify screw loosening using a relevant cyclic loading protocol in the sacrum). qCT scans showed the mode of failure was screw toggle, as has been described clinically, and thus Hypothesis #1 is accepted (an *in vitro* cyclic loading protocol producing clinically-relevant screw loosening is possible). Thus, the hollow screw does not appear efficacious in this model and Hypothesis #2 is rejected (the novel hollow screw would outperform the solid screw). Therefore, its use in the sacrum is not recommended, which is consistent with previous literature cautioning its use in other vertebral bodies (Ferguson *et al.*, 2002).

The second study included in this thesis (Chapter 3) aimed to create motion in a multi-segment spine through the use of a spinal loading simulator. The simulator was designed and built as a modification to an existing Instron® materials testing machine, using its two actuators, axial and off-axis, to successfully produce unconstrained pure applied moments of flexion-extension, lateral bending, and axial rotation (*i.e.* Hypothesis #3 is accepted – a modified materials testing machine could produce motion in a multi-segment spine). Motion of the specimen was tracked using a camera and custom-written LabVIEW™ software for 2D planar tracking and kinematic analysis to determine motion parameters, such as range of motion and neutral zone. Based on an experimental validation study, the repeatability of the simulator was very strong, with a maximum standard deviation of 1.7° (based on all the segmental rotations calculated). The

reproducibility of the simulator was also promising (*i.e.* Hypothesis #4 is accepted – the motions produced could be quantified in a repeatable and reproducible manner). The spinal loading simulator proved to be an effective and reliable method of producing spinal motion in an *in vitro* setting (*i.e.* Objective #2 – to design a spinal loading simulator).

4.2 STRENGTHS AND LIMITATIONS

4.2.1 Screw Loosening Study

This was the first known study to quantify pedicle screw loosening using cyclic flexion-extension bending moments applied to the screw in an *in vitro* sacral model. This was a clinically relevant loading mode as *in vivo* loosening has been previously shown to be the result of cyclic loading of the screw, and the largest bending moments occur in flexion-extension. Furthermore, the use of the custom optical tracking system allowed for real-time analysis of the screw angulation relative to bone (*i.e.* loosening with bone). This was essential to the study, as the load to achieve complete screw pull-out was not used as a testing measure, or believed to be appropriate. Also, maintaining the screw within bone allowed for qCT scans of the sacra both pre- and post-loading to provide further insight into the mechanism of failure for each screw.

Limitations may have existed as a result of the *in vitro* nature of the study. Potential *in vivo* benefits may exist in the clinical setting, such as bone growth over time, which cannot be duplicated in the laboratory. This would clearly be of benefit to the hollow screw; however, the overall goal of this *in vitro* study was to evaluate the fixation available in the S1 pedicle in the immediate post-operative period. If the pedicle screw

design cannot provide adequate stability to withstand cyclic loading in this initial time frame, the fixation system would likely fail through loosening and the clinical goal of achieving fusion would not occur. While bone growth into the hollow screw would no doubt increase the long-term stability, without such initial stability, bone ingrowth could never take place.

4.2.2 Spinal Loading Simulator

There have been previous examples of spine loading devices built as a modification to an actuator of a material testing machine (Cunningham *et al.*, 2003; Crawford *et al.*, 1995; Callaghan and McGill, 2001), but this was the first reported use of a tri-axial machine (*i.e.* two actuators), in combination with the custom modification components (*i.e.* loading arms, potting fixtures, and counterbalance), to create continuous physiologic spinal motion. Based on the initial results, this design has been shown to produce highly repeatable loading patterns, and reproducible results.

A potential drawback to the current design of the simulator was that it required a reconfiguration of the apparatus and rotation of the specimen between applying flexion-extension and lateral bending. While the reproducibility results showed that reconfiguring the apparatus produced similar results, with only a reasonably small percent difference, there was additional time involved in setting up the new configuration and potential for unnecessary error. This drawback could be accounted for in a future design with the addition of a third actuator to produce either flexion-extension or lateral bending without reconfiguring the apparatus.

The custom 2D optical tracking system used in the validation study was not ideal for this application. When simulating one physiologic motion of the spine (*i.e.* flexion-

extension), motions in other planes also occur due to the complex spinal geometry and passive stabilizers. Small out-of-plane rotations could not have been detected by the tracking system used; however, it was reasonable to assume that these rotations were significantly smaller than the primary rotation being produced as a result of the loading applied. Commercial 3D tracking systems are available, such as the Optotrak Certus™, and would be an asset to this testing protocol, but these systems are very expensive. Designing a custom 3D system would have been possible, but was beyond the scope of the current work. In contrast, the 2D system used in this study was relatively inexpensive, required only one camera view, and was shown to have produced results similar to those obtained with 3D methods for the motions studied.

Finally, the goal of a spinal loading simulator is to produce motions of a spine specimen similar to those experienced *in vivo*. However, the ability to create these motions in a laboratory environment is highly difficult, if not impossible, as the true physiological loading conditions are not completely known. Thus, the limitation exists in all spinal loading simulators that true physiology of the spine cannot be fully reproduced. As such, these devices are meant only to provide a close representation of what researchers and surgeons believe happens in the spine during its complex loading scenario. Therefore, any resulting data captured from *in vitro* studies are only a possible indication of what would occur *in vivo*.

4.3 FUTURE DIRECTIONS

With the completion of these two initial studies, the groundwork has been laid for considerable future work in spine biomechanics in Western's Biomechanical Testing Laboratory. The majority of this work will come in the continued development and

improvement of the spinal loading simulator for the assessment of surgical methods and devices. Numerous components of the design still need to be properly addressed to provide a closer representation to the *in vivo* scenario. These include ideas such as improving the actuator control methods and more accurately, and specifically, quantifying the segmental loading.

Based on current literature, one potential concept to be considered is the incorporation of a compressive follower load along the spine, as a method to simulate the compressive loading of the *in vivo* spine due to the weight of the head and torso. This concept has gained popularity in other spinal loading simulators (Patwardhan *et al.*, 1999; Niosi *et al.*, 2006), yet the effects of the application of follower load versus the actual compressive load on the spine in the body remain not well understood.

Eventually, it is hoped that the complications associated with fusion in the multi-segment spine can be evaluated, such as adjacent-level effects. Furthermore, there are many new devices entering the market to counteract these effects, based on the concept of dynamic stabilization. Through the use of the simulator as a tool for the assessment of orthopaedic interventions, these devices could be thoroughly evaluated on a motion preservation basis. Before any studies can take place, however, a 3D optical tracking system will be required, such as the Optotrak Certus™. This has become the standard measurement tool for tracking spinal motion and would be a more robust system than that of the custom design used for this work.

In addition to the simulator work, the cyclic loading protocol used to assess pedicle screw loosening shows significant promise for future comparative studies. This protocol can now be used to readily test other screw types, a variety of screw design

factors (*i.e.* length and diameter), and the possible addition of cement and similar new biomaterials to increase fixation strength. This loading protocol could also be adapted to evaluate pedicle screw loosening in a multi-level instrumented specimen using the spinal loading simulator.

4.4 CLINICAL RELEVANCE

Biomechanical testing of the spine has developed and evolved over the past few decades as an essential method for evaluating new surgical methods and components. By evaluating the benefits, or harms, of the concepts, these biomechanical testing protocols, and their associated results, have provided invaluable assistance to the clinician and, more importantly, to the patient.

As seen in the initial study in Chapter 2, the novel hollow screw was less resistant to loosening when compared to a conventional solid pedicle screw in this sacral model under cyclic loading. While the results do not improve the fixation capabilities for lumbosacral fusion, the biomechanical research performed in this study does provide important clinical information regarding the potential use of a hollow screw in sacral fixation. Future development for sacral screw designs should continue to improve the ability to maintain fixation in trabecular bone under dynamic cyclic loading.

Similarly, the development of spinal loading simulator has provided an essential platform for numerous surgical methods and components to be evaluated and quantified. Simulator research and biomechanical testing has a large impact on clinical methods in the treatment of spinal disorders, and this can only be expected to continue for the near future.

4.5 REFERENCES

Callaghan,J.P. and McGill,S.M. (2001) Intervertebral disc herniation: studies on a porcine model exposed to highly repetitive flexion/extension motion with compressive force. *Clin.Biomech.(Bristol., Avon.)* **16,** 28-37.

Crawford,N.R., Brantley,A.G., Dickman,C.A., and Koeneman,E.J. (1995) An apparatus for applying pure nonconstraining moments to spine segments in vitro. *Spine* **20,** 2097-2100.

Cunningham,B.W., Gordon,J.D., Dmitriev,A.E., Hu,N., and McAfee,P.C. (2003) Biomechanical evaluation of total disc replacement arthroplasty: an in vitro human cadaveric model. *Spine* **28,** S110-S117.

Ferguson,S.J., Winkler,F., and Nolte,L.P. (2002) Anterior fixation in the osteoporotic spine: cut-out and pullout characteristics of implants. *Eur.Spine J.* **11,** 527-534.

Niosi,C.A., Zhu,Q.A., Wilson,D.C., Keynan,O., Wilson,D.R., and Oxland,T.R. (2006) Biomechanical characterization of the three-dimensional kinematic behaviour of the Dynesys dynamic stabilization system: an in vitro study. *Eur.Spine J.* **15,** 913-922.

Patwardhan,A.G., Havey,R.M., Meade,K.P., Lee,B., and Dunlap,B. (1999) A follower load increases the load-carrying capacity of the lumbar spine in compression. *Spine* **24,** 1003-1009.

Schramm,M., Krummbein,S., Kraus,H., Pitto,R.P., and Schmidt,R. (2003) Anterior vertebral body screw pullout testing with the hollow modular anchorage system--a comparative in vitro study. *Biomed.Tech.(Berl)* **48,** 356-361.

APPENDIX A: ANATOMICAL GLOSSARY

This appendix provides a list of anatomical terms used throughout this body of work to assist the lay reader (taken from Merriam-Webster's Medical Dictionary, Bethesda, MD). http://www.nlm.nih.gov/medlineplus/mplusdictionary.html

Annulus Fibrosus: A ring of fibrous tissue.

Anterior: Situated at or directed toward the front; opposite of posterior; refers to the front of the body when in the anatomical position.

Anteromedial: Directed from the front towards the mid-line of the body.

Arthrodesis: The surgical immobilization of a joint so that the bones grow solidly together.

Articular: Of or relating to a joint.

Atlas: The first vertebra of the neck.

Axial Rotation: The act of rotating the spine about the superior-inferior axis.

Axis: The second vertebra of the neck.

Bicortical: Passing through two cortical walls.

Cancellous Bone: A spongy, lattice-like structure of bone.

Caudal: Situated in or directed toward the hind; inferior to another structure, in the sense of being below it.

Cervical: The vertebrae immediately behind (posterior to) the skull and above the thoracic vertebrae.

Coccyx: A small bone that articulates with the sacrum and that usually consists of four fused vertebrae which form the terminus of the spinal column.

Contralateral: Occurring on, affecting, or acting in conjunction with a part on the opposite side of the body.

Cortical Bone: The dense, outer layer of bone; a hard shell surrounding cancellous bone.

Cranial: Directed toward the skull, superior to another structure, in the sense of being above it.

Decorticate: To remove all or part of the cortical bone.

Disc Degeneration: Deterioration of the physical structure of the intervertebral disc.
Extension: Rotation of the spine about the medial-lateral axis in a posterior direction.

Facet Joints: A synovial joint between the superior articular process of one vertebra and the inferior articular process of the vertebra directly above it.

Flexion: Rotation of the spine about the medial-lateral axis in an anterior direction.

Frontal Plane: A vertical plane that divides the body into anterior and posterior portions.

Fusion: The surgical immobilization of a joint.

Graft: To implant (living tissue) surgically.

Inferior: In anatomy, used in reference to the lower surface of a structure, or to the lower of two (or more) similar structures.

***In Situ*:** In the natural or original position or place.

***In Vitro*:** In an artificial environment outside the living organism.

***In Vivo*:** Within the living organism.

Intervertebral Disc: The tough elastic discs that are interposed between adjacent vertebrae.

Kyphosis: Outward curvature of the thoracic region of the spinal column resulting in a rounded upper back.

Lateral: Denoting a position farther from the median plane or mid-line of the body or a structure; refers to being away from the mid-line of the body when in the anatomical position.

Lateral Bending: Rotation of the spine about the anterior-posterior axis to left or right sides.

Laxity: The state of being loose.

Ligament: A band of fibrous tissue connecting bones or cartilages, serving to support and strengthen joints.

Lordotic: Forward curvature of the lumbar and cervical regions of the spinal column.

Lumbar: The vertebrae between the thoracic vertebrae and sacrum.

Lumbosacral: Of, relating to, or being the lumbar and sacral regions.

Medial: Situated towards the mid-line of the body or a structure.

Monocortical: Passing through one cortical wall.

Motion Segment: A unit of the spine used to describe the general mechanical behaviour of a region of the spine; consists to adjacent vertebrae, as well as the intervertebral disc and connecting ligaments.

Musculoskeletal: Involving both musculature and skeleton.

Neurologic: Relating to neurology; the branch of medicine concerning the structure, functions, and diseases of the nervous system.

Neurovascular: Involving both nerves and blood vessels.

Nucleus Pulposes: An elastic mass lying in the center of each intervertebral disc.

Orthopaedics: The branch of surgery dealing with the preservation and restoration of the function of the skeletal system, its articulations, and associated structures.

Osseous: Composed of bone.

Osteoporosis: A condition that is characterized by decrease in bone mass with decreased density and enlargement of bone spaces producing porosity and brittleness.

Osteotomy: A surgical operation in which a bone is divided or a piece of bone is excised (as to correct a deformity).

Pathology: The anatomic and physiological deviations from the normal that constitute disease or characterize a particular disease.

Pediatric: A branch of medicine dealing with the development, care, and diseases of children.

Pedicles: Two short pieces of bone that form the lateral sides of the vertebral arch connecting the arch to the vertebral body.

Pelvis: The bony structure located at the base of the spine.

Physiological: In accordance with or characteristic of the normal functioning of a living organism.

Posterior: Directed toward or situated at the back; opposite of anterior; refers to the back of the body when in the anatomical position.

Process: A prominent or projecting part of an organism or organic structure.

Proximal: Situated next to or near the point of attachment or origin.

Sacral: Region of the spine containing the sacrum and coccyx.

Sacroiliac: The region of the joint between the sacrum and the ilium.

Sacrum: A large, triangular bone formed by five fused vertebrae at the base of the spine; exists below the lumbar region and above the coccyx.

Sagittal Plane: The median plane that divides the body into left and right lateral sides.

Scoliosis: A lateral curvature of the spine.

Spondylolisthesis: Forward displacement of a lumbar vertebra on the one below it producing pain by compression of nerve roots.

Superior: Situated above, or directed upward.

Synovial Joint: A joint surrounded by a capsule that is filled with a lubricating fluid.

Thoracic: The vertebrae between the cervical and lumbar vertebrae.

Thoracolumbar: Of, relating to, arising in, or involving the thoracic and lumbar regions.

Trabecular Bone: See Cancellous Bone.

Transverse: Extending from side-to-side; at right angles to the long axis.

Transverse Plane: A horizontal plane that divides the body into superior and inferior portions.

Vertebra: The individual, irregular bones that make up the spinal column.

APPENDIX B: TRACKING METHODS FOR 2D MOTION ANALYSIS

In this thesis, a 2D optical tracking system was used to record the motion of beads attached to bodies of interest (*i.e.* screws and vertebrae) using pre-existing and custom-written LabVIEW™ software. This appendix describes the approach used to find the *x,y* locations of all the tracking beads in the camera's field of view (FOV). Tracking was accomplished using a pattern-matching approach; however, the methods differed slightly between the programs used for screw loosening (Chapter 2) and multi-segment spine motion (Chapter 3). The program written to track screw loosening was the initial version and used colour analysis to find the locations of the beads. Comparatively, segmental spine motion was an evolved version of the program, where black and white (B&W) analysis was used to track the motion of an increased number of beads (*i.e.* attached to each of four vertebrae).

In the screw loosening setup, two purple beads were attached to both the rod, rigidly connected to the screw, and another two purple beads to the sacrum (Figure B.1A). Since the same size and colour beads were utilized, the program used one of these beads as the template image to compare against other beads in the FOV. This was accomplished by taking a screenshot of the camera's FOV prior to loading. The template bead image was created by "cutting" it from the original screenshot and "pasting" the bead to its own image file (Figure B.1B).

Using the Vision Acquisition tools provided with LabVIEW™ software (program names shown in quotes), the template image saved was read into the program and its image learned by "IMAQ Learn Color Pattern." Camera data were continuously acquired at a resolution/colour space of 640 x 480/YUV (4:1:1) from the camera using "IMAQ1394 Grab Acquire." Each image collected by the camera was scanned with

"IMAQ Match Color Pattern" to find the similar matches in the FOV to the template image, based on a certain matching score achieved up to the number of matches requested (*i.e.* four matches for four beads). The pattern-matching program then recorded the *x,y* pixel location for all beads found in the FOV. In addition to these four beads, two additional "imaginary beads" were also calculated based on known distances from the recorded beads. This was done to help define the rigid-body motion for each object (*i.e.* screw and bone) without having to add additional beads to the FOV, which would have slowed down the capture rate. One of these beads was located roughly at the screw-bone interface, determined through an initial measurement using digital calipers from the nearest bead on the rod. The other was located near the two beads on the sacrum such that together the three beads produced approximately a right angle triangle. Pixel location data for these six beads (four real, two imaginary) were collected throughout the entire loading protocol. Further details related to the LabVIEW™ programs used for this purpose are found in Appendix C (Figures C.1 – C.4).

In the segmental motion study, marker blocks were rigidly connected to each vertebra. This allowed vertebral body motion to be tracked relative to adjacent vertebrae. In each marker, three tracking beads, with same size and shape as the loosening study, were inserted in the block to track its rigid-body motion. Since four vertebrae were used in the experimental validation study of the spinal loading simulator, a total of twelve beads needed to be tracked to quantify the motion produced.

Thus, an evolved version of the LabVIEW™ tracking program was designed such that more beads could be recorded over a larger capture resolution, since the segmental motion took place in a much larger area than screw loosening. As such, it was necessary

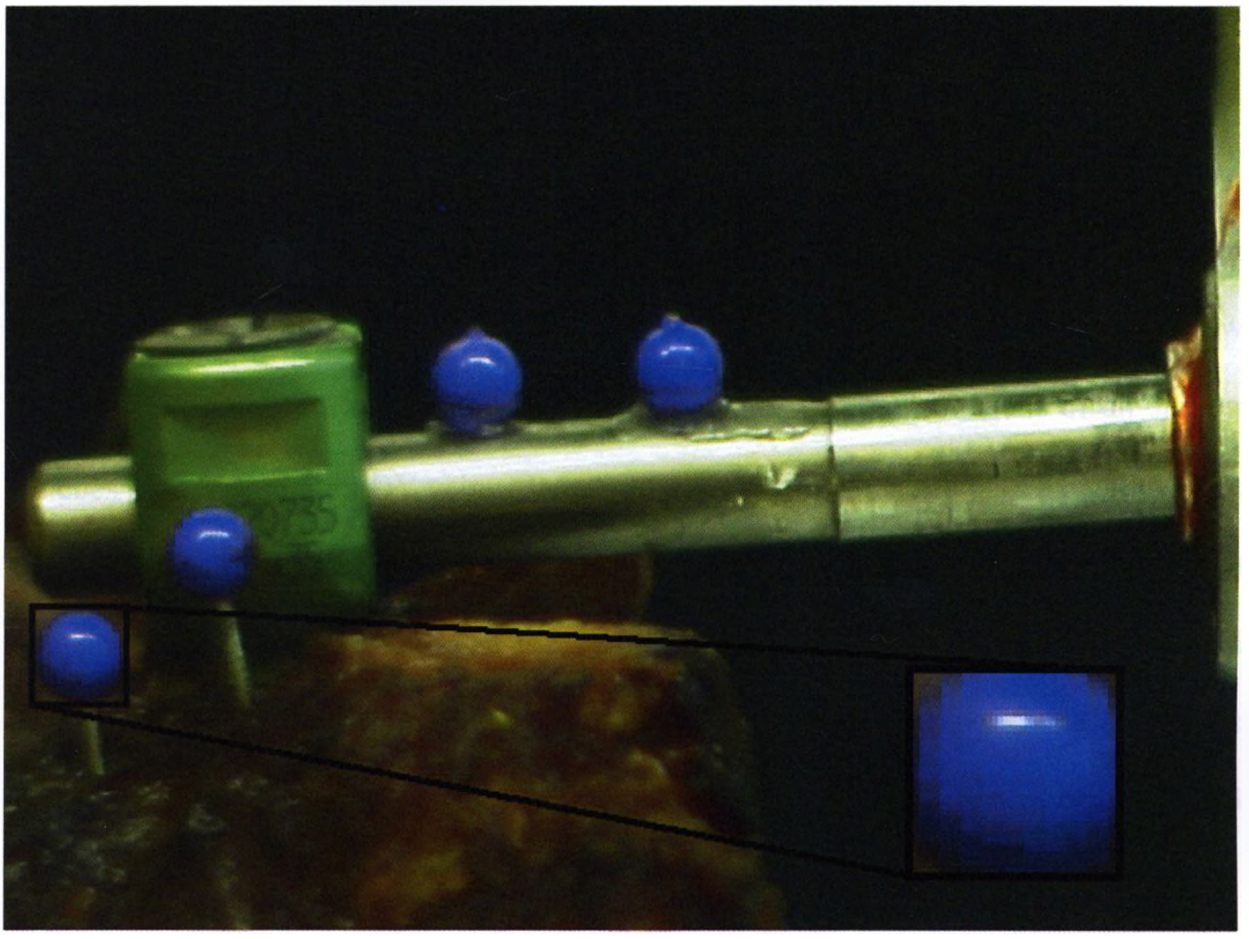

Figure B.1 **Camera Image from Screw Loosening Study**
This screenshot of the camera's field of view (FOV) shows the four tracking beads (two on screw, two on bone) used to record loosening of the screw with respect to bone. The colour pattern-matching approach used in the custom-written LabVIEW™ software used a saved template image (INSET) of one bead to match against other beads found in the FOV.

to switch from a colour video feed to a B&W feed so that more data could be recorded at the same rate. This new program used a resolution/colour space of 1280 x 960 Y (Mono 8).

The mechanics of this new program were also altered slightly from the screw loosening program. Rather than using a saved template file, the template image desired could be selected as a rectangular region of interest directly on the camera's video output window. Once a bead was highlighted, the template could be learned by the program using "IMAQ Extract" and "IMAQ Learn Pattern 2" (Figure B.2A). Similar to the screw loosening program, it would then find and record the *x,y* pixel locations of all similar matches in the camera's FOV using "IMAQ Match Pattern 2", based on a matching score and desired number of matches (Figure B.2B). After the bead locations were recorded throughout the range of motion of the specimen, the *x,y* pixel locations for the found beads were sorted into different columns of data based on marker blocks. Further details about these refined LabVIEW™ programs used for tracking and data analysis are found in Appendix C (Figures C.5 – C.8).

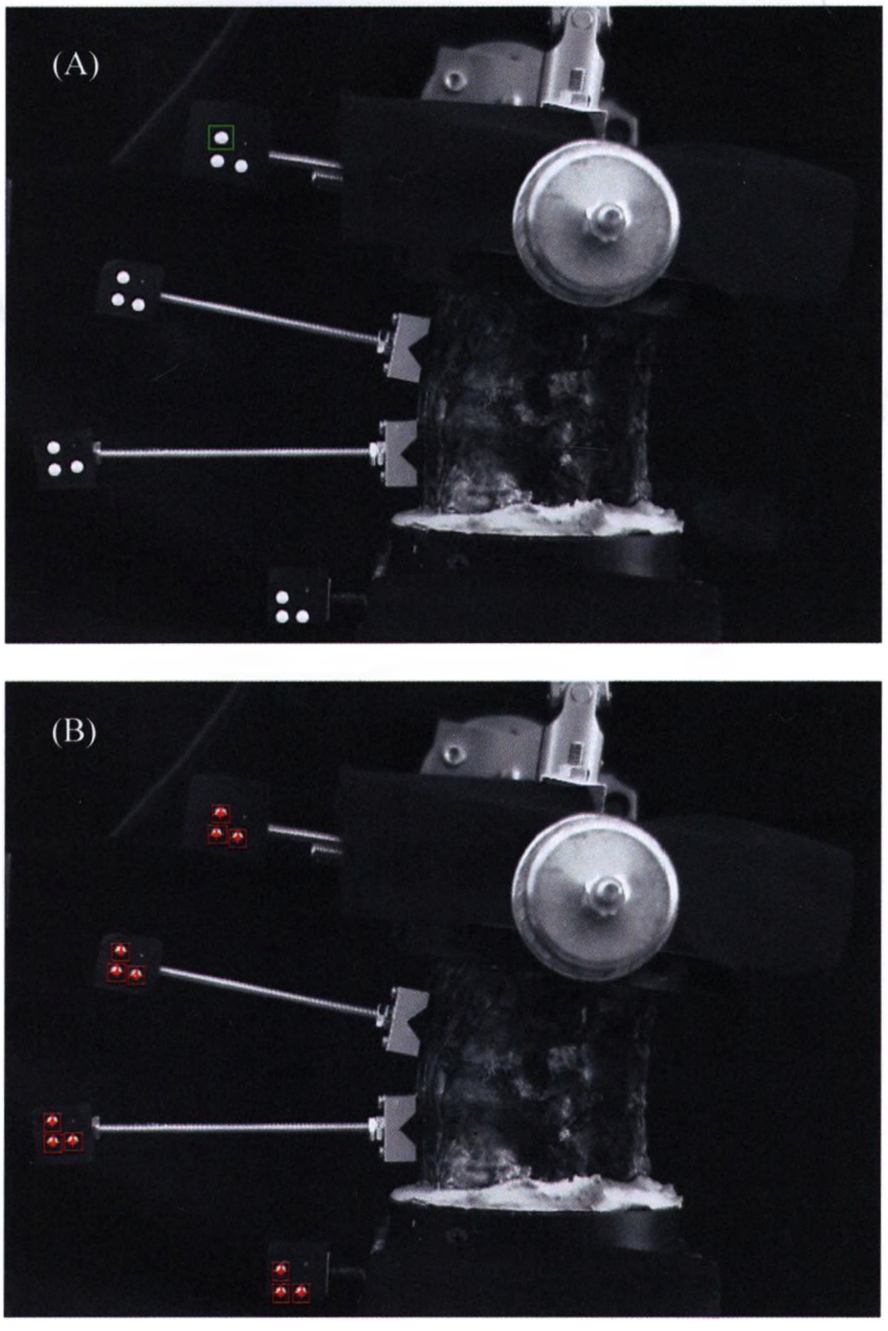

Figure B.2 **Camera Images for Segmental Motion**
(A) To locate the beads found in the camera's field of view (FOV), one bead was chosen as the template for the pattern-matching approach by highlighting the bead with a rectangular box. (B) Once learned, the template image was searched for in each image of the camera's FOV with found matches recorded and shown on the output window.

APPENDIX C: LABVIEW™ PROGRAMS FOR MOTION TRACKING AND POST-HOC ANALYSIS

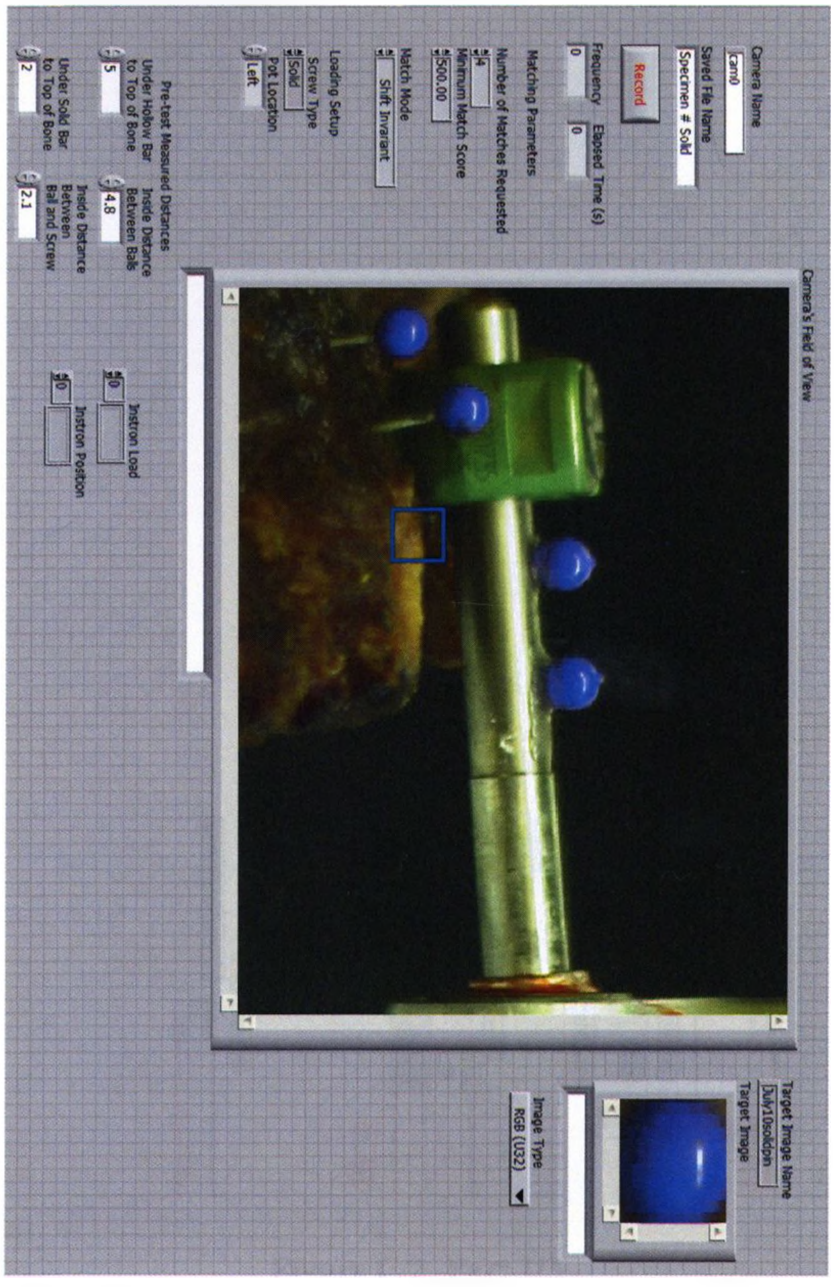

Figure C.1 **Front Panel from LabVIEW™ Program to Track Screw Loosening**
Parameters for the 2D motion tracking of the screw relative to bone were input on the front panel. These included the number of matches requested (*i.e.* number of beads), minimum match score, match mode, screw type (solid or hollow), and pot location relative to the Instron® actuator (left or right). In addition, the pre-measured distances from the furthest tracking bead on the rod to the point where screw inserted into bone (approximated by the blue highlighted box) were also input to create an "imaginary" bead location. The imaginary bead was used to represent the screw's displacement in the bone throughout the test, since it was continuously recorded as a fixed distance from the beads in motion on the rod (assuming the screw and rod to be one rigid body). During the test, the camera field of view window displayed the real-time tracking of the beads.

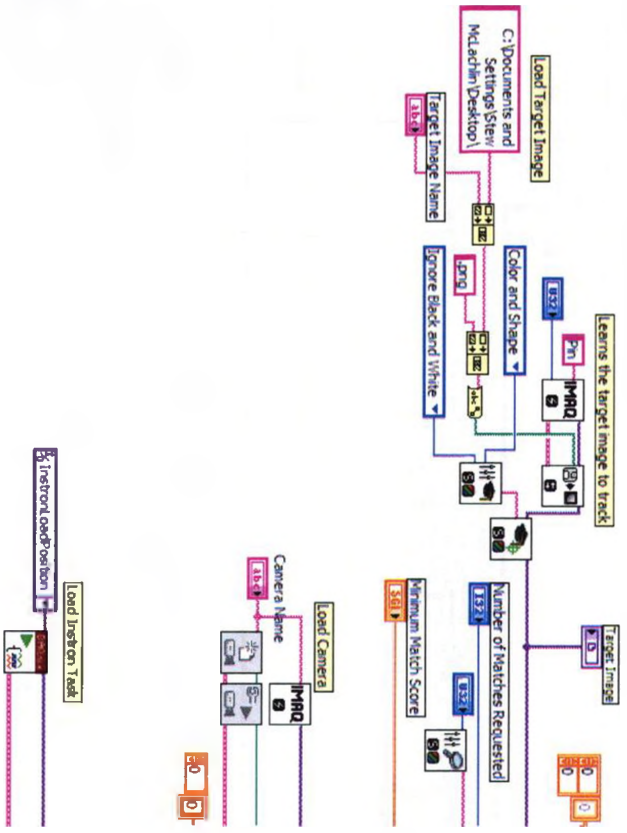

Figure C.2 -Part 1/3

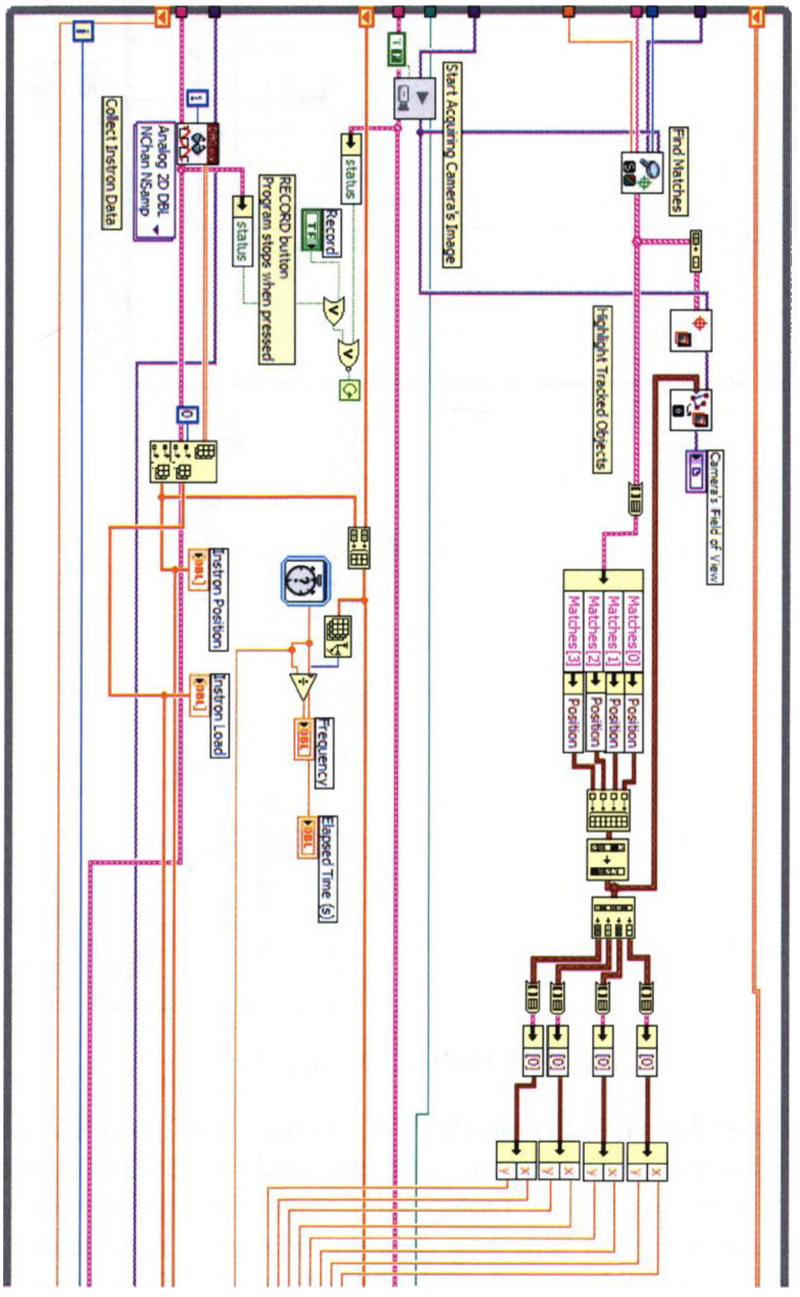

Figure C.2 -Part 2/3

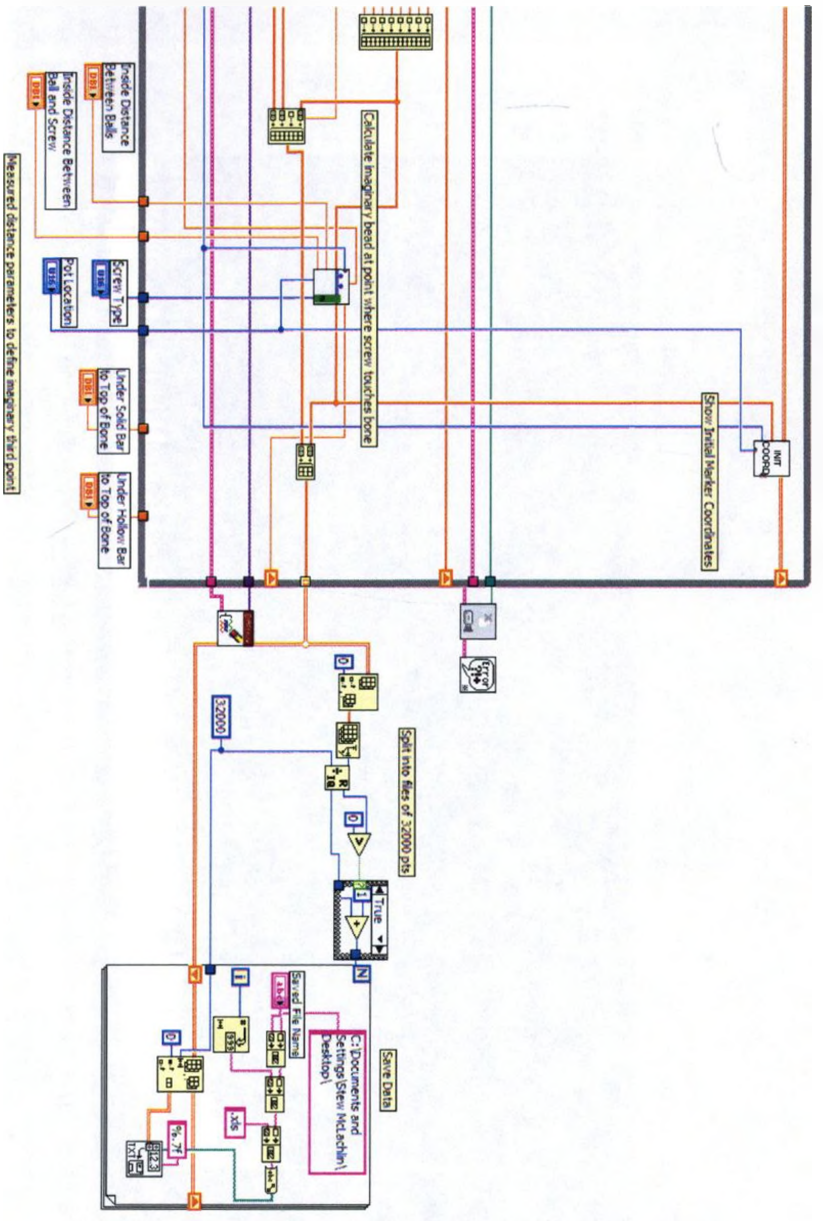

Figure C.2 -Part 3/3

Figure C.2 **Back Panel from LabVIEW™ Program to Track Screw Loosening**
Before collecting data, the program read the template image file of the desired bead and learned its colour pattern to match during the test. Camera data were continuously fed into the program, with each image scanned to find areas that matched the template image (based on a certain score achieved) up to the maximum number of matches requested. The position of an "imaginary" bead was calculated in the tracking program, based on fixed distance to the beads on the rod, to represent where the screw edge contacted bone throughout the test. Pixel *x,y* locations were saved to an Excel file following the test for the two beads on the bone, two on the rod, as well as for the calculated position of the imaginary bead.

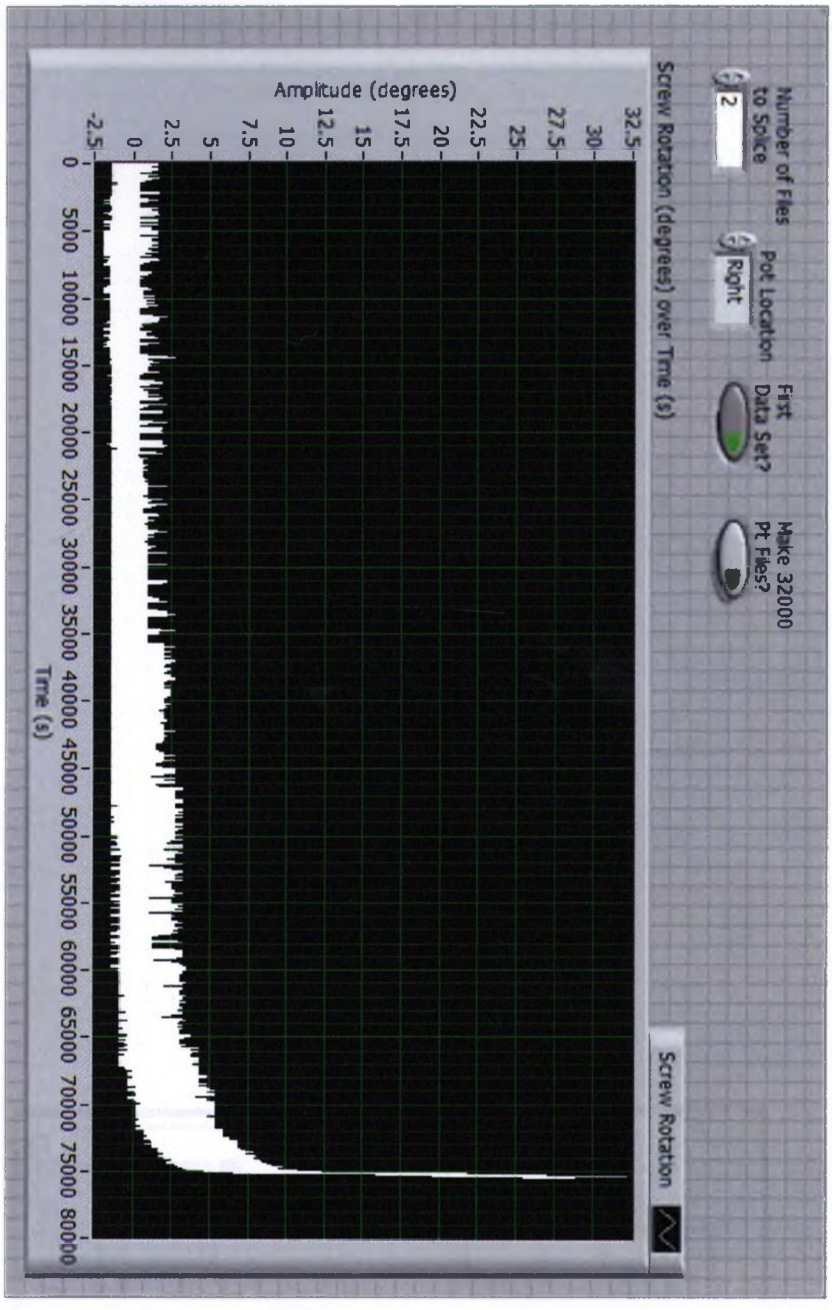

Figure C.3 **Front Panel from LabVIEW™ Program to Analyze Screw Rotation**
Pixel *x,y* locations recorded during the test for the screw and bone were analyzed to assess the screw's rotation relative to bone. On the front panel of the program, the user was required to select the number of files to splice together (if more than one had been recorded by the tracking program). As well, the pot location was selected to ensure the proper data columns were analyzed. The first data set button was selected to shift the initial rotation of the screw to represent zero degrees of rotation relative to bone. Once the positioned data had been analyzed using vector algebra and Euler angle analysis, the screw's rotation relative to bone over time was displayed on screen.

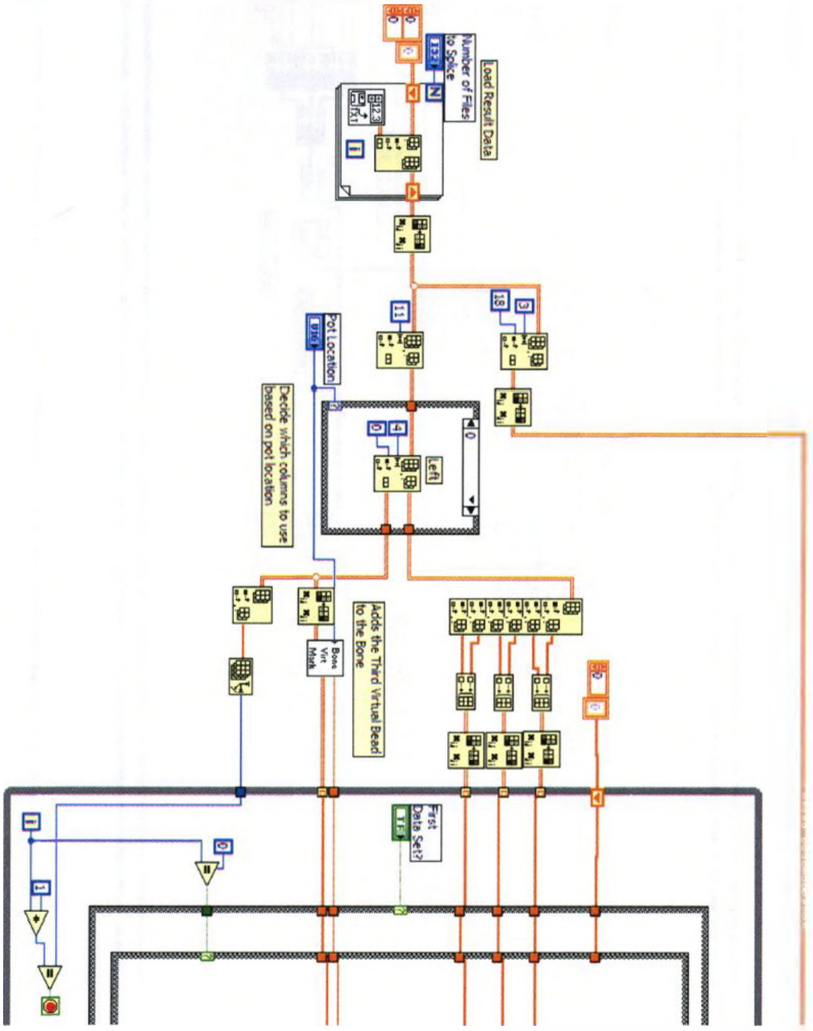

Figure C.4 -Part 1/3

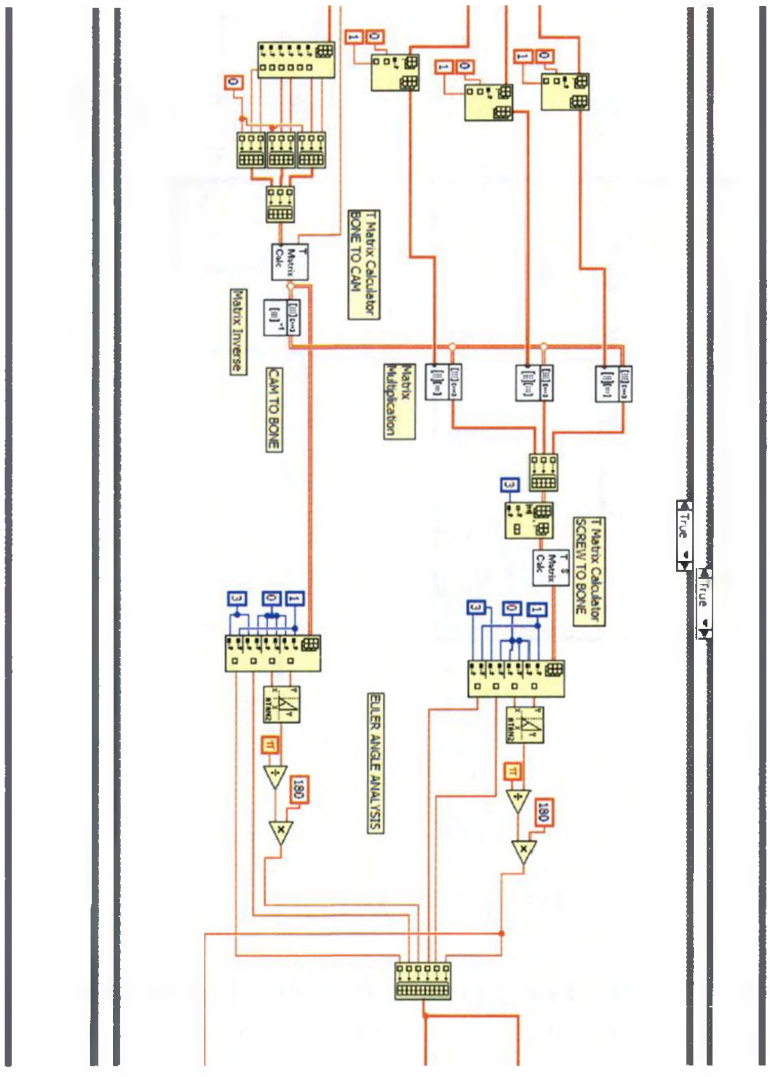

Figure C.4 -Part 2/3

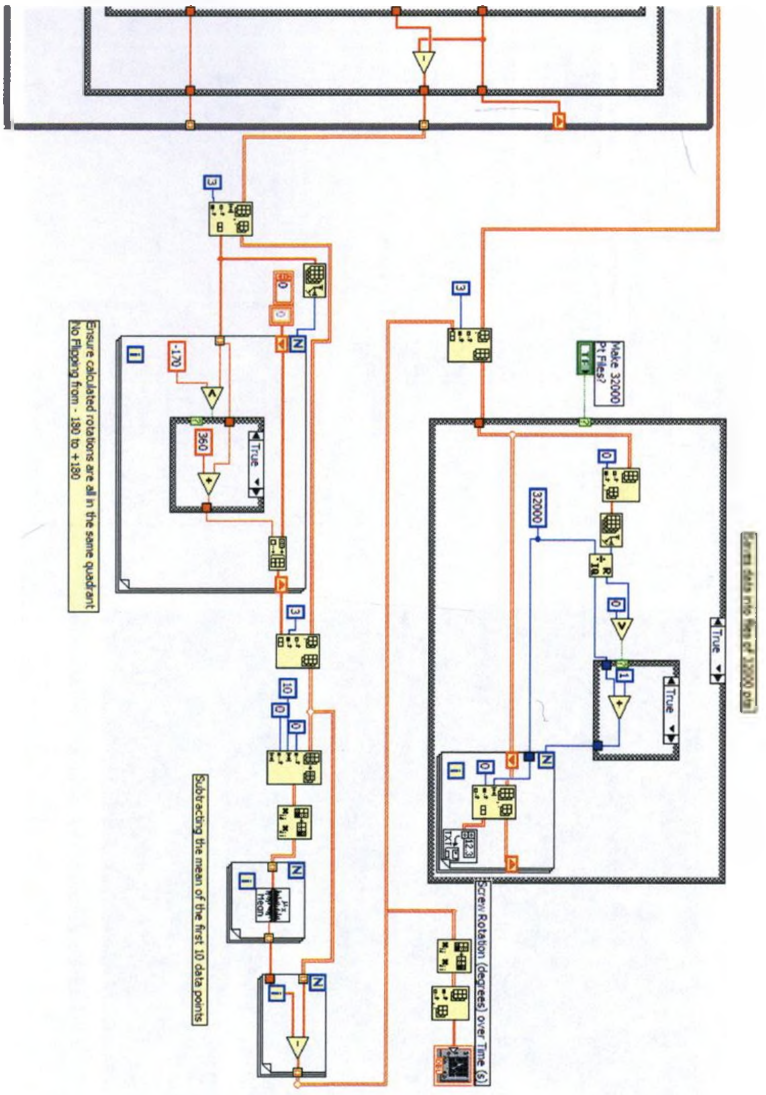

Figure C.4 -Part 3/3

Figure C.4 **Back Panel from LabVIEW™ Program to Analyze Screw Rotation**
Data collected from the tracking program was read and analyzed by the program to determine the screw's rotation throughout the test relative to bone. Before analyzing the data, a "virtual" bead was added on the bone based on initially creating a right-angled triangle with the other tracked beads on the bone. This position was then re-calculated for each row of collected data to maintain the same initial distance to the beads on the bone. Using the three beads tracked and calculated (2 real and 1 imaginary) for both the rod and bone, local coordinate systems could be defined. Rotation (R) matrices were then calculated to define the rotation of each object relative to the camera. The rotation of the rod (and screw) relative to bone could be calculated using matrix multiplication methods (*i.e* ${}^{BONE}_{ROD}[R] = {}^{CAM}_{BONE}[R]^{-1}\,{}^{CAM}_{ROD}[R] = {}^{BONE}_{CAM}[R]\,{}^{CAM}_{ROD}[R]$). Finally, using ZYX Euler angle analysis, screw rotations in the 2D plane were determined relative to bone. Analyzed rotations were shifted to centre the initial rotation at zero degrees and saved to an Excel file.

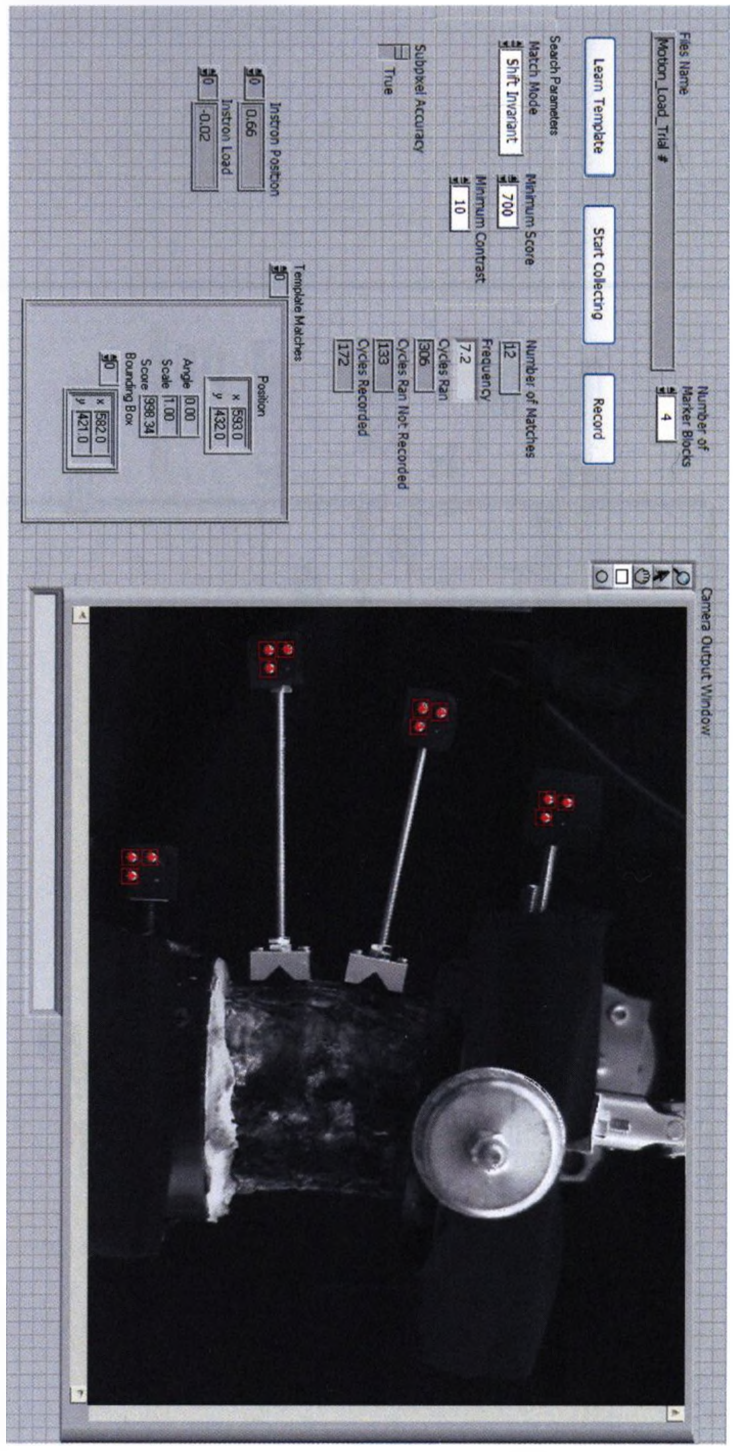

Figure C.5 **Front Panel from LabVIEW™ Program to Track Segmental Motion** Parameters for the 2D motion tracking of the segmental rotations of the spine were input on the front panel, the number of marker blocks to find. The camera's field of view window displayed the real-time tracking of the beads. The template to match was created by highlighting a box around one bead found in the camera's field of view, and clicking the "learn the template" button. Once the motion was ready to be recorded, the "start collecting" button was pushed. After the loading of the specimen was finished, data collection was stopped by pressing "record."

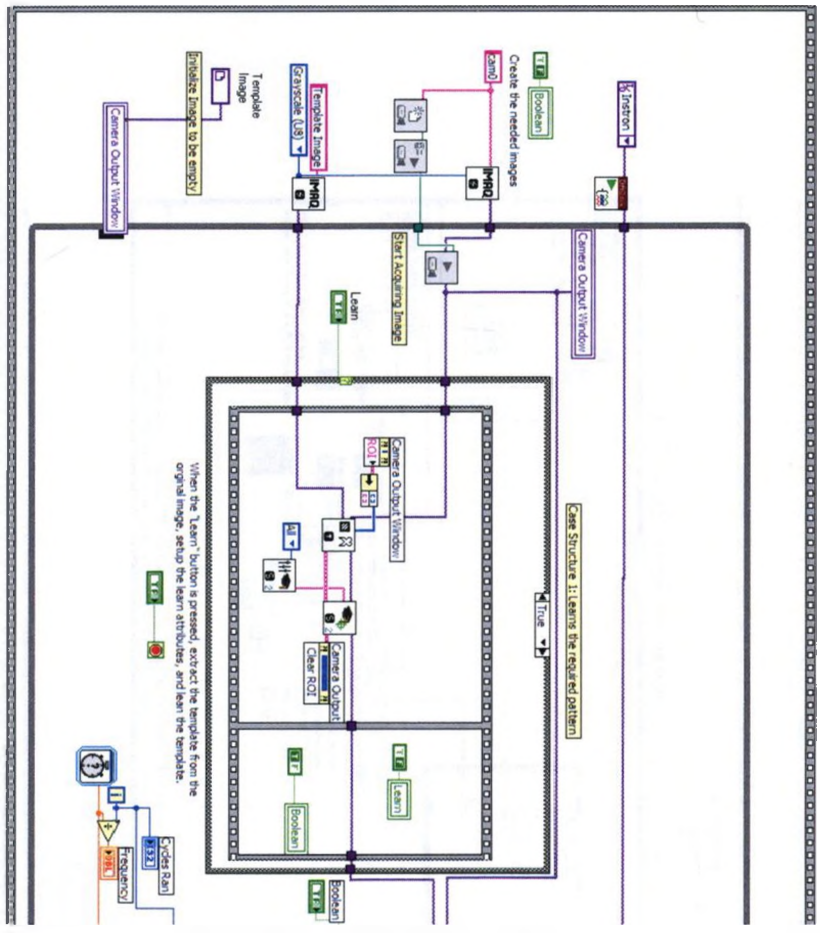

Figure C.6 -Part 1/4

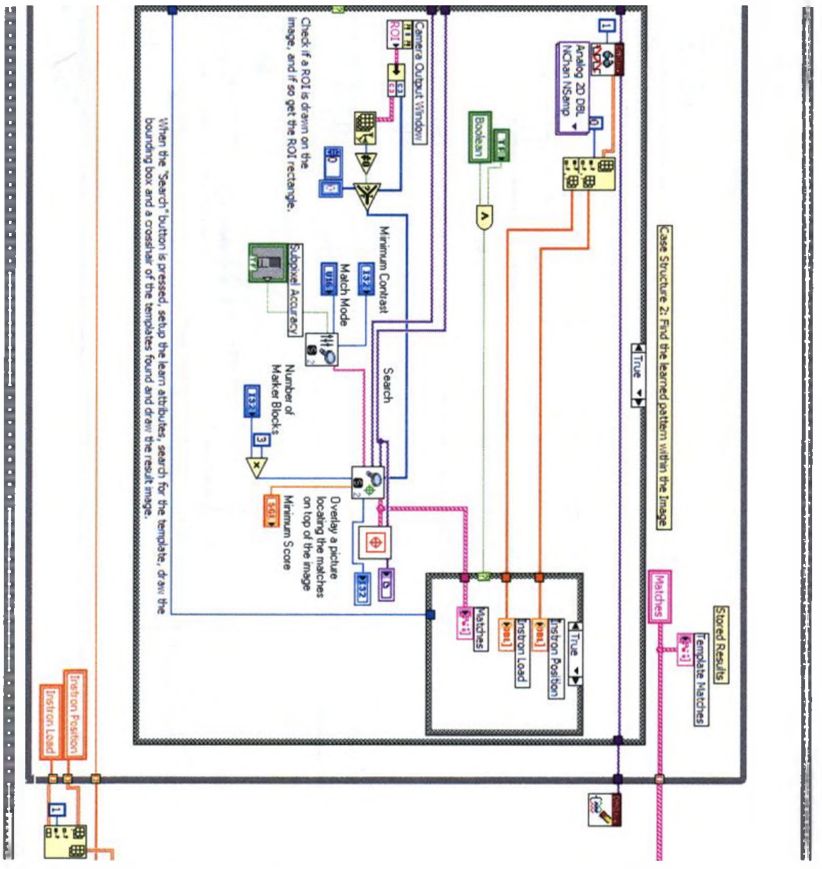

Figure C.6 -Part 2/4

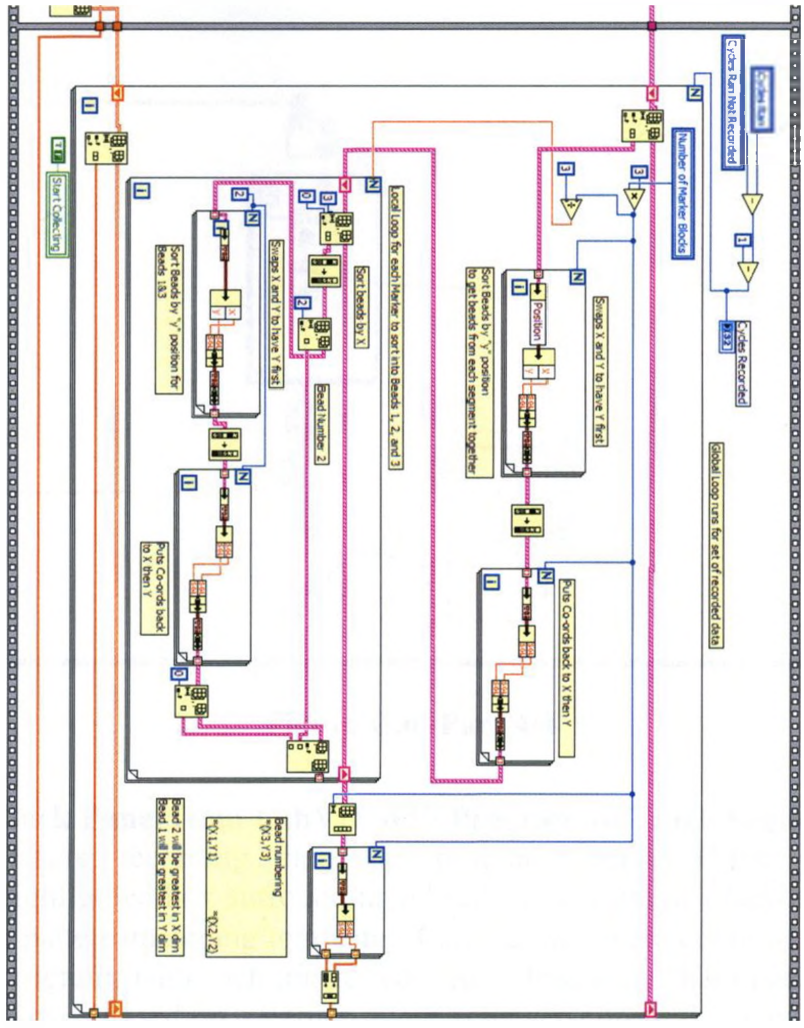

Figure C.6 -Part 3/4

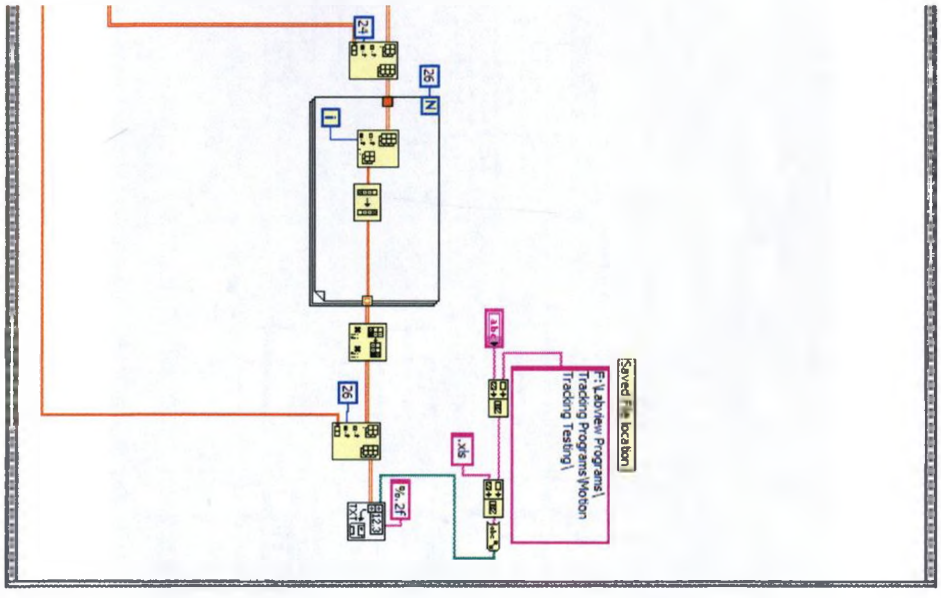

Figure C.6 -Part 4/4

Figure C.6 **Back Panel from LabVIEW™ Program to Track Segmental Motion**
Before recording data, the program extracted the pattern from a highlighted box surrounding a bead in the camera's field to view to create a pattern-matching template. Camera data were continuously fed into the program, with each image scanned to find areas that matched the template image (based on a certain score achieved) up to the maximum number of matches requested. Once recording, the *x,y* pixel location for each the matched bead was determined along with the Instron® load and position data at that time. After the loading protocol was complete, bead and Instron® data were recorded, sorted, and saved to an Excel file.

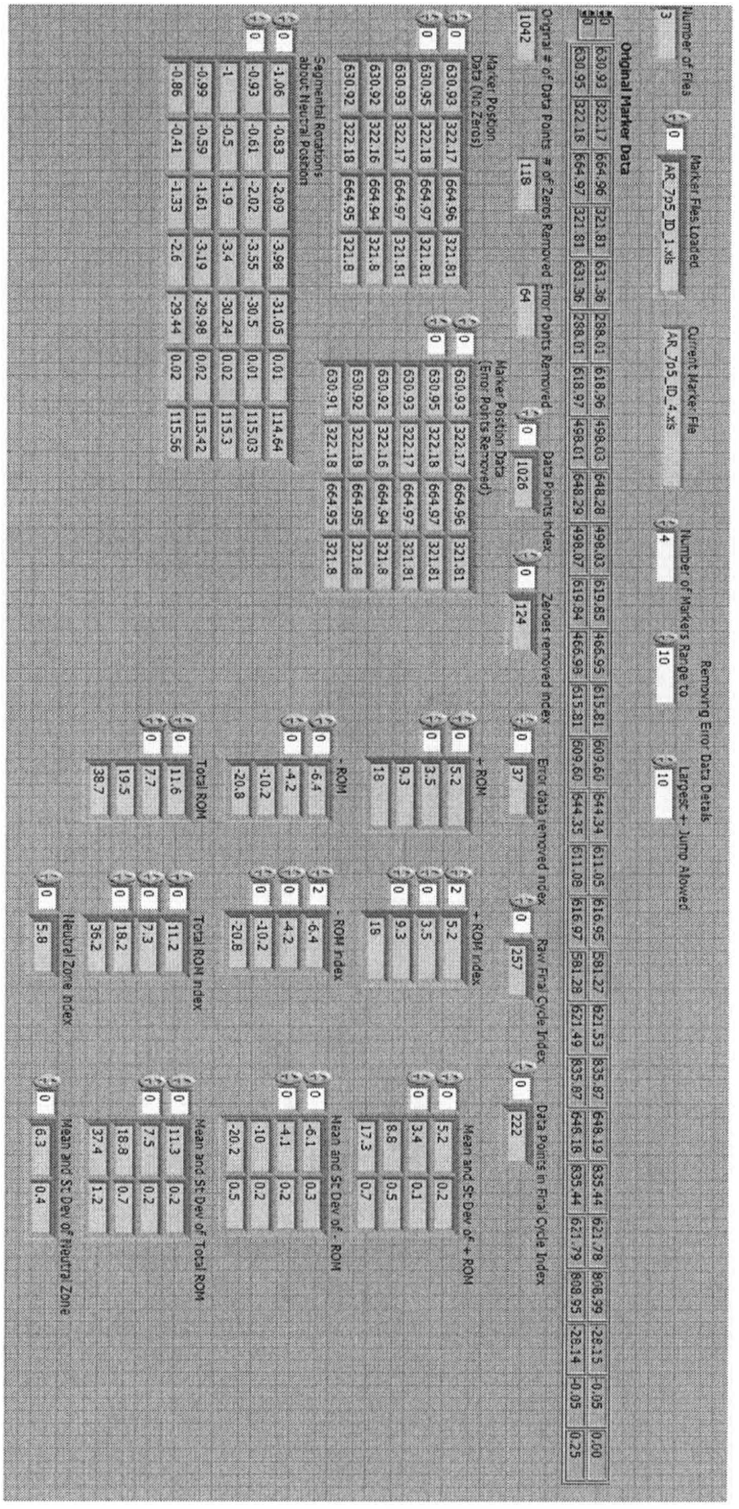

Figure C.7 **Front Panel from LabVIEW™ Program to Analyze Spine Motion**
Data for each vertebra were analyzed for each trial of the specific motion and applied moment to determine the segmental and overall range of motion of the specimen, as well as the overall neutral zone. The analyzed data were output to the front panel, including means and standard deviations for the three trials performed for each motion / applied moment grouping.

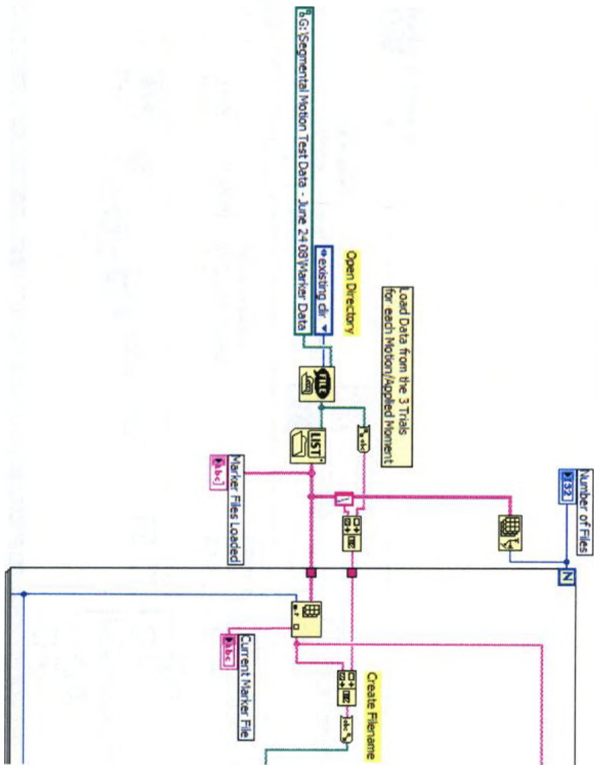

Figure C.8 -Part 1/4

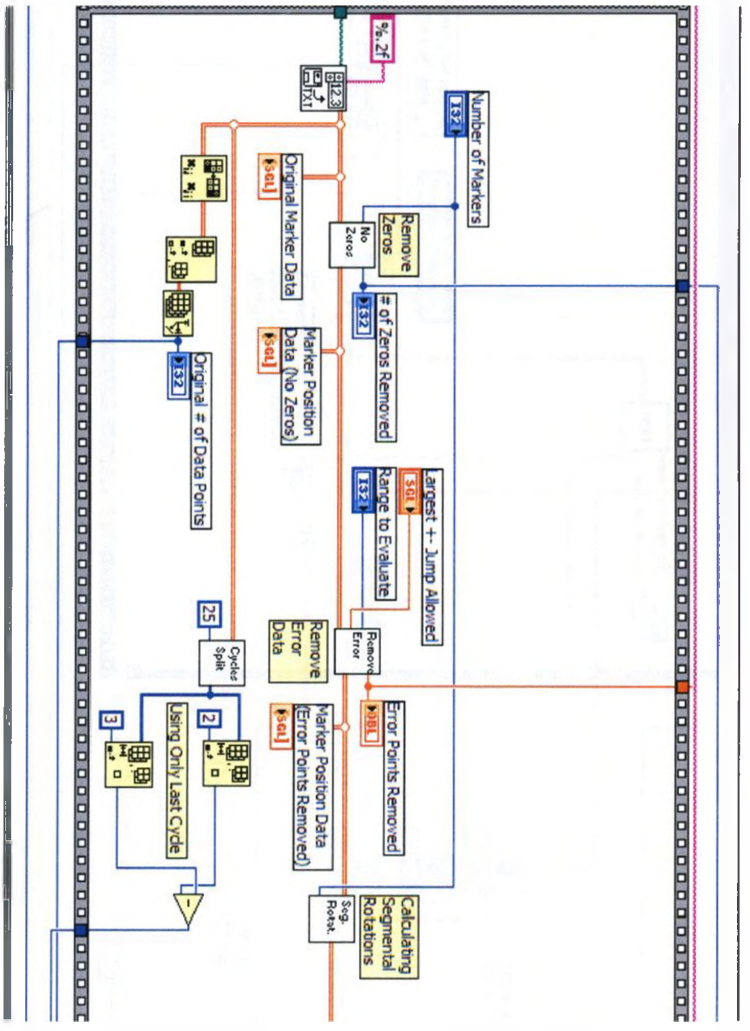

Figure C.8 -Part 2/4

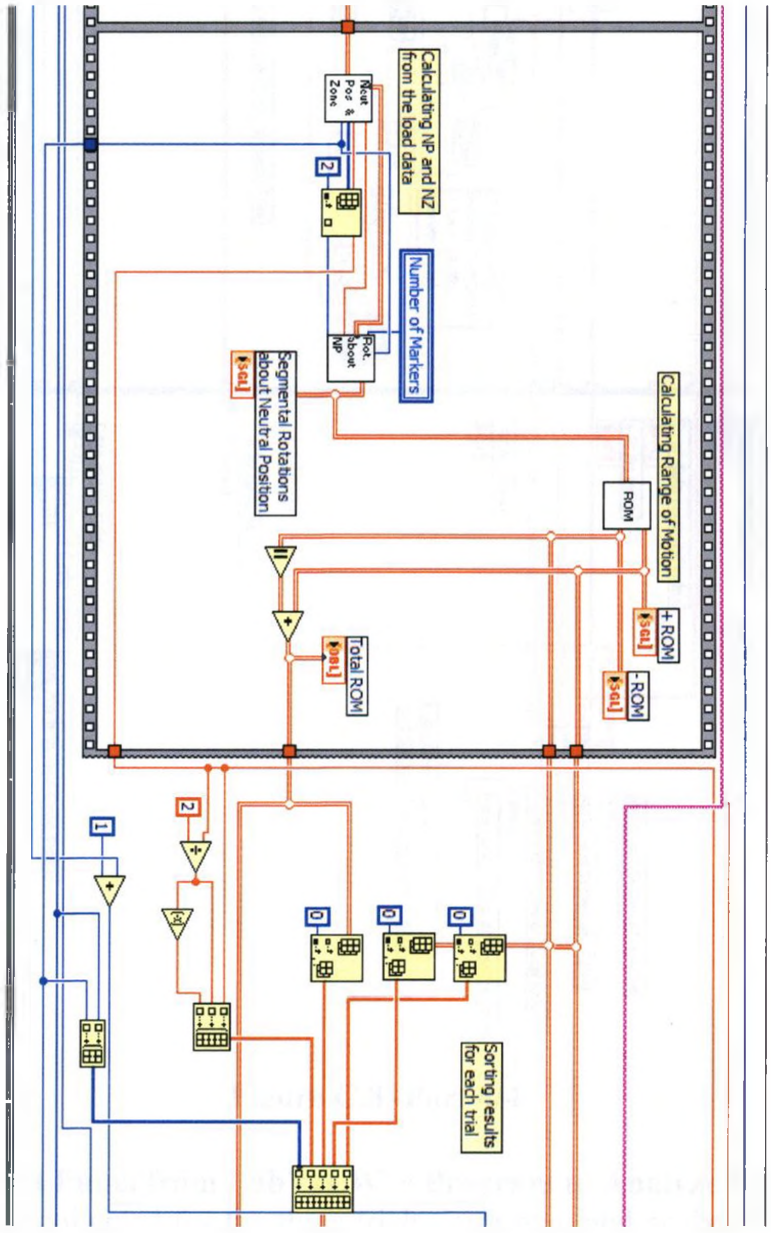

Figure C.8 -Part 3/4

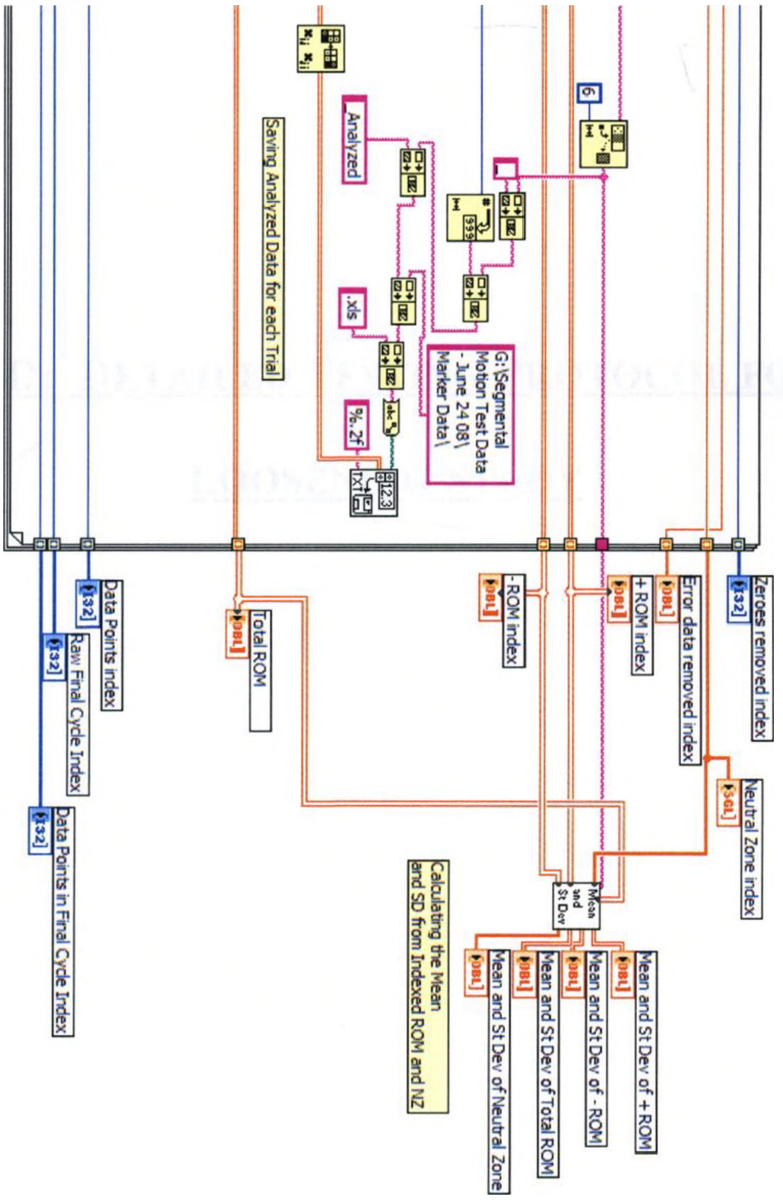

Figure C.8 -Part 4/4

Figure C.8 **Front Panel from LabVIEW™ Program to Analyze Spine Motion**
Data collected for the three trials were read and analyzed by the program to determine the segmental motion parameters. After removing the erroneous data (zeroes and large jumps in the data), the segmental (*i.e.* L1-L2) and overall (*i.e.* L1-L4) rotations were calculated using vector algebra and ZYX Euler angle analysis. Using the last cycle of data from each trial, the neutral zone, neutral position, and ranges of motion were calculated, along with the means and standard deviations for these values for the three trials.

APPENDIX D: DETAILED TESTING PROTOCOL FOR SCREW LOOSENING STUDY

The complete testing procedure to create screw loosening in the sacrum is described below. The level of detail included is such that another operator, given access to the required software tools, could follow these steps to reproduce the material presented in Chapter 2 of this thesis.

A) Pre-testing Day

1) Hollow and solid screws inserted into cadaveric sacrum by orthopaedic surgeon
2) Pedicle insertion site (left or right) randomly selected for the screw types
3) Sacral specimen remained frozen until the day prior to testing
4) Place specimen in sink to thaw overnight

B) Potting Protocol

1) Insert extra screws (*i.e.* drywall screws) into specimen for additional fixation
2) Check bone height in PVC tube, remove some bone from the caudal end if height outside PVC greater than 2 – 3 cm
3) Create cement mixture by combining 8 cups of Denstone cement with approximately 480 mL of water for cement mix
4) Place PVC tube overtop of paper towels on the workspace
5) Insert cement mix into PVC tube surrounding all sides of the specimen (use a stick to force cement into hard to reach areas)
6) Use a level on the sacral endplate to achieve proper alignment
7) Let sit for at least 1 hour for cement to harden

C) Experimental Setup

1) Setup the pot location on the left side of the Instron® actuator (screw insertion side already randomly selected)
2) Orient the PVC in the mounting fixture so the screw to be tested lies vertical
3) Connect the rod with tracking beads attached using surgical tools provided for the screw being tested
4) Insert 2 tracking beads into specimen: one along the axis of the screw, up from the bone, and another almost touching the bone, but positioned approximately 1 cm horizontally closer to the sacral endplate from the previous bead
5) Beads should be clearly visible from a lateral view; remove any bone obstructing this view
6) Cover the side of the screw with black electrical tape to create solid backdrop for tracking beads in bone
7) Lock the PVC pipe in position in fixture using set screws

D) Instron Setup

1) Check height of rod compared to Instron® actuator to ensure enough travel can occur in the actuator, adjust crosshead if necessary
2) Fine balance 250 N load cell (*i.e.* tare to 0 N)

3) Set Load/Position Limits
    a. Load +50 N, -250 N
    b. Position ± 30 mm, depending on initial position
4) Reduce actuator proportion, integral, and derivative (PID) settings to small values (P = -20, I = 0, D = 0)
5) Leave Specimen Protect ON
6) Pass the connecting rod from the screw through the ball joint connected to the actuator
7) Align fixture on testing platform so that the screw and joint are in the same vertical plane and set at a distance of 40mm between the edge of the ball joint and the centre of the screw
8) Turn Specimen Protect OFF
9) Setup Loading protocol using WaveMaker™ program
    a. 1000 cycle blocks, 1 Hz, Relative ramp loading
    b. A load of ±12.5 N should be used in the first block based on the set distance to create applied moments starting at ±0.5 Nm
    c. Increase compressive load by -12.5 N in each subsequent block to increase flexion moment by -0.5 Nm
    d. Save loading protocol

E) Camera Setup

1) Setup camera in front of Instron® and place black backdrop behind potting fixture
2) Run Measurement & Automation (M&A) Explorer to check camera settings
3) Select GRAB camera stream and adjust camera position accordingly:
    a. Fit the beads within the camera window
    b. Perpendicular to screw edge
4) Stop GRAB and select SAVE IMAGE as "Date.Screw Type.png", SAVE settings and close camera window in M&A
5) Create template image of pin
    a. Open saved image in MS paint and highlight one bead and "cut" it from the image
    b. Open a new image and "paste" the bead image
    c. Centre purple circle in screenshot (should be around 50 x 50 pixels)
    d. Save bead image as "Date.Screw Type.pin.png"
6) After this point, do not adjust camera position for current screw being tested

F) LabVIEW™

1) Open LabVIEW™ program "Sacral Screw Tracking.vi" (Figure C.1)
2) Change file name to open on the front panel to specimen # and screw type (*i.e.* "0511055Hollow")
3) Change template image name on front panel to "Date.Screw Type.pin.png"
4) Change saved folder path on back panel to specimen #
5) Measure the described distances for current screw setup
    a. Inside distance between balls on rod
    b. Distance between closest ball and screw edge
    c. Distance between lower edge of bar and bone (standard for solid at 2 mm)

6) Input values on to program front panel
7) Click the LabVIEW™ "Start" arrow to start data collection
8) To record data, must click the RECORD button

G) Starting the Loading Protocol

1) Check to ensure that four bead locations are displayed on the camera's output window by briefly running "Sacral Screw Tracking.vi"
    a. If not found correctly, re-run camera setup and change bead selected as the template image
2) Tune actuator control
    a. Use loop tuning tool provided
    b. Create a target sine wave at 1 Hz with an amplitude of ±6.25 N (0.25 Nm), with a mean load 0 N
    c. Increase the proportional gain (P) of the actuator until the actuator's response can achieve a close match to the target shape
3) Actual Test
    a. Re-start "Sacral Screw Tracking.vi"
    b. Start loading protocol in WaveMaker™

H) Ending Testing

1) Allow loading to continue as long as there is no significant screw motion
2) End test when gross screw loosening within bone is clearly evident
3) IMPORTANT: Press RECORD in "Sacral Screw Tracking.vi" first, then press STOP in WaveMaker™ program
4) Repeat procedure steps C – H for the opposing side screw

APPENDIX E: DETAILED TESTING PROTOCOL FOR SIMULATOR VALIDATION

The following steps outline in detail the complete testing procedure used to set-up and test with the spinal loading simulator. The level of detail included is such that another operator, given access to the required software tools, could follow these steps to reproduce the material presented in Chapter 3 of this thesis.

A) Materials Required

1) Multi-segment spine cadaveric specimen, including L1-L4
2) Cranial and caudal potting fixtures
3) 2 cut pieces of 4" PVC pipe
4) Denstone™ (3 - 4 cups minimum)
5) Extra screws (*i.e.* drywall screws) for height adjustments and additional fixation
6) Surgical tools (*i.e.* scalpels and cortical bone screws)
7) Marker blocks (and means of attachment) for optical motion tracking

B) Pre-testing

1) Remove most soft tissue (muscles) from bone, including remaining disc tissue on cranial and caudal ends
2) Leave ligaments and discs intact for usable segments
3) Specimen remained frozen until night before testing
4) Thaw overnight in sink

C) Connecting Mounting Brackets to Vertebrae

1) Mounting brackets are required on L2 and L3 vertebrae for attachment of optical tracking marker blocks
2) Align the mounting bracket along the superior-inferior axis on the most anterior point of the vertebral body
3) Connect the bracket to the vertebral body using cancellous bone screws

D) Potting Cranial End (*i.e.* L1)

1) Insert two extra screws directly caudally into L1 to act as a height adjustment tool
2) Find the appropriate height of the specimen in the PVC (only want the body of top vertebrae to be in cement – disc must be able to move) and adjust screw depth as necessary
3) Adjust specimen orientation such that the cranial endplate of the L3 vertebral body lies horizontally
4) Add extra screws into the body of L1 for added cement fixation, if possible add screws through PVC pipe into vertebral body
5) Check that the specimen fits in the PVC with the additional screws
6) Setup paper towel on bottom of cranial potting fixture to prevent cement contact with fixture

7) Put PVC piece in fixture before potting, with all walls attached
8) Mix approx 2 cups of Denstone™ with 120 mL of water in a sealed plastic bag
9) Tear off one corner of the bag to pour out the cement while still partially liquid
10) Slowly add wet cement around specimen using a stick to move cement into place
11) Fill to height required
12) Support the specimen for the first 5 minutes to ensure its position will be maintained while the cement sets
13) Allow 20-30 minutes for the cement to fully harden

E) Potting Caudal End (*i.e.* L4)

1) Add additional screws into the body of L4 for added cement fixation
2) Connect the cranial potting fixture, with specimen attached, to the axial loading arm
3) Setup the caudal potting fixture below the loading arm on the movable mounting plate
4) Place paper towel and PVC tube in caudal fixture
5) Lower the specimen using the Instron® axial actuator to the height required (want the lowest vertebral body entirely potted, but with adjacent cranial disc exposed)
6) Ensure L3 vertebral body lies horizontally, make adjustments if necessary
7) Move mounting plate so that the specimen is centered in the caudal fixture and bolt the mounting plate to testing platform
8) Mix approx 2 cups of Denstone™ with 120 mL of water in a sealed plastic bag
9) Tear off one corner of the bag to pour out the cement while still partially liquid
10) Raise specimen again and add some initial cement into the PVC tube held in the potting fixture
11) Lower specimen into the liquid cement in the PVC and continue to add cement until correct height is reached, using the stick to move the cement into the hard to reach areas
12) Allow 20-30 minutes to set

F) Simulator Setup

1) Remove the specimen and PVC from the potting fixtures
2) Depending on the loading performed, connect the off-axis loading arm and deadweight counterbalance to the cranial potting fixture, which is supported from above by the axial loading arm (if performing axial rotation, do not connect the off-axis loading arm and counterbalance)
3) Tare both AMTI load cells to zero load to remove the machine weight from their readings
4) Remove the off-axis loading arm and counterbalance along with two walls from the cranial fixture, and raise actuator to maximum height

5) Remove two walls from the caudal fixture
6) Place the specimen back on the caudal fixture, ensuring to align its axes with the motion about to be performed (*i.e.* if performing flexion-extension, align the anterior-posterior axis to be perpendicular to the off-axis actuator; this will required rotating the PVC in the potting fixture)
7) Fix the specimen in position by adding the two walls again to the caudal fixture
8) Lower the cranial fixture until slight contact with the cranial PVC occurs, easier to see with walls removed (a small compressive load should appear on the axial channel as well)
9) Fix the cranial fixture to the PVC by reattaching the walls
10) Reattach the off-axis loading arm and counterbalance if performing flexion-extension or lateral bending at this point

G) Tuning Load Control of Axial Actuator

1) Set axial load channel to load control
2) Ensure reasonable position limits are set (action: system stop)
3) Set load limits at ±100 N (action: unload)
4) Set starting Proportion, Integral, and Derivative control to small values (P = 0, I = 0, D = 0)
5) Use loop tuning tool provided with the Instron® software
6) Create an aggressive target square wave signal at 0.5 Hz with an amplitude of ±20 N with a mean load of -10 N
7) Increase the proportional gain (P) of the actuator until the actuator's response can achieve a close match to the target shape desired
8) Alter the Integral (I) and Derivative (D) as necessary

H) Loading Protocol

1) Set the loading arm rotation channel to be in position control and keep the axial load channel in load control
2) Using the desired loading arm (*i.e.* dependent upon the motion being performed), manually rotate the loading actuator to find the positions targets corresponding to the desired applied moment levels (*i.e.* 2.5 Nm, 5 Nm, and 7.5 Nm)
3) Record the position targets for each applied moment level
4) Create a new "Method" loading protocol using the WaveMatrix™ program (see Figure 3.5)
    i. Loading protocol consists of three full loading cycles to the desired applied moment (*i.e.* ±2.5 Nm, ±5 Nm, or ±7.5 Nm)
    ii. Use relative ramp waveforms (rotation) in sequential blocks to create cyclic rotation of the specimen (use rotations slightly larger than those found with the manual rotations, such that the desired load is sure to be reached)
    iii. Create a waveform event for reaching the target applied moment so that it begins the next rotation (*i.e.* changes direction) once the load target has been achieved

iv. Set the axial load (and axial torque channel if applying flexion-extension or lateral bending) to an absolute ramp waveform maintain a small compressive load (-10 N) (or no applied moment respectively) throughout the test
v. Save the Method

I) Camera Setup

1) Insert 3 tracking beads into the Delrin® marker block so that they will be seen by the camera for the specific motion being applied
2) Attach the aluminum rods and marker blocks to the mounting brackets on the exposed vertebrae, and separate marker blocks to each of the cranial and caudal potting fixtures
3) Cover the visible testing area with a black sheet to prevent unwanted pattern-matches from being detected by the camera
4) Setup camera in front of the Instron®
5) Run Measurement & Automation (M&A) Explorer to set camera settings to appropriate values (1280x960 Y (mono 8) 7.5 fps)
6) Select "Grab" camera stream and adjust camera position accordingly to fit the marker blocks within the camera window, being sure to account for their additional movement once the loading starts (see Figure C.5)
7) Manual adjust the camera's focus on the beads in the window for the clearest view of the beads (use the zoom tool to increase the size of the beads for easier adjustment)
8) Stop Grab and close the camera window in M&A
9) After this point, do not adjust camera position for current motion

J) LabVIEW™

1) Open "Planar Tracking – Segmental Motion.vi" (Figure C.5)
2) Change file name to save on the front panel to include motion type, applied moment, and trial # (*i.e.* "AR_7p5_1")
3) Input the # of marker blocks to be tracked on the program front panel
4) Click the LabVIEW™ "Start" arrow to start camera data collection, video should be shown in the camera output window
5) Using the rectangle box tool on the camera output window, draw a box around a bead of interest in the output window
6) Select "Learn Template" on the front panel
7) Matched beads should be shown in output window, if not all beads found, repeat procedure starting from Step 4

K) Starting the Loading Protocol

1) Select a new Test and run the Method created for the current motion in WaveMatrix™
2) Click "Start Collecting" on the front panel of the LabVIEW™ program
3) Click OK to start loading in the WaveMatrix™

L) Finishing the Protocol

1) The WaveMatrix™ test finishes after the loading cycles are complete
2) Click "Record Data" in the LabVIEW™ program to save the tracked motion

M) Continuing Loading Protocol

1) Run the Test created in WaveMatrix™ for 3 trials of same motion and applied moment level without changing any settings (*i.e.* re-run Steps J – L) to assess repeatability
2) Run the protocol for three levels of applied moment with the same motion (*i.e.* 2.5 Nm, 5 Nm, and 7.5 Nm of axial rotation) (*i.e.* re-run Steps J – M1)
    a) Change the relative ramp waveform settings in WaveMatrix™ to adjust to the new applied moment
    b) Change the event detection to account for the new applied moment
3) Run the protocol for the three different motion types (*i.e.* flexion-extension, lateral bending, and axial rotation) (*i.e.* re-run Steps F – M2)
    a) Reconfigure the simulator, camera and specimen between each motion
4) Run an addition setup of the first motion applied for one applied moment level (Steps F – M2) to assess reproducibility
    a) Reconfigure the simulator, camera, and specimen
    b) Only one applied moment level needs to be run in Step M2

N) Reconfiguring the Simulator

1) Simulator needs to be reconfigured for between the different motions
2) For flexion-extension,
    a) Specimens should be aligned with its anterior-posterior axis perpendicular to the off-axis actuator
    b) Off-axis loading arm and deadweight counterbalance need to be connected
    c) Marker blocks should be oriented to view the tracking beads from a lateral perspective
3) For lateral bending,
    a) Specimens should be aligned with its anterior-posterior axis parallel to the off-axis actuator (same as axial rotation)
    b) Off-axis loading arm and deadweight counterbalance need to be connected
    c) Marker blocks should be oriented to view the tracking beads from a frontal view perspective
4) For axial rotation,
    a) Specimens should be aligned with its anterior-posterior axis parallel to the off-axis actuator (same as lateral bending)
    b) Off-axis loading arm and deadweight counterbalance need to be disconnected
    c) Marker blocks should be oriented to view the tracking beads from a superior perspective of the horizontal plane
    d) Camera moved to location above the specimen
5) For each reconfiguration, simulator setup should follow the procedure described in Step F